IOWA STATE UNIVERSITY
Digital Repository

Retrospective Theses and Dissertations

Iowa State University Capstones, Theses and Dissertations

1981

Laser excited Shpol'skii spectroscopy for the selective excitation and determination of polynuclear aromatic hydrocarbons

Yen Yang
Iowa State University

Follow this and additional works at: https://lib.dr.iastate.edu/rtd

 Part of the Analytical Chemistry Commons

Recommended Citation
Yang, Yen, "Laser excited Shpol'skii spectroscopy for the selective excitation and determination of polynuclear aromatic hydrocarbons " (1981). *Retrospective Theses and Dissertations*. 6863.
https://lib.dr.iastate.edu/rtd/6863

This Dissertation is brought to you for free and open access by the Iowa State University Capstones, Theses and Dissertations at Iowa State University Digital Repository. It has been accepted for inclusion in Retrospective Theses and Dissertations by an authorized administrator of Iowa State University Digital Repository. For more information, please contact digirep@iastate.edu.

www.manaraa.com

8122572

YANG, YEN

LASER EXCITED SHPOL'SKII SPECTROSCOPY FOR THE SELECTIVE EXCITATION AND DETERMINATION OF POLYNUCLEAR AROMATIC HYDROCARBONS

Iowa State University

PH.D. 1981

University
Microfilms
International 300 N. Zeeb Road, Ann Arbor, MI 48106

Laser excited Shpol'skii spectroscopy for the selective excitation and determination of polynuclear aromatic hydrocarbons

by

Yen Yang

A Dissertation Submitted to the
Graduate Faculty in Partial Fulfillment of
The Requirements for the Degree of
DOCTOR OF PHILOSOPHY

Department: Chemistry
Major: Analytical Chemistry

Approved:

Signature was redacted for privacy.

In Charge of Major Work

Signature was redacted for privacy.

For the Major Department

Signature was redacted for privacy.

For the Graduate College

Iowa State University
Ames, Iowa

1981

TABLE OF CONTENTS

LIST OF TABLES

LIST OF FIGURES

CHAPTER 1. INTRODUCTION

Although comparisons of the mutagenic or carcinogenic potency of various chemical substances are subject to considerable uncertainty, there is little doubt that selected compounds in the polynuclear aromatic hydrocarbon (PAH) series are among the most potent known. For example, the higher than normal incidence of cancer among chimney sweeps and workers in the coal tar, creosote, coal gas, coke, and cutting oil industries, where exposure to PAHs is localized, has been extensively documented in the past (1). In the years ahead, man seems destined to experience an increasing burden of exposure to low concentrations of PAHs from more extensive and diffuse sources, e.g. aerosol emissions from the stacks of coal fired utility boilers, or fugitive emissions from coal gasification or liquefaction and from oil shale recovery operations.

The assessment of the potential health effects of this increased environmental loading by the PAHs is rendered difficult by:

a. the large range of potency found among structural isomers of compounds with the same number of condensed rings and among the various alkylated derivatives (2-4);

b. the enhancement of carcinogenicity through synergistic effects (5); and

c. the absence of reliable data bases.

The three factors just mentioned impose several stringent requirements on analytical methodologies required for collecting data bases, especially if a comprehensive health effects assessment is the goal. Among these requirements are adequate powers of detection, the capability to distinguish between structural isomers and alkylated species of the same parent compound, acceptable sample through-put, and acceptable reliability.

During the past decade, there have been significant advances in developing analytical methodologies addressed to meeting these needs. These methodologies are usually based on first isolating the PAHs as a compound class followed by isolation of the individual PAHs, or their structural isomers or alkylated derivatives, via: (a) thin layer chromatography; (b) capillary column gas chromatography with flame ionization detection or mass spectroscopic characterization; (c) gas-liquid chromatography using nematic liquid crystal columns; and (d) high performance liquid chromatography with fluorescence detection. A critical test for any of these techniques is their capability of achieving efficient and adequate resolution of individual, high-potency, structural isomers and of alkylated species at the concentration

ratios found in environmental samples. For many of these samples, state-of-the-art methodologies do not satisfy all of the requirement stated above. As consequence, there is a continuing interest in alternative approaches, especially those that would allow the direct determination of specific high potency species without prior isolation of the individual compounds.

Optical luminescence spectroscopic approaches have been used for many years for the sensitive detection of molecular species (6-25). However, ambient temperature luminescence spectrometry has only been utilized to a limited extent in the qualitative and quantitative determinations of PAHs in complex mixtures (18-23). The limitation arises from the fact that molecular absorption and emission spectra from room temperature solutions are generally broad and featureless, because the molecules in fluid media can easily be affected by their immediate environments that shift their electronic levels. This broad feature causes severe spectral overlap, making the identification of the constituents of a complex mixture difficult.

It has long been recognized that molecular luminescence spectra can be sharpened by use of low temperature matrices. The fact that the thermal broadening contribution to the spectral bandwidth is minimal at low temperature, however, does not automatically give rise to a spectral bandwidth that satisfy the resolution requirement for complex mixture analysis. At

cryogenic temperature, the bandwidth is essentially determined by the so called "inhomogeneous broadening effect," which arises from a statistical distribution of the local environments (sites) experienced by the guest (solute) molecules in the solid matrix (solvent or host) (26). The extent to which the sites are randomly distributed determines the spreading of the electronic levels of the guest molecules, and hence the spectral bandwidth. The degree of the inhomogeneous broadening, however, depends on the orderliness of the matrix lattice. For the amorphous glass matrices which are devoid of long range order, the site inhomogeneously broadened bandwidth is of the order of 200-300 cm^{-1} (27). In contrast, the bandwidths observed for the isomorphous or polymorphous crystalline matrices are only a few wave numbers (28-30).

The guest-matrix interactions also play an important role in determining the appearance of the low temperature spectrum. In the low temperature spectrum, the vibronic bands are usually accompanied, on the longer-wavelength side in emission and on the shorter-wavelength side in absorption, by a much broader band called phonon sideband, or phonon wing. The narrow vibronic bands, which correspond to purely vibration-electronic transitions, are often called the zero-phonon or phonon-free bands, because no changes in the matrix vibrational states accompany the absorption or emission process. The broad phonon bands, on the other hand,

arise from the simultaneous creation or annihilation of matrix phonons during the electronic transition. The term "electron-phonon coupling," or "guest-host coupling" is often used to describe this process (31-35). The electron-phonon coupling is known to be both temperature and solvent dependent (26,32,33). For example, as the matrix temperature is increased, the intensity of the phonon wing usually increases at the expanse of the zero-phonon band intensity. In those matrix systems in which the guest-matrix interactions are strong, the zero-phonon bands can disappear at temperatures as low as 20 K, and the spectrum consists of only the diffuse phonon bands (28,29).

Both site inhomogeneity and electron-phonon coupling can impose problems detrimental to the analytical applications of low temperature spectroscopy from the selectivity point of view. The latter can usually be alleviated by judicious choice of matrix material and by lowering the matrix temperature. To circumvent the site inhomogeneity problem, one approach involves the utility of a narrow band excitation source, usually a laser, to excite those guest molecules in a particular environment. Because only those molecules whose electronic energy levels are in resonance with the laser frequency can be excited to fluoresce, the resulting spectrum exhibits the quasilinear feature. Usually, the observed spectral line width is determined by the linewidth

of the light source (assuming the homogeneous broadening contribution is negligible). This technique is called the fluorescence line-narrowing spectroscopy (FLNS) (26,36-38). The excitation process in FLNS can be viewed as a selection process, that is, selecting a relatively small number of approximately identical sites from the large number, broad continuum of possible ones. The major requirement for achieving fluorescence line-narrowing effect is that laser excitation be into a vibronically well-resolved region of the absorption spectrum (usually near the 0-0 absorption band). In principle, FLN effect can be achieved in any low temperature matrix, provided that the excitation bandwidth is narrow relative to the inhomogeneously broadened absorption profile.

A different approach to the site inhomogeneity problem involves the choice of suitable matrix to trap guest molecules of similar molecular structure or configuration. Because the guest molecules can substitute uniquely into the matrix lattice and become fixed in a particular environment, a significant reduction of site inhomogeneity results. This technique is called the mixed-crystal spectroscopy (27-30). One of such matrix systems is the Shpol'skii system, i.e. n-alkanes.

In 1952, Shpol'skii and his co-workers discovered that when aromatic compounds were dissolved in appropriate n-alkane

solvents and the resulting solutions were frozen to cryogenic temperature, quasilinear emissions were observed and the observed bandwidths were of the order of 1-10 cm^{-1} (39). This type of line-narrowing phenomenon is now often called the "Shpol'skii effect," named after the Russian scientist. One remarkable feature of the Shpol'skii system is that the n-alkane solvent is less specific in choosing the guest molecules than any other mixed-crystal system. The only configuration requirement for achieving quasilinear spectrum is that the n-alkane carbon skeleton chain length be equal to the longest dimension of the carbon skeleton of the guest aromatic molecules (30,40). This requirement is often called the "key and hole rule." This rule, however, is not so restrictive as it was initially proposed (41). For example, the quasilinear spectrum of anthracene has been observed in normal pentane, hexane, heptane, octane, and nonane. Usually, a single solvent, such as n-heptane, suffices for the development of quasilinear spectra of many aromatic compounds of different ring sizes. Nevertheless, serious mismatches of n-alkane chain length with guest molecular dimension may still lead to severe line broadening. When this happens, the observed bandwidth can be as broad as those observed in amorphous systems, despite the fact that a Shpol'skii solvent is utilized. To date, hundreds of

organic compounds of various compound classes are known to exhibit quasilinear emissions (42). Some representative compound classes are shown in Figure 1.

In addition to the quasilinear feature, the weak phonon wings are another distinct characteristic of Shpol'skii spectra. The weak phonon wings arise from the weak interactions between the guest molecules and the n-alkane matrix lattice (31-33). As a result of this weak electron-phonon coupling, it is often sufficient to decrease the matrix temperature to 77 K to observe quasilinear emissions, which is often found difficult for other types of mixed-crystal systems (30,40).

In spite of the aforementioned advantages of Shpol'skii systems, the Shpol'skii effect spectra are usually complicated with the multiplet structures that are observed repeatedly throughout the vibronic lines. These multiplets may consist of as many as ten lines, and the splitting among these lines may vary from a few wave number to several hundred wave numbers. The complexity of the multiplet structure is generally related to the symmetry of the guest molecules, that is, the most complex structure of multiplets are characteristic of low-symmetrical molecules (43). In addition, the number of lines in the multiplets, their relative intensities, and wavelengths depend on such parameters as the choice of host (40,44), cooling rate (45,46), matrix temperature (47), excitation wavelength

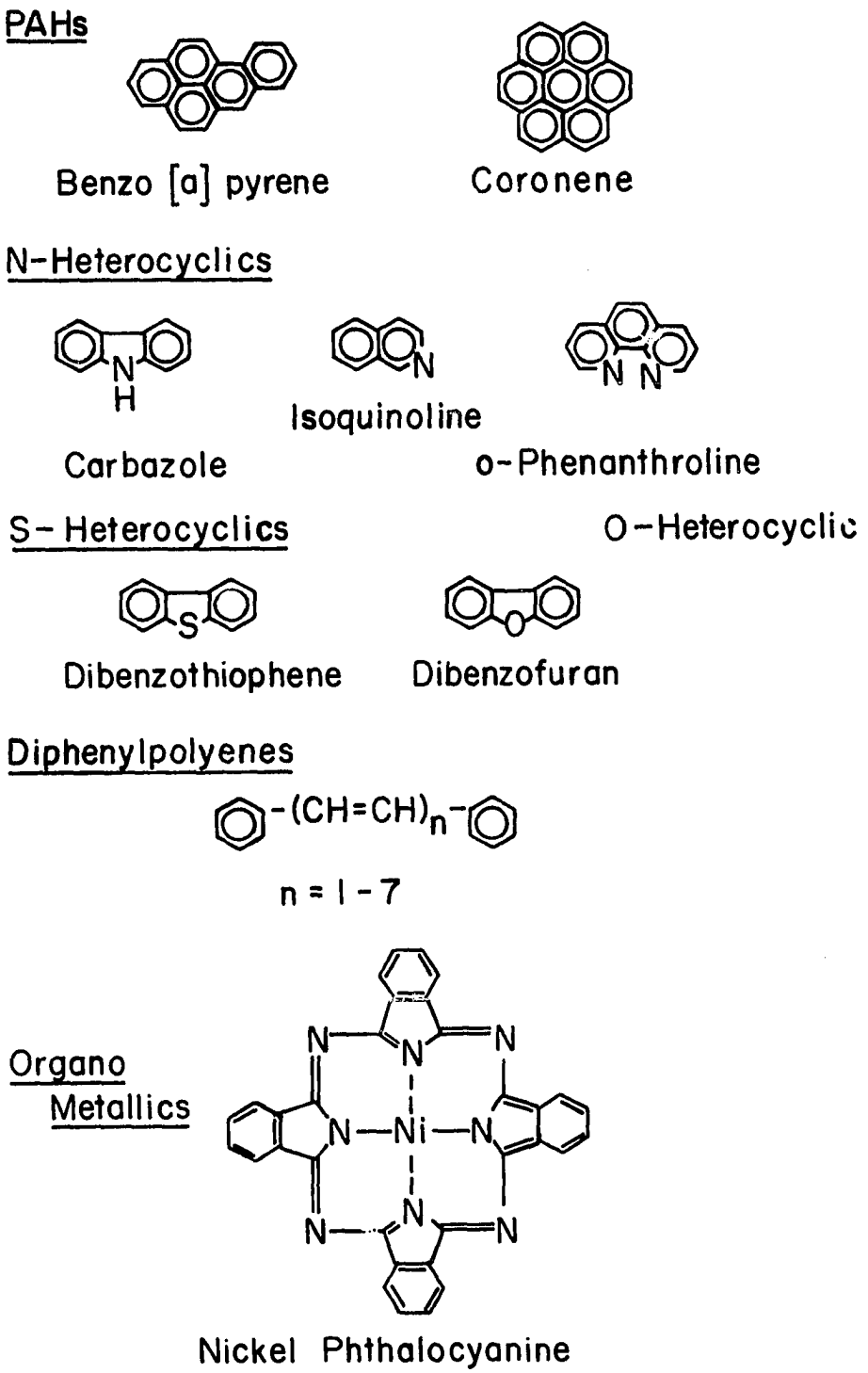

Figure 1. Organic compound classes for which Shpol'skii effect has been observed.

(48), and concentration (49). For example, the fluorescence spectrum of benzo[a]pyrene exhibits quintets in n-hexane, quartettes in n-heptane, and singlets in n-octane, when the sample solution is frozen rapidly and observed at 77 K (50). The origin of multiplet structure was initially proposed by Shpol'skii as the results of guest molecules occupying different, well-defined lattice sites. He suggested that the nonequivalent lattice sites were provided by different rotational isomers of the n-alkane host molecules (30,40). There is now general agreement that those multiplets arise from several orientations of the guest molecules in the solidified n-alkane cage (51-54). These different orientations result in different local environments that lead to nonequivalent crystal field effects, and hence multiple site spectra. The direct experimental confirmation of this interpretation was first performed by Svischev (55), who showed that the guest molecules do exist in several effectively different environments by exciting one component of the doublet multiplet of coronene in n-heptane at 77 K; he then observed the fluorescence only from the corresponding half of the doublet in emission. Subsequently, Svischev's results have also been confirmed by other investigators utilizing laser excitation of the fluorescence as well as phosphorescence of one of the coronene sites (56).

The dependency of Shpol'skii effect spectra on concentrations has also been of great concern in the past (49,57-60). Typically, two kinds of concentration behaviors of quasilinear spectra have been observed. In the first kind, quasilinear emissions were observed at low concentrations. As concentration increases, diffuse bands appear to superimpose the quasilinear spectrum. As for the second kind of behavior, the spectra consist of diffuse bands at low concentrations. With an increase of concentration, the spectra become quasilinear ones, but with accompanying of diffuse bands. Shpol'skii has interpreted these totally different concentration behaviors as follow (61): In the first case, the guest and host molecules are of comparable sizes, and the quasilinear emissions at low concentrations are due to the matrix-isolated guest molecules, whereas the broad emissions at low concentrations in the second case are the result of severe site inhomogeneous broadening, presumably because of mismatch of molecular sizes. The appearance of quasilines at high concentrations in the second case is associated with the alignment effect of the solvent crystal lattice near the guest molecules. An increase of concentration causes an increase of the extent of orderlines of the guest molecules relative to the host, and hence leading to a decrease of site inhomogeneity. The broad emissions observed at high concentrations are due to the aggregates of

the guest molecules.

Analytical applications of both Shpol'skii spectroscopy (62-70) and FLNS in organic glasses (71-73) for the analysis of PAH mixtures have been documented. An alternate approach, which involves a different sample preparation procedure, is matrix isolation spectroscopy (MIS) (27,74-80). In MIS, a liquid or solid sample is vaporized under vacuum, and mixed with a large excess of a dilute gas, i.e. matrix gas. This gaseous mixture is then deposited onto the cold surface in a cryostat. The deposited solid, which is subjected to spectroscopic analysis, is usually at a temperature of 20 K or less. The matrix gases commonly employed include nitrogen, argon, and xenon, etc. inert gases. Because of the physical isolation of sample molecules from each other and the low matrix temperature, the resulting spectral bandwidth are much narrower than those observed in fluid media. Typical bandwidths of PAHs under MIS conditions are of the order of 50-200 cm^{-1} (78). Recently, other types of matrix materials, such as n-heptane and perfluorohexane, have been employed to improve spectral resolution (78,79). When the Shpol'skii solvent was used, spectral linebroadening was observed (81), and annealing of the sample matrix at a temperature below the matrix melting point was required to restore the orderliness of the lattice matrix (78). When perfluorohexane used as the matrix, the site

selection technique (to be discussed in detail later in this thesis) was employed to provide narrow-lined emissions (79). The most significant advantage of MIS appears to be the suppression of aggregate formation at relative high analyte concentrations.

Based on the criteria indicated earlier that an analytical technique should be rapid, selective, sensitivity, and quantitative, none of the aforementioned, low temperature based techniques is completely satisfactory in these regards. The major potential drawback of FLNS in organic glasses lies in the inherent broad absorptive features. In complex mixtures, especially those containing alkylated PAHs, overlap of the broad absorption bands may seriously impair the selectivity. The major shortcoming of MIS appears to be the tedious and sophisticated sample preparation procedures involved, which are generally not reproducible. Moreover, MIS is only applicable to those samples which can be vaporized without accompanying thermal decomposition. As for the conventional Shpol'skii spectroscopy, the principal difficulty arises from the inherent multiple-site characteristic. Because all of the PAH molecules occupying different lattice sites can be excited to emit under conventional broad band excitation (UV or X-ray), spectral interferences have been a problem in the analysis PAH mixture spectra.

During the past decade, lasers have been used more and more in analytical spectroscopy and luminescence spectroscopy has been a particularly fertile area for laser applications (82,83). Because the number of photons emitted by a sample increases linearly (up to the point of saturation) as the number of photons put into the sample, the best signal levels are obtained with high power laser excitation. However, the sensitivity advantage of laser excitation cannot be fully appreciated unless the absorbers in the sample are also of comparable narrow bandwidth as the laser. Thus, Shpol'skii spectroscopy coupled with laser excitation, i.e. laser excited Shpol'skii spectroscopy (LESS), can offer some distinct advantages over the FLNS and MIS alternatives in terms of sensitivity as well as selectivity. The sharp absorption bandwidth (FWHM of 1 to 10 cm^{-1}) exhibited by PAHs in frozen Shpol'skii hosts facilitates selective excitation of the luminescence of a specific compound in mixtures through narrow band laser excitation (84). When selectivity is enhanced through selective excitation, the spectral resolution in emission is immaterial, and a high resolution spectrometer is not required. Moreover, because of this narrow absorptive feature, narrow band lasers can provide more effective excitation of PAH luminescence, and consequently an enhanced detection sensitivity.

This dissertation describes the development of LESS as an analytical technique for the direct characterization of complex mixtures of PAHs. Qualitative and quantitative aspects of LESS are discussed. The applications of LESS to the direct determination of PAHs in liquid fuels are demonstrated. Finally, analytical data are presented and compared with those obtained by independent chromatographic techniques.

CHAPTER 2. EXPERIMENTAL FACILITIES

A block diagram of the LESS system is shown in Figure 2. The components used in the present study are summarized in Table 1. A more detailed description of the entire system and instrumental features is given below.

Excitation Sources

In the early phase of this investigation, a laboratory constructed nitrogen laser was utilized to excite a dye laser. The N_2 laser, a super-radiant discharge, had a peak power of 200 kW, a repetition rate of 20 pps, and a pulse width of approximate 8 ns at 337.1 nm with an output spectral bandwidth of less than 0.1 nm. This laser was normally operated at 10 kV with an operating N_2 gas pressure of 100 Torr in the laser channel.

Later, the N_2 laser was replaced with a Lambda Physik excimer multigas laser. The recent commercial introduction of the excimer laser as a pump source not only extended the fundamental tuning range down to 310 nm, as compared to 355 nm of the N_2 laser, but also increased the dye laser peak power by an order of magnitude, to several megawatts in the UV and visible. The excimer laser is a gas laser that uses a mixture of a rare gas and a halogen as the active medium. The choice of gas mixture determines the output wavelength. Generally a broad

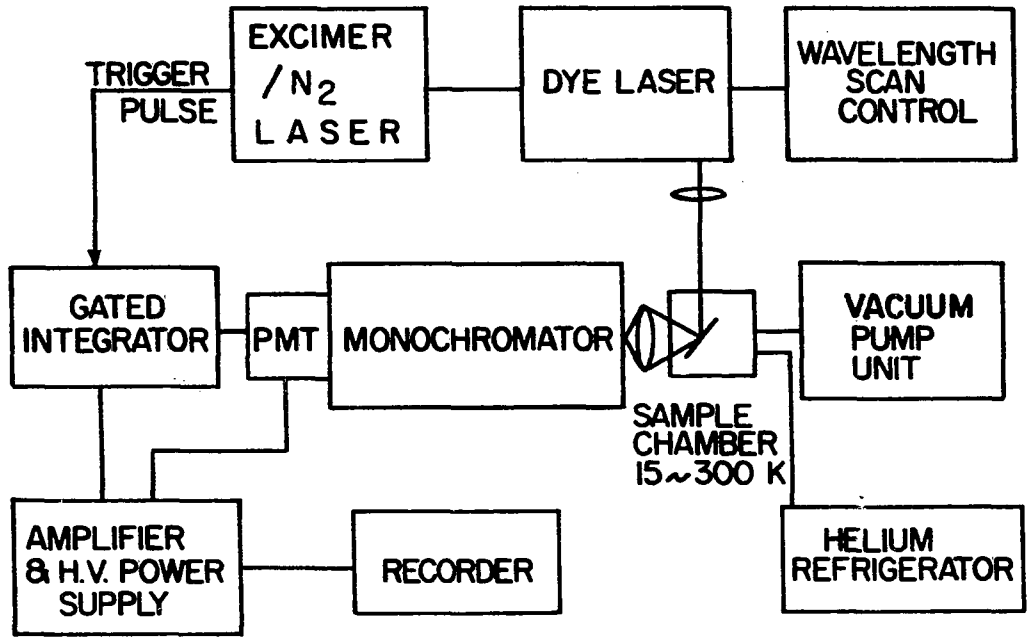

Figure 2. Block diagram of the experimental facilities utilized for the observation of LESS.

Table I. Experimental components of LESS system

Component	Model No.	Manufacturer
A. Laser System		
Excimer multigas laser	EMG 101	Lambda Physik, West Germany
N_2 laser	——	Ames Laboratory constructed
Dye laser	FL 2000	Lambda Physik, West Germany
Dye laser scan controller	FL 500	Lambda Physik, West Germany
B. Spectrometer System		
Monochromator (0.5 m)	82-000	Jarrell-Ash, Waltham, MA
Monochromator (0.64 m)	HR-640	Instruments SA, Inc., Metuchen, NJ
Monochromator stepping motor controller	980015	Instruments SA, Inc., Metuchen, NJ
C. Detector and Signal Processing		
Photomultiplier	R955	Hamamatsu Co., Middlesex, NJ
HV power supply	110	Pacific Photometric Instrument, Emeryville, CA
Boxcar averager	162/164/165	Princeton Applied Research, Princeton, NJ
Strip chart recorder	5210-5	Houston Instrument, Austin, TX
D. Refrigeration and Vacuum System		
Cryogenic refrigerator	CSW-202	Air Products and Chemicals Inc., Allentown, PA
Diffusion		NRC Equipment Co., Newton, MA
Vacuum pump	1397	Welch Scientific Co., Skokie, IL
Thermocouple and emission regulated ion gauge	710	NRC Equipment Co., Newton, MA

spectral region, from 157 nm with F_2 to 10.6 μm with CO_2, can be covered. In the present study, XeCl was employed as the active medium. This medium was obtained by mixing 60 mbar of xenon, 80 mbar of 5% hydrogen chloride in helium and 1110 mbar of helium (as the buffer gas). Both Xe and HCl gases were of ultra-high purity (>99.99%) and were obtained from Cryogenic Rare Gas Laboratory, Inc., Newark, New Jersey.

The XeCl laser, radiating at 308 nm, had a temporal band width of ~10 ns and normally operated at a power level of ~2 MW, a repetition rate of 30 pps and power supply high voltage of 25 kV.

The Lambda Physik dye laser basically follows the design of Hänsch (85), utilizing a holographic grating, beam expanding telescope, dye cell, and outcoupling mirror in the oscillator stage. In addition, the dye laser comprises an amplifer stage where emission from the oscillator is further amplified. The grating, in connection with a conventional sine bar mechanism, can be either scanned linearly in wavelength or set at a specific wavelength by a wavelength controller. The dye laser output had a beam FWHM (full width at half maximum) of 0.01 - 0.03 nm.

The three dyes used for tuning the laser were PBD {2-(4-biphenylyl)-5-phenyl-1,3,4-oxadiazole}, BBQ {4-4'''-bis-butylactyloxy-quaterphenyl}, and stilbene-3, for 355 to 465 nm wavelength region. The experimental conditions employed with these three dyes to excite the luminescence of various PAHs are shown in Table 2. All of the dyes were obtained from

Table II. Experimental conditions of laser dyes

Dye	Pump Laser	Dye Solvent	Concentration, M		Wavelength Peak, nm	Wavelength Range, nm
			Oscillator	Amplifier		
PBD	N_2	toluene/ ethanol (50/50)	5×10^{-3}	5×10^{-3}	365 , 380	360 - 385
	XeCl	cyclohexane	3.6×10^{-4}	1.2×10^{-4}	360	355 - 390
BBQ	N_2	toluene/ ethanol (50/50)	2.5×10^{-3}	2.5×10^{-3}	385	375 - 400
	XeCl	cyclohexane	3.6×10^{-4}	1.2×10^{-4}	370	360 - 400
Stilbene-3	XeCl	cyclohexane	3.6×10^{-4}	1.2×10^{-4}	425	405 - 465

Interactive Radiation Inc., Northvale, New Jersey. The dye solutions, when in operation, were circulated through the dye cells to avoid thermal decomposition. Change of the dye solutions usually did not require retuning of the laser unless the refractive index of the dye solvent changes.

Optical System

The optical schematic diagram of the LESS system is shown in Figure 3. Optical alignment was performed using a continuous wave He-Ne laser with emission at 632.8 nm (C. W. Radiation, Inc., Mountain View, CA). The exciting laser was focused along an axis perpendicular to the dye laser axis (transverse pumping) with a cylindrical lens so that a thin line of fluorescence appeared across the front of the dye cell. Dye concentrations were chosen (Table 2) so the excitation light was totally absorbed within a short distance of entering the solution. The excitation laser pusles are so intense that an almost total population inversion between vibrational levels of the first excited singlet state and higher energy vibrational levels of the ground state can be obtained for the dye molecules within that small excited region. A beam expanding telescope (25X), consisting of diverging and converging lenses, was used between the grating and the dye cell to decrease the bandwidth of the laser by filling the grating. The holographic diffraction grating with 2440 grooves/mm, used in the first order, diffracted light at a specific wavelength determined by the angle of the

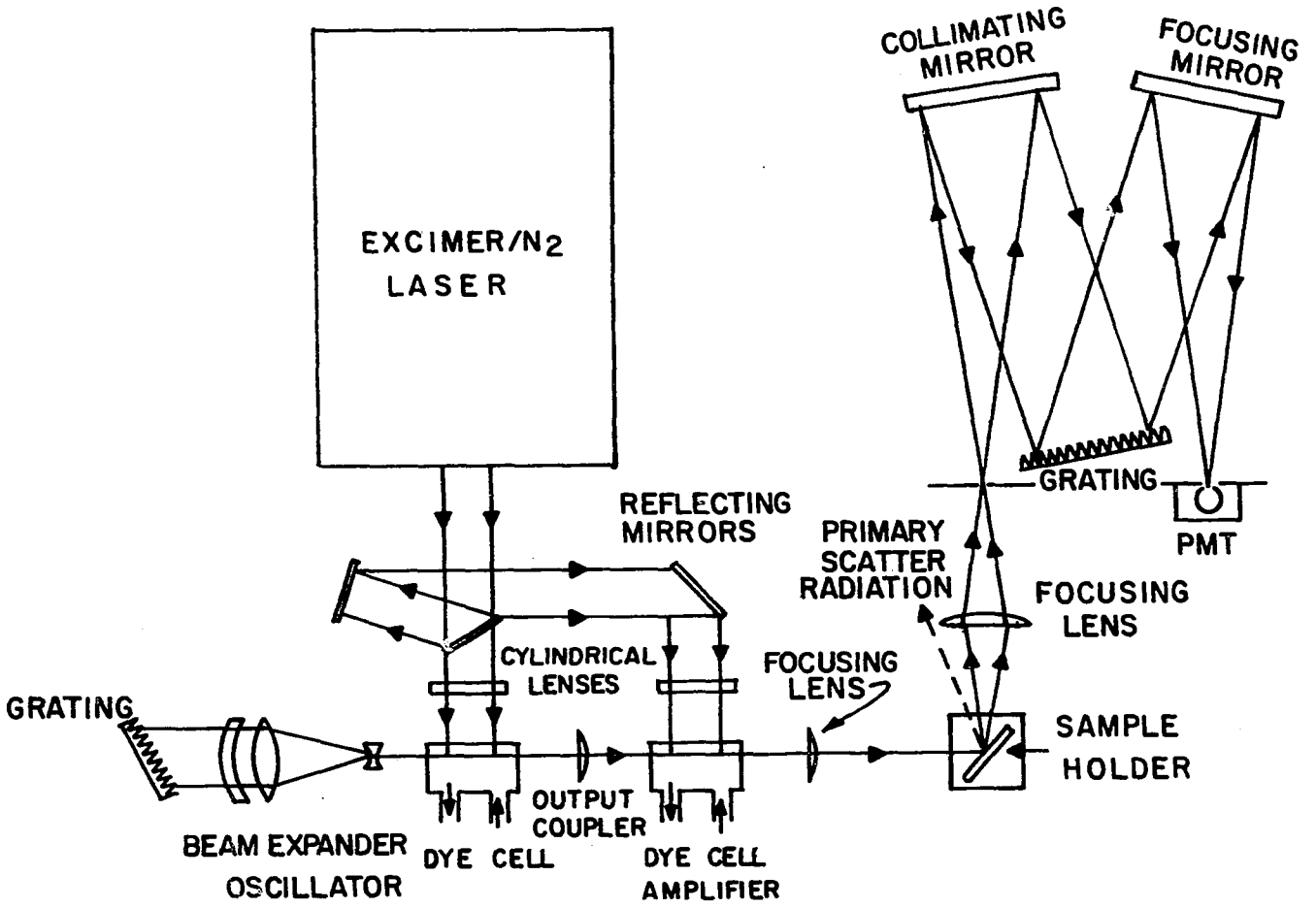

Figure 3. Optical schematic diagram of the LESS system.

grating back through the excited region of the dye cell. Although an etalon could have been placed between the beam expander and the grating to achieve narrower bandwidth, this was not done in our investigation because the laser bandwidth (~1 cm^{-1}) is already narrower than the Shpol'skii bandwidth (~1-10 cm^{-1}). The other end of the oscillator cavity was the output coupler, a f=150 mm plano-convex lens. The plane surface faced the dye cell and served as a 4% feedback mirror. The convex side was used to focus the oscillator beam into the amplifier. The sideways position of the lens can be changed to steer the beam into the amplifier cell.

As shown in Figure 3, the oscillator was pumped only by a portion of the direct pump beam. Approximately 65% of the pump beam radiation was split off by a quartz plate and guided via a 1-1.5 ns optical delay line, comprising two reflecting mirrors (R=98%), into the amplifier dye cell. The optical delay line assured that the amplifier was only pumped when the oscillator emitted the small bandwidth beam instead of the superradiance at the beginning of the pulse.

The output radiation of the dye laser was focused by another f=150 mm plano-convex lens onto the front surface of the solidified sample. The sideways position of the lens can also be changed to steer the laser beam to a point at the sample surface so that the luminescence axis is in correct alignment with the optical axis of the monochromator. The excited luminescence was focused by a 100 mm focal length, 76.2 mm diameter plano-convex, fused silica lens onto the entrance slit of the

monochromator. This lens was positioned at twice the focal length from the entrance slit and sample surface center with the emission axis perpendicular to the exciting laser beam. To avoid collecting the laser radiation scattered off the sample holders optical window surfaces by the luminescence focusing lens, the sample holder was so positioned that the angle between the sample face and the laser beam in the horizontal plane was about 55^{o}.

The monochromator was a f/8.6, 0.5-m focal length equipped with a plane grating having reciprocal linear dispersion of 1.6 nm/mm in the first order.

In the later phase of this study, a 0.64-meter Czerny-Turner monochromator (Figure 3) was utilized to disperse the luminescence. This f/5.7 monochromator was equipped with a 110 X 110 mm, plane holographic grating having 1200 groove/mm and a reciprocal linear dispersion of 1 nm/mm. In any event, both spectrometers were usually operated at a spectral bandpass of 0.1 nm. All of the optical components shown in Figure 3 were securely mounted on an optical table obtained from Newport Research Corporation, Fountain Valley, CA.

Sample Holder, Vacuum Sample Chamber and Refrigeration

The sample holder used in this study is sketched in Figure 4. The body of the sample holder was made of oxygen-free high conductivity copper. A fused quartz disc was used as the optical window, sealed to

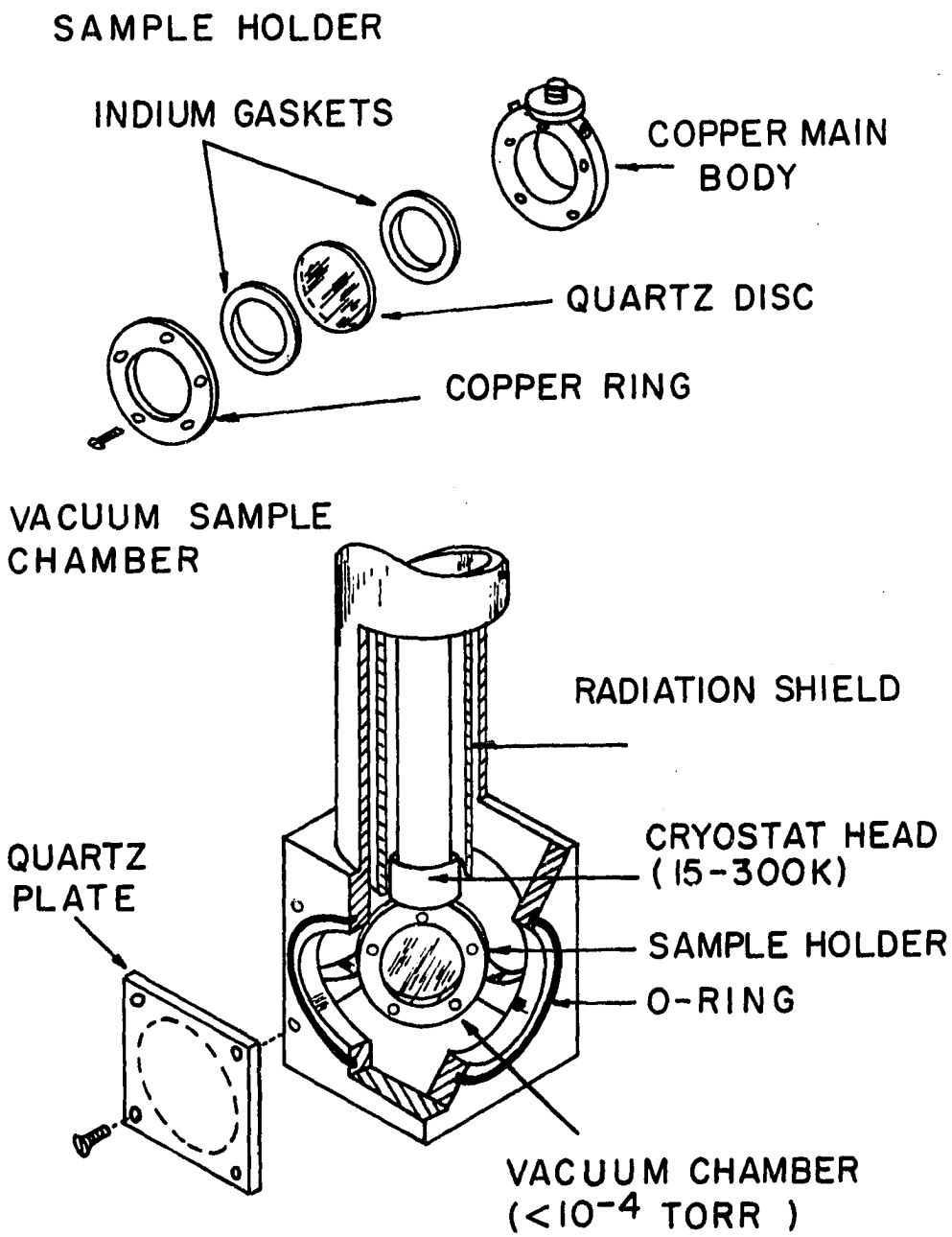

Figure 4. Sample holder (top) and vacuum sample chamber (bottom) used with the LESS system.

the holder main body with indium gaskets and copper retaining ring. The sample solution, ~0.7 mL, was injected into the holder with syringe through one of the filling ports. The holder was mounted in thermal contact with the cryostat head through an indium washer.

The cryostat head along with the sample holder was inserted into the sample vacuum chamber from the top as shown in Figure 4. The stainless steel vacuum chamber, securely mounted on the optical table, had four 1-3/8-in diameter viewing ports, each being at 90^{o} and sealed with a O-ring and a square quartz plate. A radiation shield was placed between the cryostat head and the chamber walls to minimize radiation contact with the cryostat cold surface. Thermal isolation of the sample was achieved by evacuation of the sample chamber via a 2-in diameter diffusion pump in series with a mechanical pump.

The cryogenic system was a water cooled, closed-cycle helium refrigerator that provided sample temperatures between 15 to 300 K. Thus, this system was capable of examining the spectra of solids, either frozen or vapor-deposited, and liquids, as well as gases. Figure 5 shows the fluorescence intensity and spectral half-bandwidth dependences on temperature of a B[a]p/n-octane (50 ppb) frozen solution. These data were obtained with a monochromator bandpass of 0.1 nm. It is seen in this figure that the observed spectral bandwidth is decreased with decreasing temperature, and the fluorescence intensity dependence exhibits the reverse trend. All of the samples in this study were examined at 15 K for optimum selectivity and sensititity.

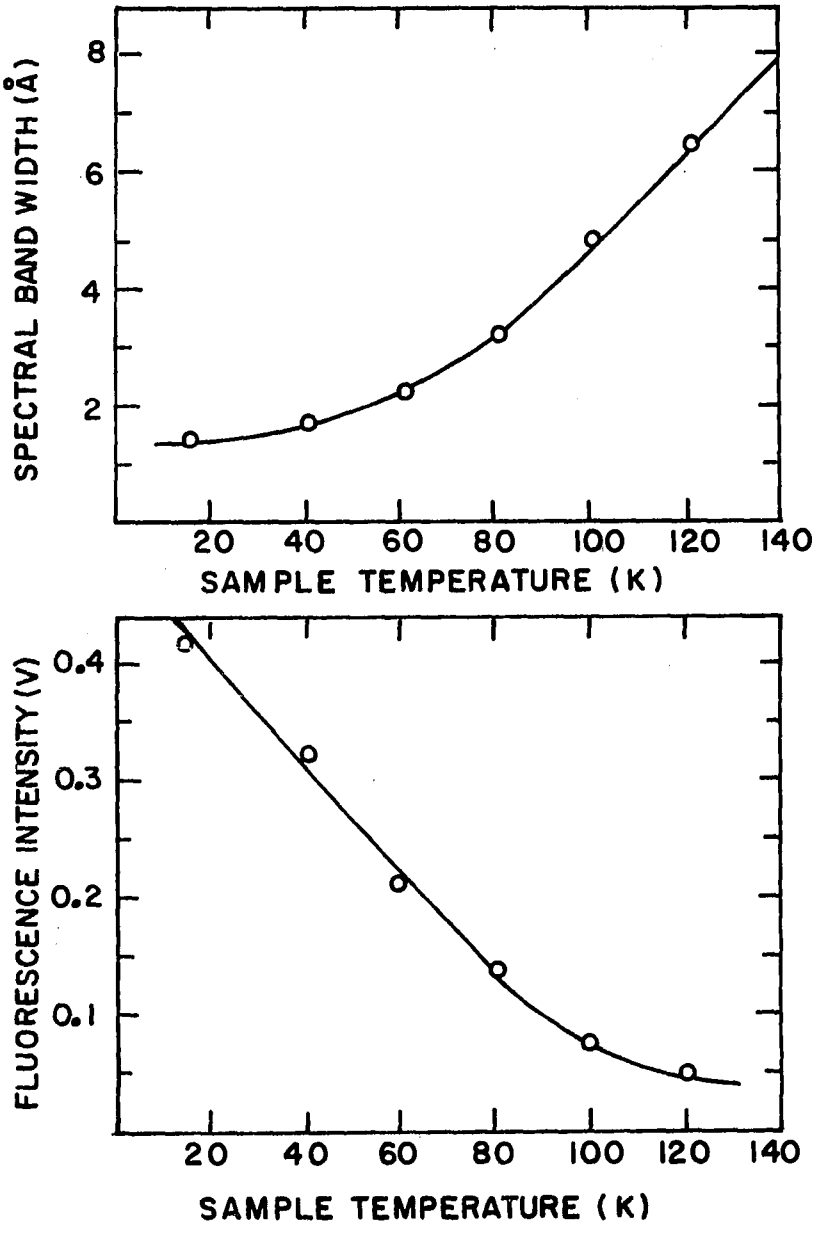

Figure 5. Fluorescence spectral half-width (top) and fluorescence intensity (bottom) dependences on temperature for benzo[a]pyrene in n-octane.

Detector

A side-on Hamanatsu photomultiplier tube (S-20 response) operated at 1100 V was employed as the detector. The function of the PMT was to detect the PAH fluorescence decay signal on the nanosecond time scale. Because conventional PMT wiring, e.g. flat voltage divider using resistors, distorts fast (high speed) optical signal information at the output and is unable to deliver sufficient charges to the dynodes to maintain linearity at high light level, the PMT base wiring was rebuilt as recommended by Lytle (86). A schematic diagram of the base wiring is shown in Figure 6. This wiring is designed around the squirrel-type PMT with dynode 2, 4, 6, and 8 located at the center and dynode 1, 3, 5, 7, and 9 at the outside. Because the electrons emitted from an inside dynode experience an acceleration from the electric field of the adjacent n+2 inside dynode, the voltage drop required between an inside dynode and an outside dynode is always less than in the reverse case. Thus, the 1100-V high voltage was distributed unevenly among dynodes by different resistances as depicted in Figure 6. The greatest potential was applied between dynode 8 and 9 where the current density was largest. Only moderate potential was required between dynode 9 and the wire mesh anode because of the excellent collection geometry and the repulsive field from dynode 8. The total dynode chain resistance, ~1000 kΩ, was chosen so that the resulting dynode current, ~1 mA, is amenable to the high voltage power supply output current requirement.

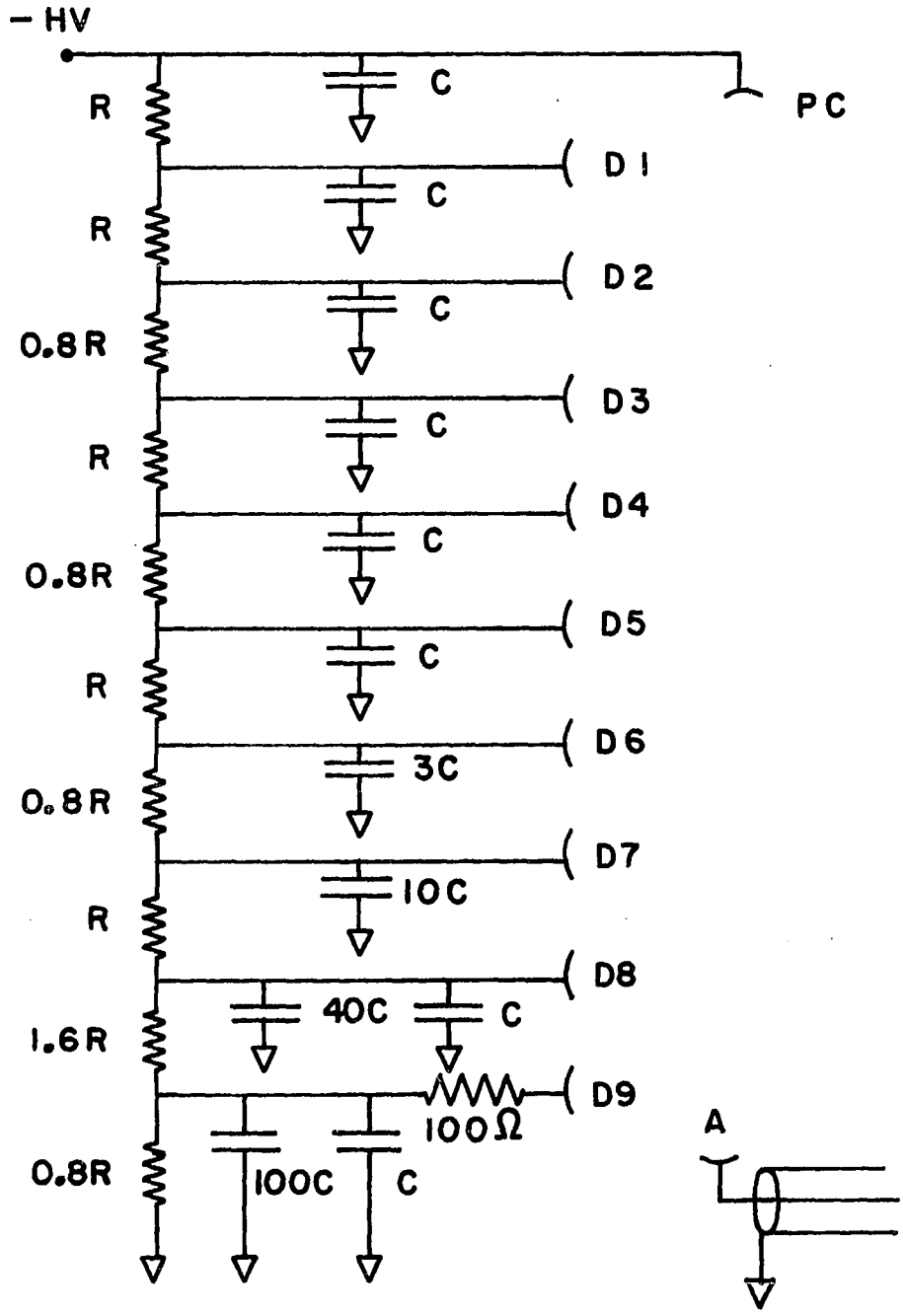

Figure 6. Wiring diagram of photomultiplier dynode chain. R=100 kΩ, C=1 nf.

To deliver the electrical charges for high peak current operation and to attain fast risetime, charging capacitors were placed at each dynode to behave as power supply as shown in Figure 6. The choice of the magnitude of capacitor was based upon three criteria:

a. The total charge stored in the capacitor should be at least ten times that used to avoid significant change in the interstage potential and to keep linearity in the output current vs. optical signal curve. For a fast output current signal of 100 mA, 1 μs wide square pulse (note that this should be the most stringent expected condition, since the maximum allowable input current for the boxcar integrator is 100 mA and the PAH decay time is usually much less than 1 μs), the charge acquired from the last dynode capacitor is 100 mA X 1 μs = 1 X 10^{-7} coulombs. The charge stored in the last dynode capacitor (100 nf) is 1 mA (dynode chain current) X 80 kΩ X 100 nf = 8 X 10^{-6} coulombs, which is more than ten times the charges required at the output;

b. There should be sufficient recharge time for all the capacitors before the next optical pulse reaches the photocathode. The recharge time is determined by the amount of charge needed in all of the capacitors and the dynode chain current. With a safety margin, the charge required to recharge all the capacitors can be estimated to be twice that needed in the largest capacitor, i.e. 2 X 10^{-7} coulombs. Thus, the recharge time would be 2 X 10^{-7} coulombs/1 mA = 0.2 ms. For a 50 pps

optical signal (note that the maximum trigger rate of the excimer laser is 30 pps), the period is 1/50 s^{-1}=20 ms, which is sufficiently longer than the recharge time of all the dynode capacitors; and

c. The average anode current should be at least 1/10 of the dynode chain current to keep the anode output linear with light intensity. For a 100 mA, 1 μs wide, and 50 pps output pulse train, the average anode current is 100 mA X 1 μs X 50 s^{-1}=5 μA, which is sufficient smaller than the dynode chain current (1 mA).

As can be noted in Figure 6, the capacitance of the capacitor is increased approximately by a factor of three, going from dynode 5 to 9, because more charges are needed as one proceeds down the dynode chain. The 1-nf capacitors used at dynode 8 and 9 serve as decoupling capacitors to preserve the frequency response characteristic associated with the 50 Ω transmission line (a coaxial cable) used at the anode. The 100 Ω resistor in series with dynode 9 serves as a damping resistor to control the instantaneous voltage swing and reduce ringing.

Signal Processing

The output of the PMT was processed with a boxcar integrator. Because the boxcar requires voltage input, an input impedance of 50 Ω was selected for current-to-voltage conversion. Such a low impedence is mandatory in order to attain fast response time. The voltage across

the input load resistor was then applied to a gain-of-one differential amplifier which in turn drove the gated integrator as shown in Figure 7. The gate was synchronized with the laser pulse through a pulse generator of the pump laser. The trigger pulse controlled the firing of the laser and activated the gate delay range circuit to allow entry of the sample input signal. Because of the gating action, the integrator only "saw" the signal for a selected aperture duration (or gate width) after each trigger. The combination of variable gate width and delay enabled discrimination between fluorescence lines with different decay rates. The timing relationship among trigger pulse, gate delay, gate width and optical signal during one trigger period is depicted in Figure 8. The boxcar had a variable gate width of 2 ns to 5 ms and a delay up to 50 ms.

As noted in Figure 7, two operation modes could be selected. If the boxcar was operated in the linear integration mode, i.e. the feedback circuit was open, the whole circuit functioned as a true integrator, and the output increased by the same amount with each repetition of the input until output overload occurred. If the boxcar was operated in the exponential averaging mode, i.e. the feedback circuit was closed, the whole circuit was equivalent to a simple RC charging circuit, that is, the output approached the input signal level exponentially in five selected RC time constants. The term "integrator" in this operation, as often used, is somewhat misleading. "Averager" would be a more appropriate name because the output is proportional to the average value of the input signal over the gate width. Once the

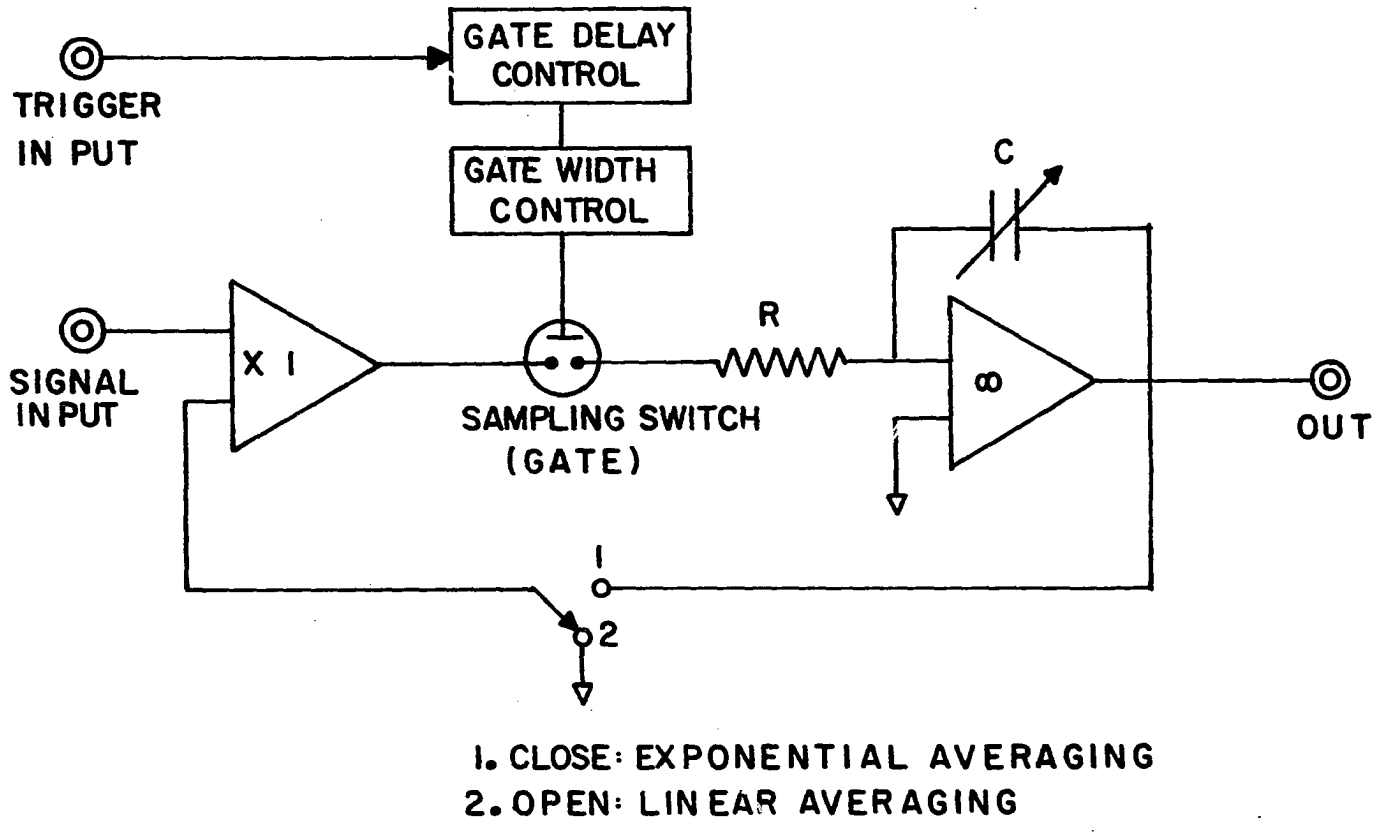

Figure 7. Simplified circuit diagram of the boxcar integrator.

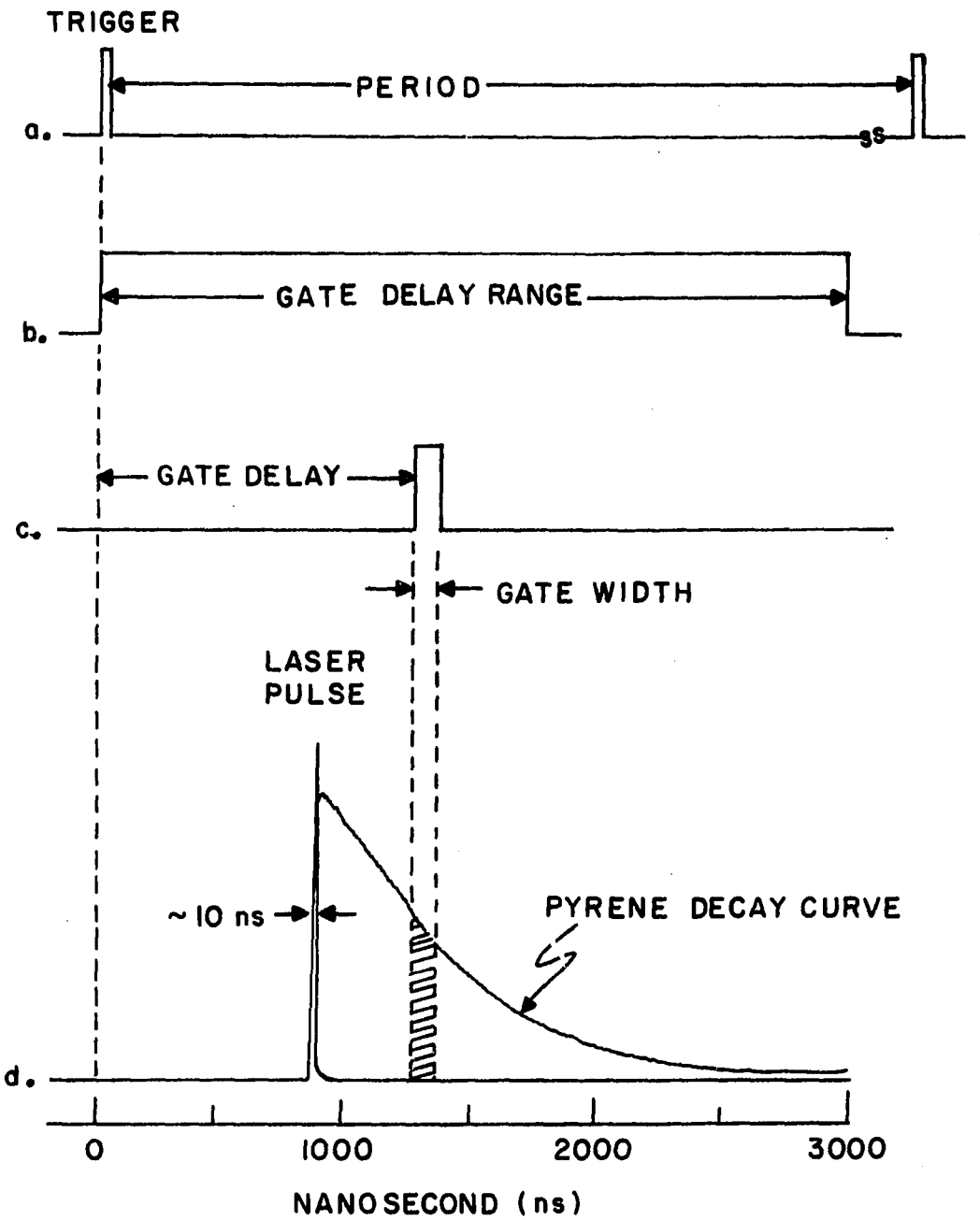

Figure 8. Timing relationship among trigger pulse, gate delay, gate width and optical signal during one trigger period.

output reaches the input level, there is no further change in the output level regardless how many repetitions occur. Since the output can reach a steady-state and exhibit a simple linear relation with the input in the exponential averaging mode, this mode was used in scan operations.

In scan operations two modes were feasible. If the gate was scanned across the input fluorescence decay signal at a fixed monochromator wavelength, the synchonous nanosecond decay profile was reproduced at the output at the scan rate. This mode of operation is illustrated in Figure 8(D), which shows the recorder tracings of the excitation laser pulse (λem=363.4 nm) and fluorescence decay curve of pyrene in n-heptane (λem=372.0 nm) obtained by scanning a two-ns gate. If the gate was fixed at a certain point of the input fluorescence decay signal, that is, at a fixed gate delay, and the output recorded as a function of wavelength, a time-resolved fluorescence spectrum could be obtained, as illustrated in Figure 9 for pyrene in n-heptane. In Figure 9(A), the gate was opened immediately after the laser pulse. At this setting the fluorescence of pyrene (decay time, 450 ns), anthracene (10 ns) and benzo[e]pyrene (100 ns) were all detected in the wavelength scan, and the spectral interferences are plainly evident in this case. If the gate delay was set at 400 ns after the laser pulse, as in Figure 9(B), the time-resolved fluorescence spectrum of pyrene resulted, and no emissions of anthracene and benzo[e]pyrene were detected, because the excited molecules of both anthracene and benzo[e]pyrene were deactivated 400 ns after excitation. A comparison of Figure 9(A)

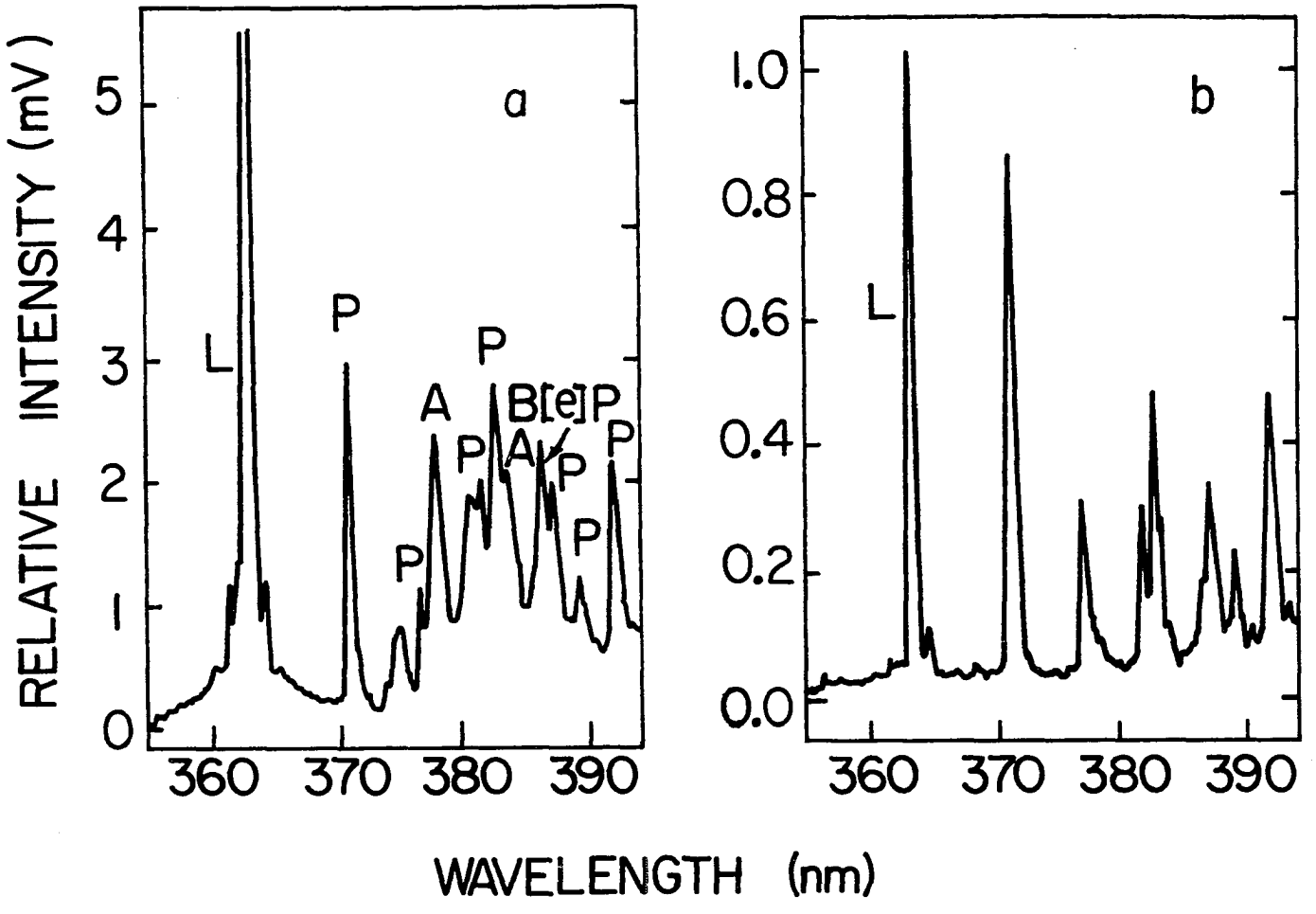

Figure 9. Time-resolved fluorescence spectra of a pyrene (P), anthracene (A), and benzo[e]pyrene (B[e]P) mixture, obtained at two different gate delays, (a) 10 ns and (b) 400 ns. λ_{ex}=363.3 nm, L=scattered laser pulse.

and 9(B) clearly reveals that time resolution can enhance selectivity, but at the expense of sensitivity. It was not a common practice to impose time-resolution technique in the present study, because spectral selectivity could usually be obtained via selective excitation.

Signal-to-Noise Improvement and Scan Rate Considerations

In addition to the gate width and delay variables, the selected RC time constant is another important experimental parameter. The time constant determines both the signal-to-noise improvement ratio and analysis time (87). As noted earlier, the time required for the boxcar output to reach its final level is five times the RC constant in the exponential averaging mode. During this 5 RC period, the number of signal repetitions sampled is 5 N, where N=time constant/gate width. The signal-to-noise improvement ratio (SNIR) is equal to the square root of the number of repetitions, assuming a white noise background. Because each repetition signal is not equally weighted in the exponential averaging mode, e.g. the output reaches 63% of its final steady-state level during the first time constant period. The signal-to-noise improvement ratio is hence given by:

$$\text{SNIR} = (2\ N)^{\frac{1}{2}} \quad \text{and} \quad N = \frac{\text{time constant}}{\text{gate width}} \qquad \text{(a)}$$

providing at least 5 N signal repetitions have occurred (88).

Although the time required for the output to reach its final level is 5 RC, the real time or the observed time constant (OTC) differs from the selected time constant by one over the duty factor because of the gating action:

$$OTC = \frac{\text{time constant}}{\text{duty factor}}$$

where duty factor is equal to the gate width times repetition rate. Thus, in real time the boxcar response time would be 5 X OTC. Thus, in a scan operation, the resolution achievable depends on the scan rate. The minimum scan rate (MIS) in a wavelength scan operation is given by the resolution element ($\Delta\lambda$) of the monochromator divided by five times the observed time constant, e.g.

$$MSR = \frac{\Delta\lambda}{5 \cdot OTC}$$

where $\Delta\lambda$=reciprocal linear dispersion X slit width. In addition to the selected time constant, the boxcar also has a signal processing time constant (SPTC) associated with an active low pass filter at the output for additional signal smoothing. Thus, the effective time constant (ETC) (88) is given by

$$ETC = \{(OTC)^2 + (SPTC)^2\}^{\frac{1}{2}}$$

and the actual minimum scan rate would be

$$MSR = \frac{\Delta\lambda}{5 \cdot ETC} \qquad (b)$$

Equations (a) and (b) show that both the time constant and gate width selected affect the SNIR and MSR. A longer time constant, or a narrower gate width would increase the signal-to-noise improvement ratio at the expense of analysis time. Therefore, the time constant should not be longer and the gate width should not be shorter than is required to reduce the noise to an acceptable level. Typical experimental conditions for boxcar integration based on both SNIR and MSR considerations are listed in Table 3. All of the experiments performed in present work employed the exponential averaging mode and wavelength scan operation.

Table III. Experimental parameters of boxcar averager

Scan rate	50 Å/min	10 Å/min
Time constant	1 s	10 s
SPTC	0.1 s	0.1 s
Gate width	100 ns	100 ns
Gate delay	0-300 ns	0-300 ns
Repetition rate	30 or 20 pps	30 or 20 pps
Monochromator bandpass	1 Å	1 Å
SNIR	4.5	14.1

CHAPTER 3. EXPERIMENTAL PROCEDURES

Chemicals, Solvents and Solution Preparations

All of the PAHs used in the LESS study are listed in Table 4. The methylated and multimethylated benz[a]anthracene were donated by Professor M. S. Newman of the Ohio State University. All of the PAHs were used as received without further purification. The n-alkane solvents, hexane, heptane and octane were either of reagent grade and purified by double fractional distillation, or obtained from Aldrich Chemical Co., Inc., Milwaukee, WI (99+% purity).

Stock solutions of the PAHs were prepared in volumetric flasks from weighted quantities of PAHs at 1000 to 100 ppm concentration level. Concentrated stock solutions were prepared to minimize absorption and decomposition effects commonly observed with very diluted solutions. PAHs which dissolved slowly were equilibrated at least three days and agitated every day for several minutes. All stock solutions were stored in the dark to avoid potential photodecomposition. Diluted solutions were prepared from the stock solutions just prior to measurements using standard syringes, volumetric pipets and volumetric flasks. Successive dilutions were utilized to prepare dilute solutions. All glassware was thoroughly washed and rinsed with ethanol and dried with air.

Table IV. Polynuclear aromatic hydrocarbons

PAH	Formula	No. of Rings	Abbreviation	Purity, %	Source
Phenanthrene	$C_{14}H_{10}$	3	Ph	98+	Analabs, North Haven, CT
Anthracene	$C_{14}H_{10}$	3	An	99	Analabs, North Haven, CT
Pyrene	$C_{16}H_{10}$	4	Py	99	Analabs, North Haven, CT
Fluoranthene	$C_{16}H_{10}$	4	FL	99	Analabs, North Haven, CT
Triphenylene	$C_{18}H_{12}$	4	Tri	98	Aldrich Chemical Inc., Milwaukee, WI
Chrysene	$C_{18}H_{12}$	4	Chr	99	Analabs, North Haven, CT
Benz[a]anthracene	$C_{18}H_{12}$	4	B[a]A	99	Analabs, North Haven, CT
Benzo[e]pyrene	$C_{20}H_{12}$	5	B[e]P	99	Analabs, North Haven, CT
Benzo[k]fluoranthene	$C_{20}H_{12}$	5	B[k]F	99.5	Joint Research Centre, Netherland
Perylene	$C_{20}H_{12}$	5	Per	99	Analabs, North Haven, CT
Perylene-d_{12}	$C_{20}D_{12}$	5	Per-d_{12}	97 atom % D	Merck & Co., Inc./Isotopes St. Louis, MO

Benzo[a]pyrene	$C_{20}H_{12}$	5	B[a]P	99+	Aldrich Chemical, Inc. Milwaukee, WI
Benzo[a]pyrene-d_{12}	$C_{20}D_{12}$	5	B[a]P-d_{12}	97 atom % D	Merck & Co., Inc./Isotopes St. Louis, MO
Benzo[ghi]perylene	$C_{22}H_{12}$	6	B[ghi]P	99	Analabs, North Haven, CT
Dibenz[ah]anthracene	$C_{22}H_{14}$	5	DiB[ah]A	97	Aldrich Chemical, Inc. Milwaukee, WI
Coronene	$C_{24}H_{12}$	7	Cor	98	Analabs, North Haven, CT
Alkylated and Multialkylated Benz[a]anthracenes					
2-Methyl-benz[a]-anthracene	$C_{19}H_{14}$	4	2-M-B[a]A	—	Ohio State University
5-Methyl-benz[a]-anthracene	$C_{19}H_{14}$	4	5-M-B[a]A	—	Ohio State University
7-Methyl-benz[a]-anthracene	$C_{19}H_{14}$	4	7-M-B[a]A	—	Ohio State University
9-Methyl-benz[a]-anthracene	$C_{19}H_{14}$	4	9-M-B[a]A	—	Ohio State University
11-Methyl-benz[a]-anthracene	$C_{19}H_{14}$	4	11-M-B[a]A	—	Ohio State University
12-Methyl-benz[a]-anthracene	$C_{19}H_{14}$	4	12-M-B[a]A	—	Ohio State University

Table IV. Continued

PAH	Formula	No. of Rings	Abbreviation	Purity, %	Source
6,8-Dimethyl-benz[a]-anthracene	$C_{20}H_{16}$	4	6,8-DM-B[a]A	—	Ohio State University
7,12-Dimethyl-benz[a]-anthracene	$C_{20}H_{16}$	4	7,12-DM-B a A	—	Ohio State University
5,7,12-Trimethyl-benz[a]anthracene	$C_{21}H_{19}$	4	5,7,12-TM-B[a]A	—	Ohio State University
6,7,8-Trimethyl-benz[a]anthracene	$C_{21}H_{19}$	4	6,7,8-TM-B[a]A	—	Ohio State University
6,8,12-Trimethyl-benz[a]anthracene	$C_{21}H_{19}$	4	6,8,12-TM-B[a]A	—	Ohio State University

Environmental Sample Preparations

The liquid fuel samples analyzed in this work are listed in Table 5.

Table V. Liquid fuel samples

Sample	Number	Source
Syncrude Oil	1106.7	
Synthoil	1202.5	
Mixed Petroleum Crude	5107.2	Oak Ridge National
Coal-Derived Fuel Oil Blend	1701.21	Laboratory,
Shale-Derived Diesel Fuel Marine Product	4610.45	Oak Ridge, TN
Solvent-Refined Coal Liquid (SRC-I) Processing Solvent	—	National Bureau of
SRC-II	—	Standards (NBS),
Shale Oil	—	Washington, D.C.
Wilmington Petroleum Crude Oil	—	

A 0.1-ml portion of the liquid fuel sample was pipetted into a 100 ml volumetric flask and diluted with n-octane solvent to the mark. The resulting solution was agitated using a mechanical shaker at room temperature for at least 10 minutes, and then left unagitated for 2 hours, agitated again for 10 minutes, and then left unagitated for several hours, usually overnight, to allow the trace n-octane-insoluble asphaltenes observed in some sample solutions settle to the bottom of the solution flask. For qualitative analysis, the solution portion of the dilute sample solution was pipetted into volumetric flask for further

dilution prior to spectroscopic investigations. For quantitative determination, the sample was initially spiked with an internal reference compound or standard additions of the analyte of interest prior to dilution. The dilution factor was chosen so that the analyte concentration in the diluted sample would fall within the linear range of its analytical calibration curve (normally, in the parts-per-billion concentration range). Usually, one trial dilution was required because of the uncertainty in the analyte concentration originally present in the sample. In any event, the total dilution factor of the liquid fuel sample usually ranged from 10^3 to 10^4.

Internal Reference and Standard Addition Methods

For quantitative determinations the internal reference principle was adopted to compensate for: (a) any variations of the sample cell position in the optical path; (b) drift in the single beam laser output; (c) possible variations in the inhomogeneity of the front surface of the sample, which may give rise to variable reflectivity; and (d) intermolecular interactions that may occur in samples of widely varying composition. A more detailed description of the internal reference as well as standard addition approach adopted for quantitative analysis is given later in Chapter 4.

Sample Cooling Procedures

Because the site distribution of solute molecules in the various crystallographic sites depends on the cooling rate, a reproducible cooling cycle is essential. Also to reduce analyte aggregate formation, a rapid cooling rate is desirable. Unfortunately, the closed-cycle helium refrigerator was not capable of providing a rapid sample-freezing in a controllable fashion. Normally a sample cooldown time of an hour was required for samples at ambient temperature down to 15 K. A sample cooling procedure was developed to circumvent these problems.

The copper sample holder containing ~0.7 mL sample solution was first immersed in liquid nitrogen. Solidification of sample was visually completed in about 20 seconds. At this stage the frozen sample in its holder was attached to the cold finger of the cryostat, which was at 100 K. The cooling down of the sample from 100 K to 15 K by the helium refrigerator was then completed in 10 minutes. The reproducibility of the cooling rate was confirmed by the reproducibility of the relative intensities in the multiple site spectra of PAHs measured at fixed excitation wavelengths during consecutive running of the same solutions.

Dye Laser Tuning Procedures

The dye laser was initially set up in front of the pump laser so that the pumping beam could be focused into both oscillator and

amplifier dye cells (by adjusting the beam splitter and reflecting mirrors as shown in Figure 3) at the height of the optical axis. The dye laser was then tuned up via the following stepwise procedures (refer to Figure 3):

1. A piece of white cardboard was placed adjacent to the grating to observe the zero order reflected by the grating.
2. The output coupler was blocked and the height position of the oscillator cylindrical focusing lens was changed until the brightest circular image appeared on the cardboard.
3. The output coupler block was removed and the output coupler, which was a plano-convex lens in a swivel mount was adjusted until a distinct diffraction pattern consisting of bright and dark vertical stripes appeared on the cardboard.
4. A piece of white cardboard was placed in front of the output coupler where a laser spot was visible.
5. The grating was turned to one end of the tuning range of the dye until the laser emission started to vanish, and then the height of the cylindrical focusing lens and the tilt of the output coupler were readjusted for improved intensity.
6. The laser was tuned further toward the end of the tuning range and the adjustment in Step 5 was repeated, if an improvement of the output intensity was observed.
7. The grating was turned back to the maximum of the tuning range, and the amplifier pump beam was blocked off.

8. The output coupler was adjusted in the horizontal and vertical planes to steer the laser beam through the amplifier cuvette so that the laser beam appeared almost unobscured.
9. The amplifier pump beam block was removed, and the focus line of the amplifier pump beam was moved up and down by adjusting the focusing lens until it coincided with the oscillator beam transversing the amplifier cuvette.
10. The laser output intensity was maximized by adjusting the output coupler, the height of the pump beam and the tilt of the focus line to obtain the best overlap in the pumped region of the amplifier cuvette.

Excitation and Emission Spectra

The excitation and emission spectra shown in this work have not been corrected for the wavelength dependency of the dye laser output, the spectrometer throughput, and the detector efficiencies. As for the excitation and emission wavelengths utilized, a detailed description of their selection processes is given in the next chapter.

CHAPTER 4. RESULTS AND DISCUSSION

Site Selective Excitation of PAH Luminescence

A typical so called "line-rich" Shpol'skii spectrum of B[a]P in n-heptane is shown in Figure 10A. In the 0-0 region of this spectrum it is easy to distinguish at least four sharp lines which result from four dominantly occupied sites. This spectrum (Figure 10A) can be considered as a superposition of slightly shifted subspectra (Figure 10B, C, D and E) of individual sites (56). As a consequence of the multiplet structures, the Shpol'skii effect spectra are generally quite complex and hence spectral interference has been a problem in the analysis of PAH mixture spectra when broadband excitation sources have been utilized (63,68).

As indicated earlier, the narrow absorption bandwidth (FWHM $10 \leq cm^{-1}$) of PAHs in n-alkane solvents is an unique feature of the Shpol'skii effect. These narrow absorption bandwidths gave us the capability of selectively "tuning in or out" of specific site spectra through utilization of narrow bandwidth, turnable dye laser excitation. Thus, by tuning the laser wavelength to an absorption transition of a specific site, each site was selectively excited as shown in Figure 10B, C, D, and E. The excitation wavelengths used for each site correspond to the same transitions separated only by 3 to 6 Å. It is also seen from this figure that the Shpol'skii spectra are relatively sensitive to excitation wavelengths.

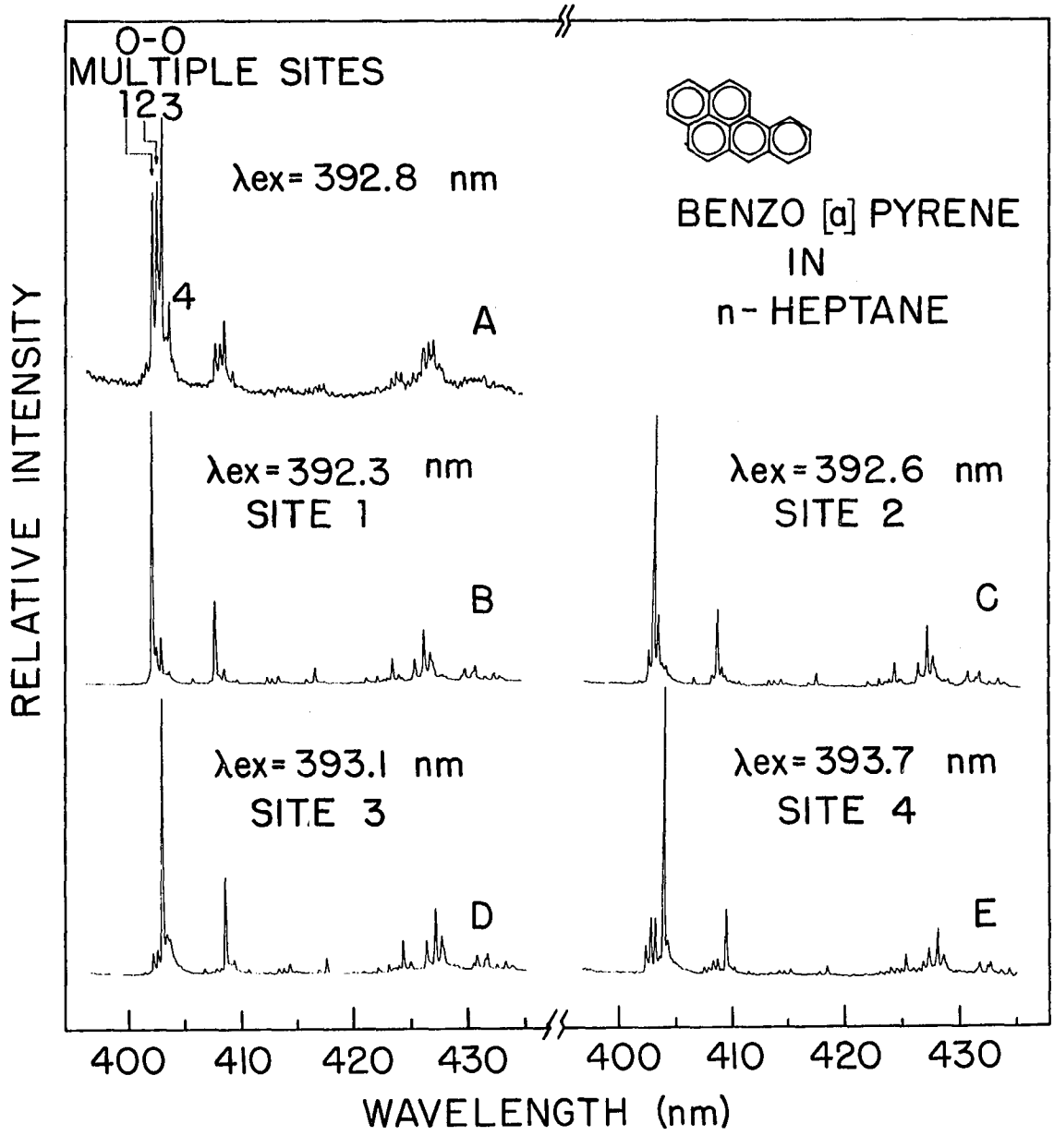

Figure 10. Selectively excited fluorescence spectra of individual sites of benzo[a]pyrene in n-heptane.

To further illustrate the site selection technique in LESS, spectrum A in Figure 11 represents the nonselective excitation at a tuned wavelength of 364.5 nm of 11-M-B[a]A in n-octane. Nonselective excitation at 364.5 nm into the congested region of the upper vibrational manifold of the excited singlet state leads to the emission of spectra of 11-M-B[a]A molecules occupying at least three different lattice sites. The multiple emissions from the 0-0 transitions which occur at 384.8, 385.2 and 386.0 nm, are labelled 1, 2, and 3 in Figure 11A. If the monochromator is peaked on 384.8 nm while the tunable dye laser output is scanned through the intervals shown for spectrum B, the excitation spectrum of molecules occupying site 1 may be obtained. The resulting spectrum (Figure 11B) clearly shows that the best wavelength to excite the fluorescence emission from site 1 molecules is 374.7 nm, i.e. at the wavelength of the most intense peak in Figure 11B. If the laser radiation is now tuned to 374.7 nm, the spectrum of site 1 molecules as shown in Figure 11B' may be recorded. In an analogous fashion, the best laser wavelengths for exciting site 2 and 3 molecules were determined to be 375.1 and 375.8 nm respectively (the most intense peaks in Figure 11C and 11D). The resulting fluorescence spectra from these sites are shown in Figure 11C' and 11D'. The identical appearances (except the wavelengths being shifted with respect to one another) of the excitation spectra as well as the emission spectra in Figure 11 explain the fact that the PAH molecules in each site act as independent absorbers and emitters. It should be noted that the relative intensities of the 0-0 multiplets shown in Figure 10A and 11A do not indicate the

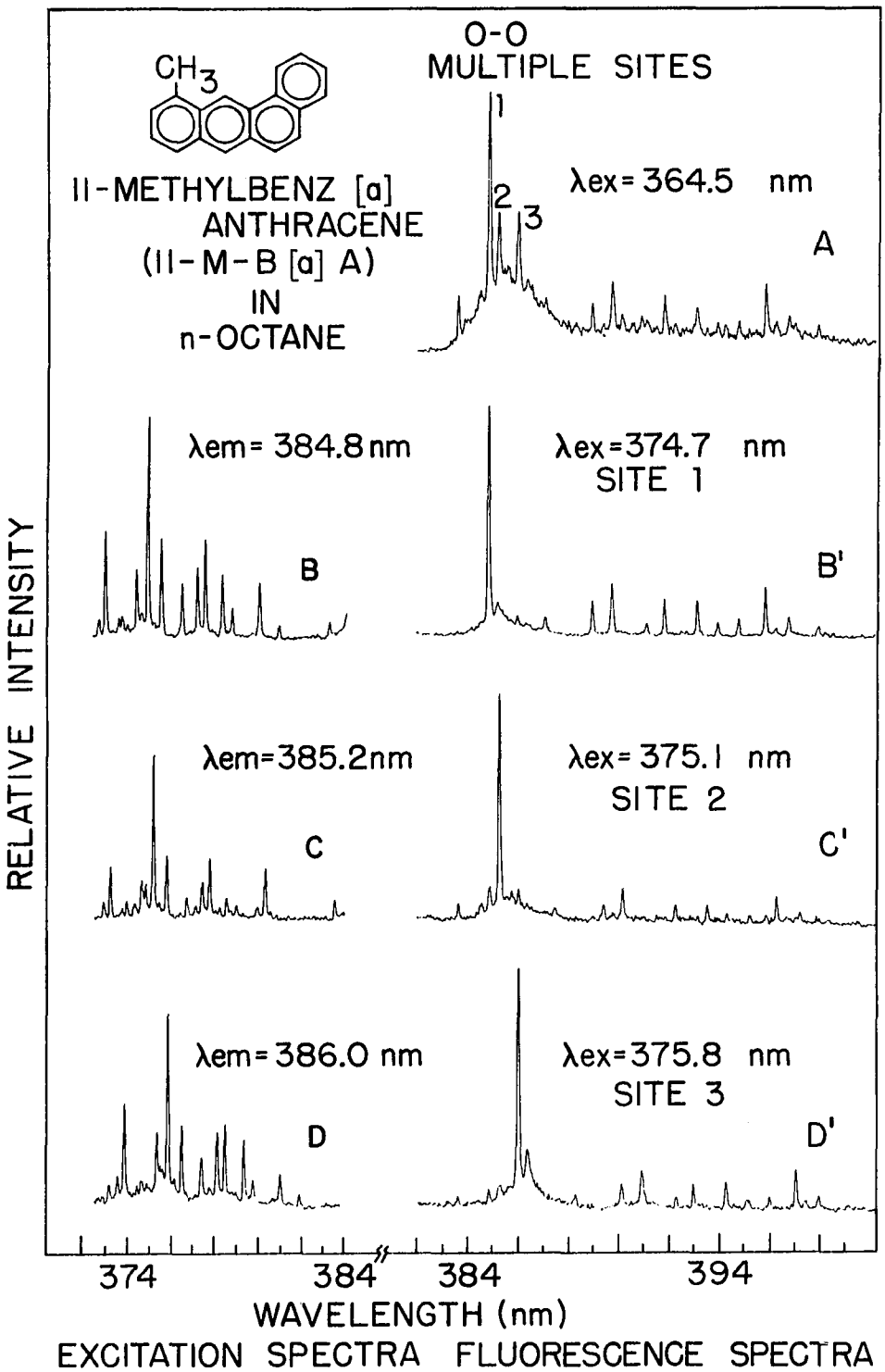

Figure 11. Selectively excited fluorescence spectra of individual sites of 11-methylbenz[a]anthracene in n-octane.

relative site concentrations, unless the molecules in all the sites are evenly excited with a broadband light source.

The capability of exciting these site specific spectra not only enhances specificity but also provides added flexibility in the event that spectral interferences by other sample constituents invalidates the use of one site specific line. Should such interferences occur, other interference-free, site specific lines may usually be selected.

Observed Luminescence Spectra of PAHs

Based on the site specific excitation technique discussed above, the luminescence spectra of some 15 selected PAHs were recorded in n-octane at 15 K, as shown in Figure 12A to 12P. The specific site that gave the most intense luminescence was selected for excitation of these PAH emissions. The excitation wavelengths (λex), as can be noted in the figure captions were selected from the corresponding excitation spectra over the 360-435 nm spectral region that exhibited the optimum resolution and intensity. It should be noted, however, that these excitation wavelengths may differ from those selected in a real analytical situation. In multicomponent samples, overlaps of absorption bands might necessitate use of another excitation wavelength for a particular compound.

The wavelength assignments made for the principal emission maxima of pyrene, benzo[e]pyrene, benz[a]anthracene, dibenz[a,h]anthracene,

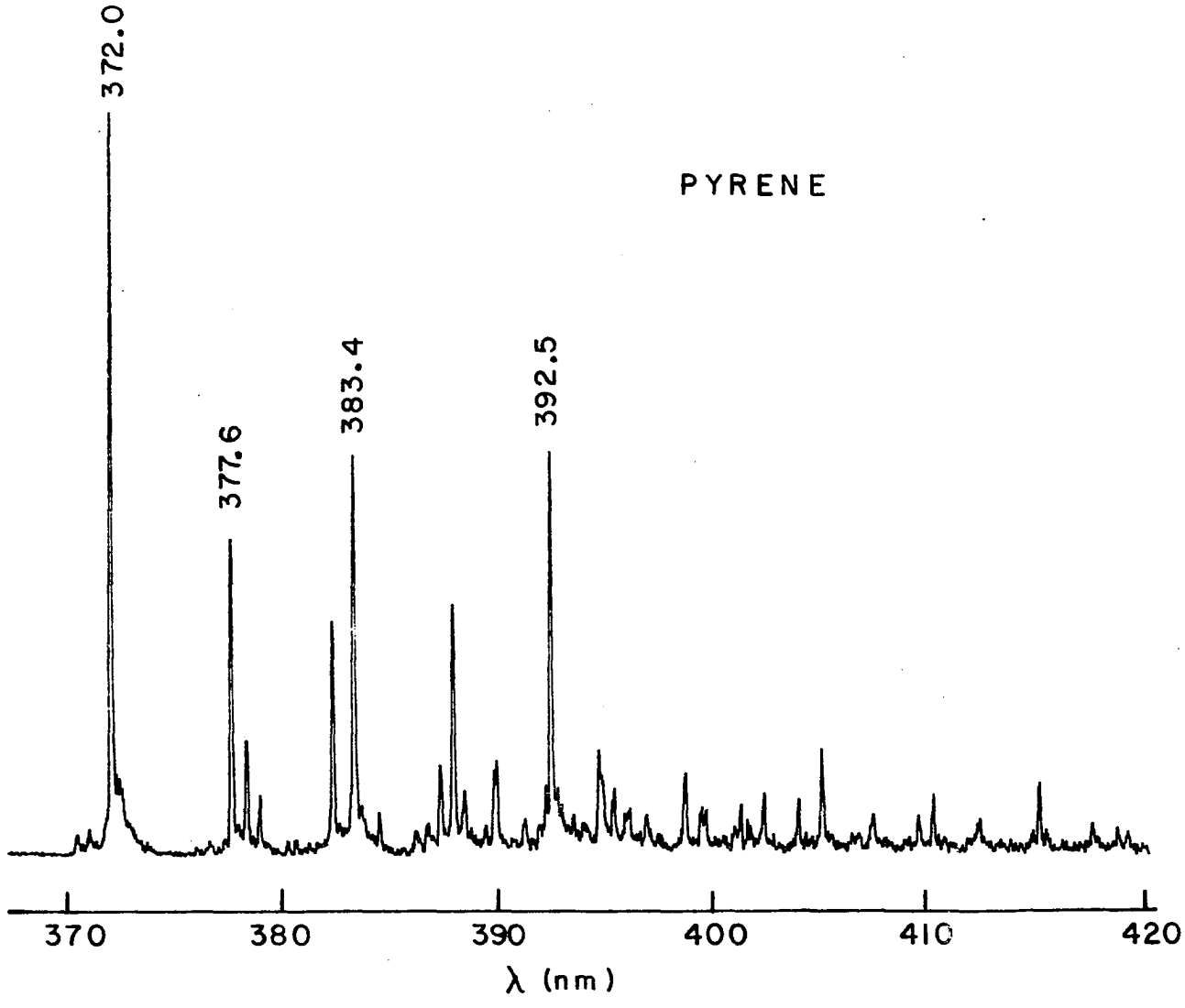

Figure 12A. LES spectrum of pyrene in n-octane. λ_{ex}=363.3 nm.

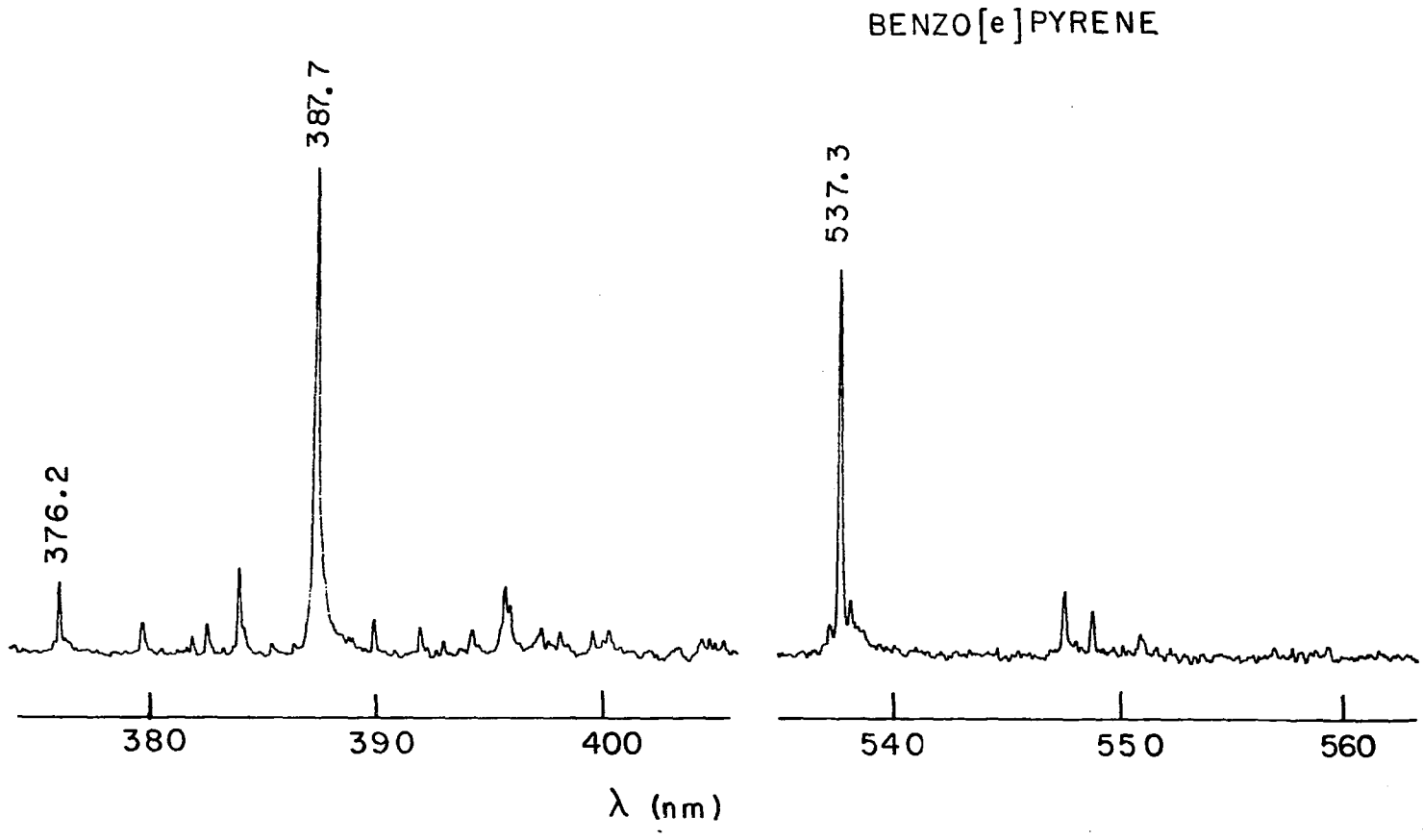

Figure 12B. LES fluorescence (left) and phosphorescence (right, 10 ms gate delay) spectra of benzo[e]pyrene in n-octane. λ_{ex}=365.6 nm.

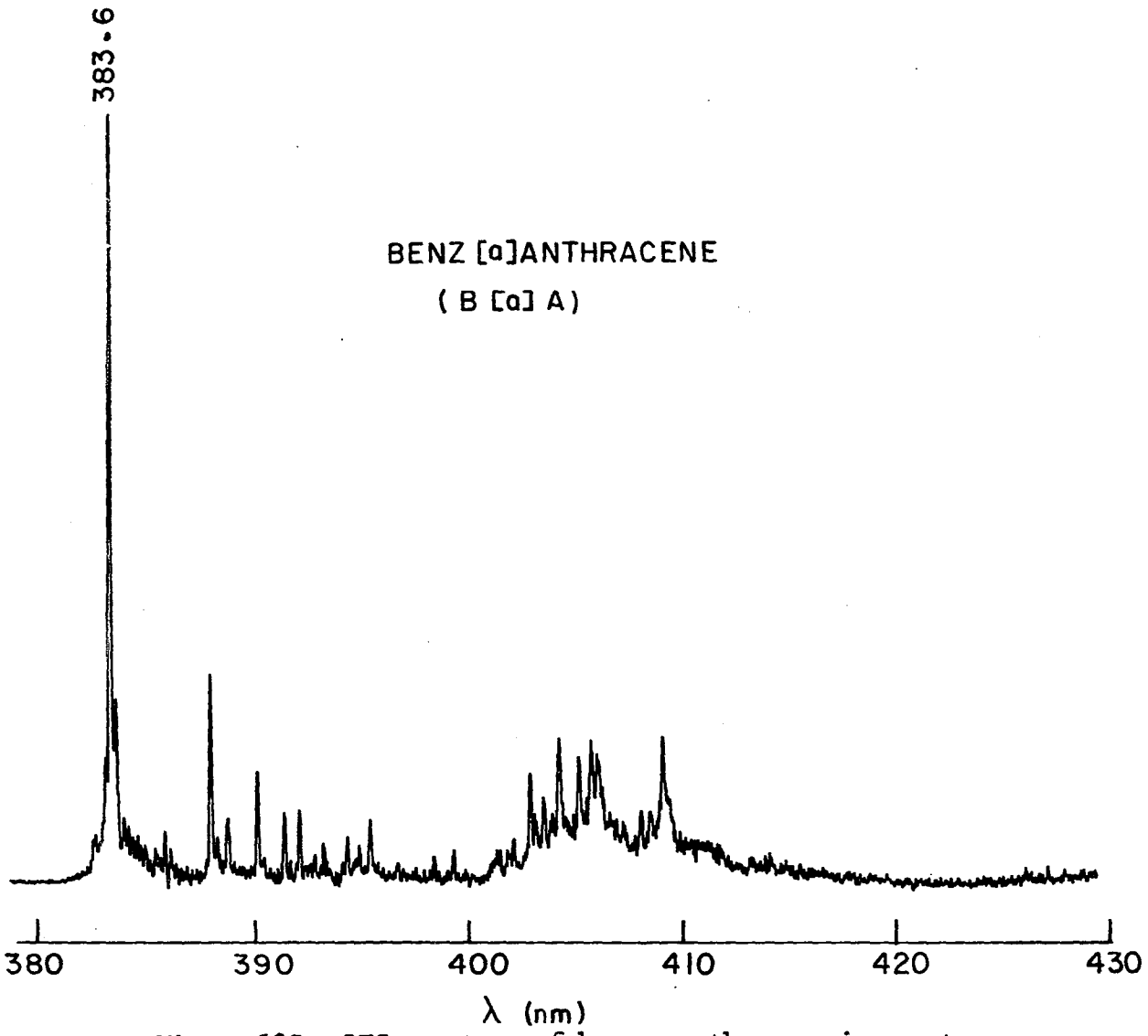

Figure 12C. LES spectrum of benz[a]anthracene in n-octane. λ_{ex}=376.9 nm.

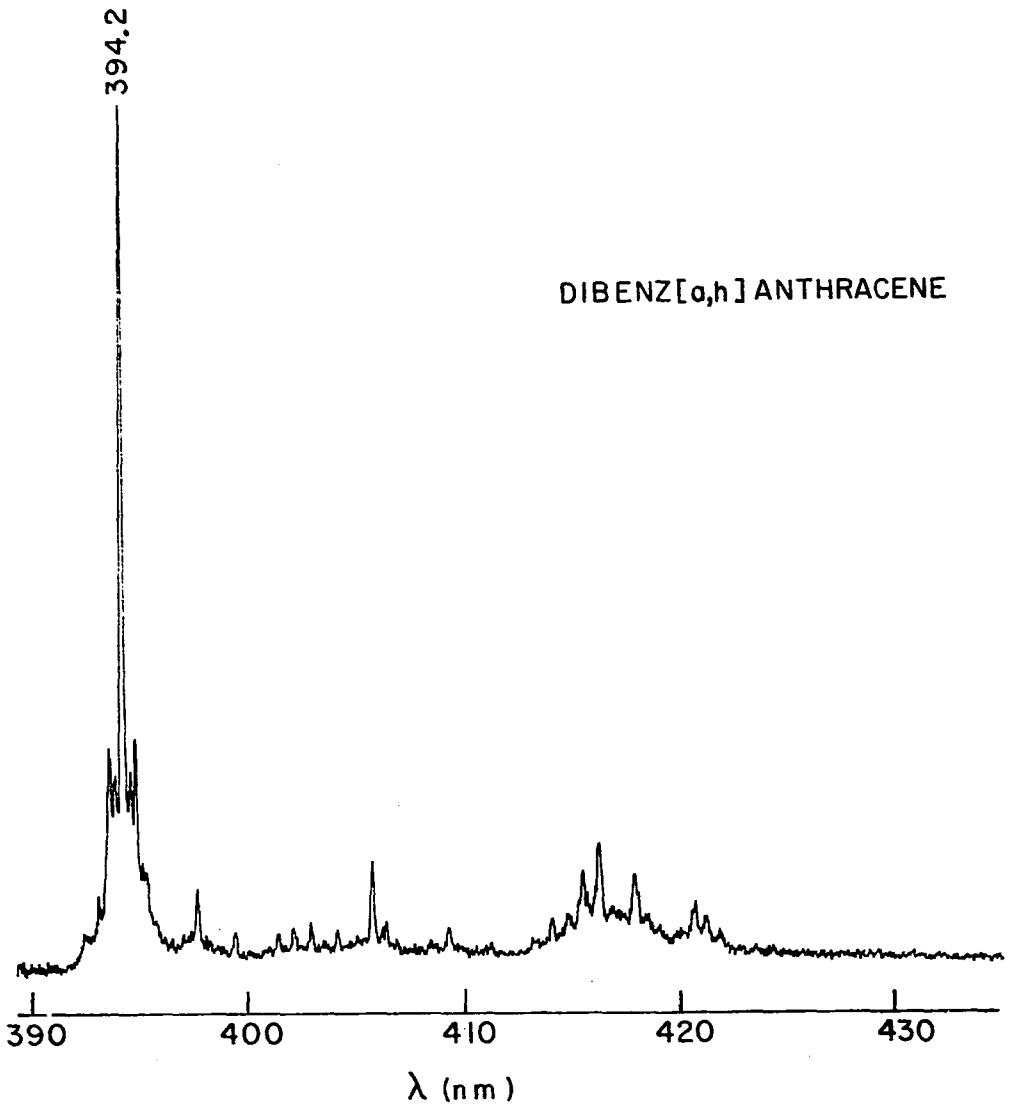

Figure 12D. LES spectrum of dibenz[a,h]anthracene in n-octane. λ_{ex}=373.6 nm.

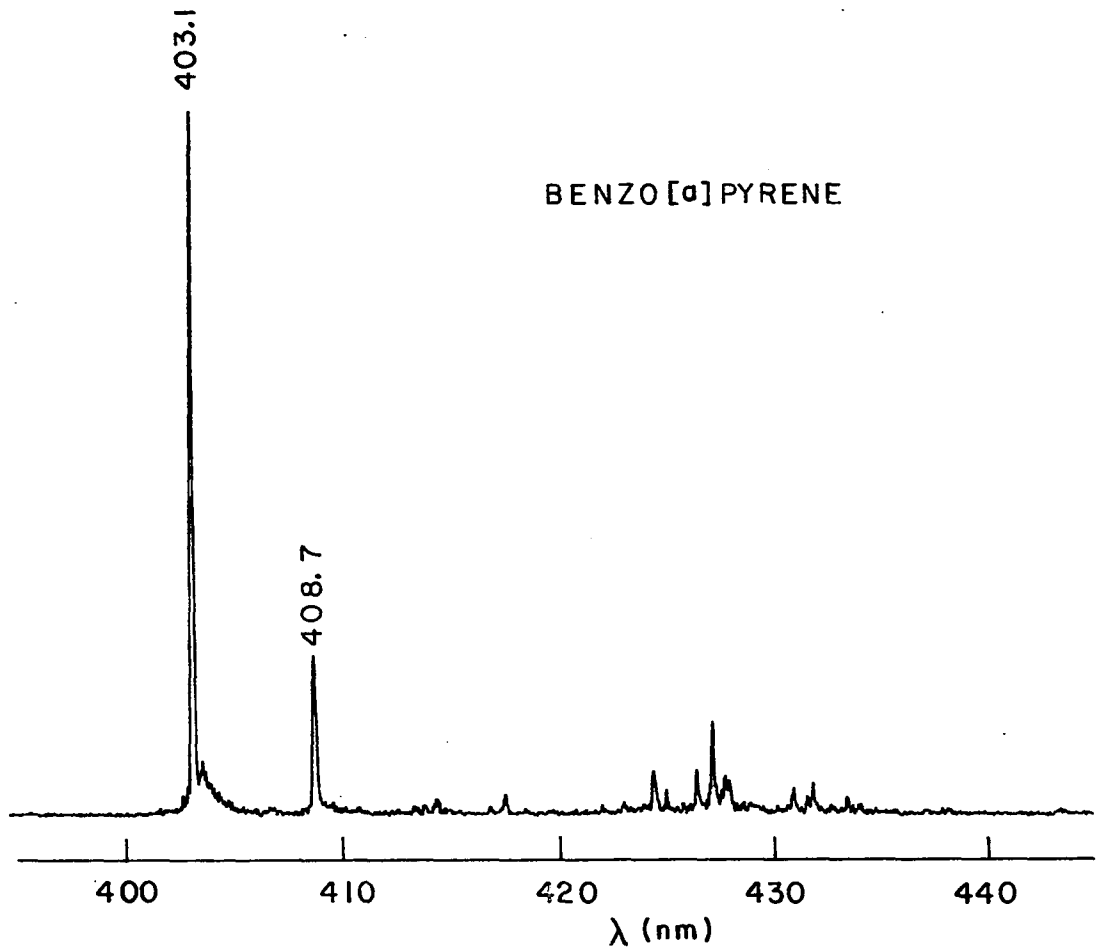

Figure 12E. LES spectrum of benzo[a]pyrene in n-octane. λ_{ex}=380.2 nm.

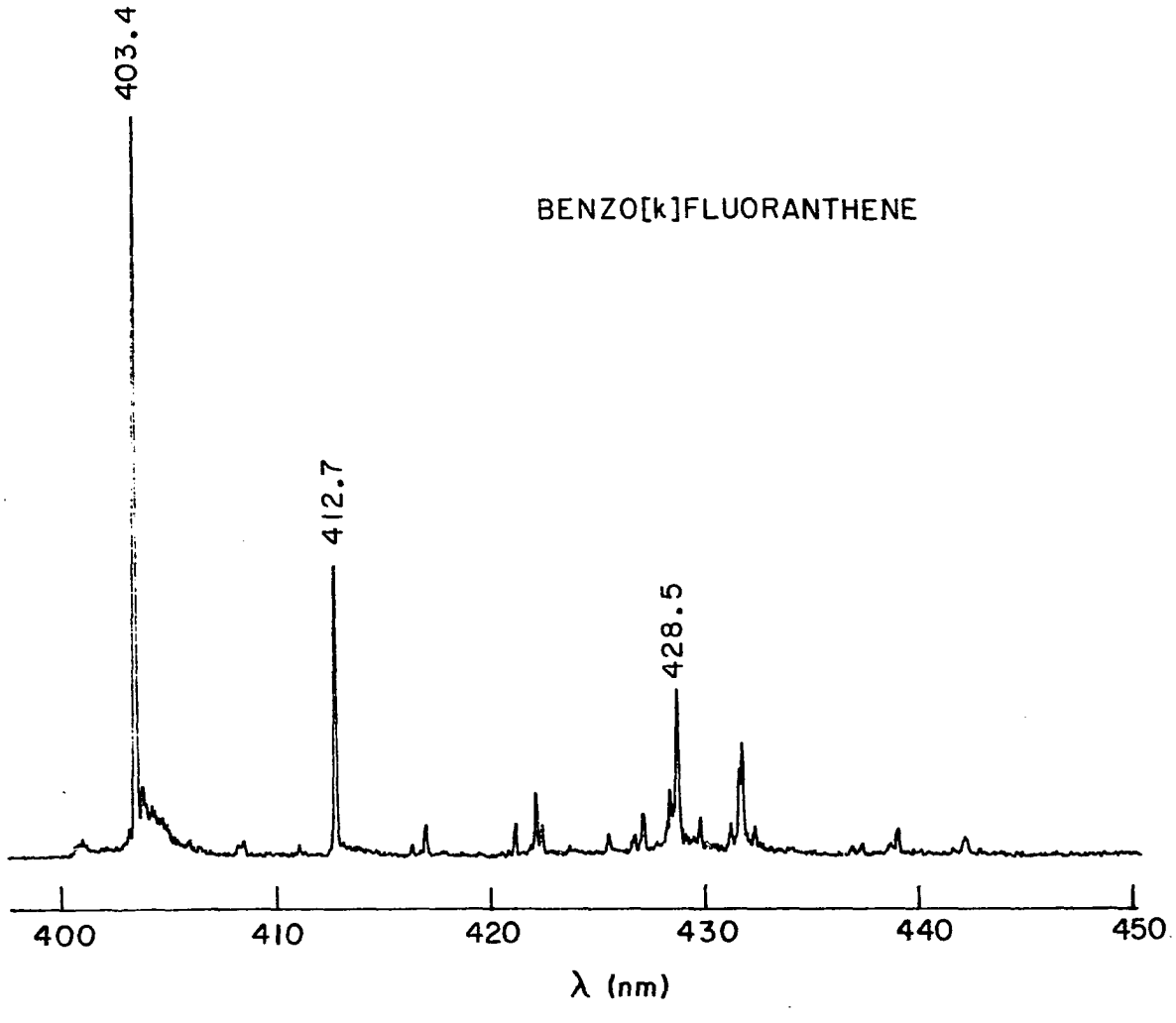

Figure 12F. LES spectrum of benzo[k]fluoranthene in n-octane. λ_{ex}=378.9 nm.

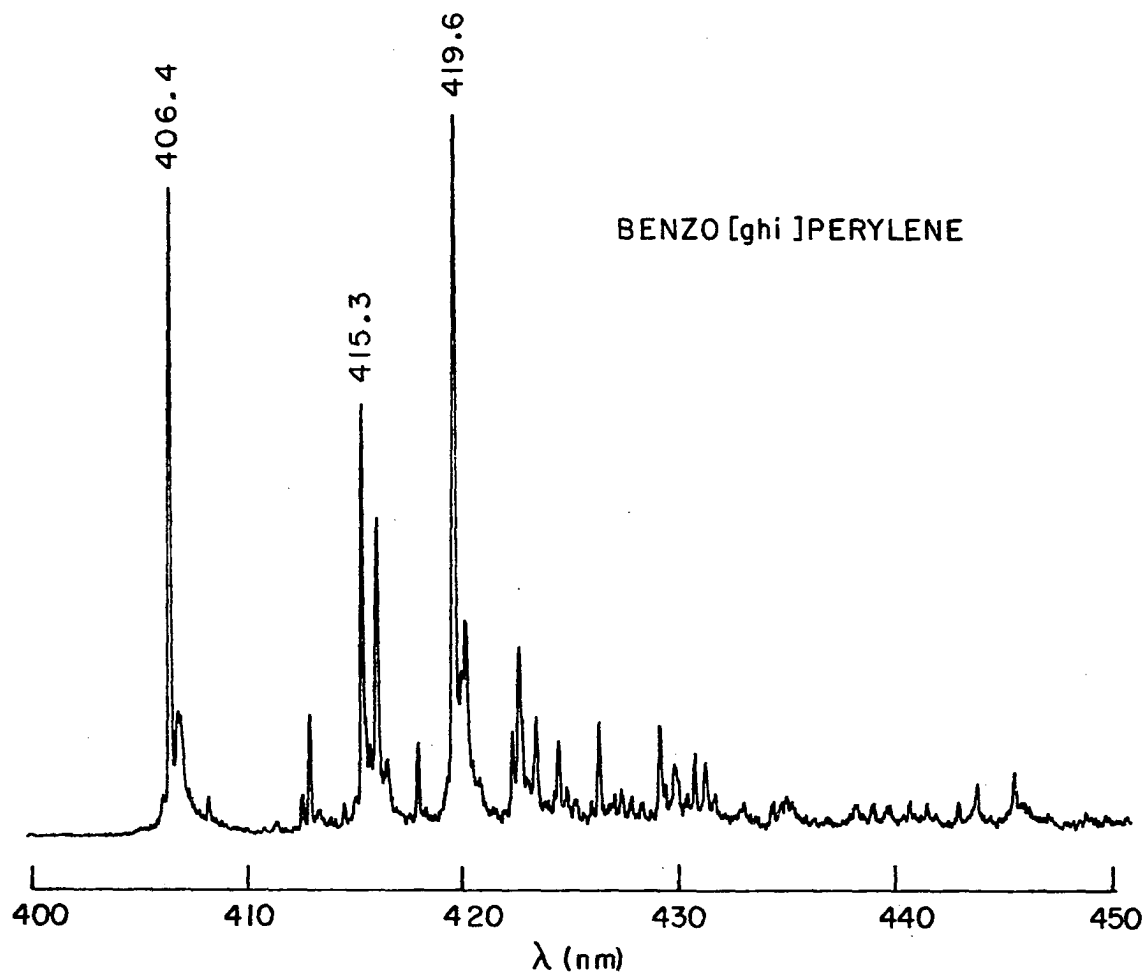

Figure 12G. LES spectrum of benzo[ghi]perylene in n-octane. λ_{ex}=365.8 nm.

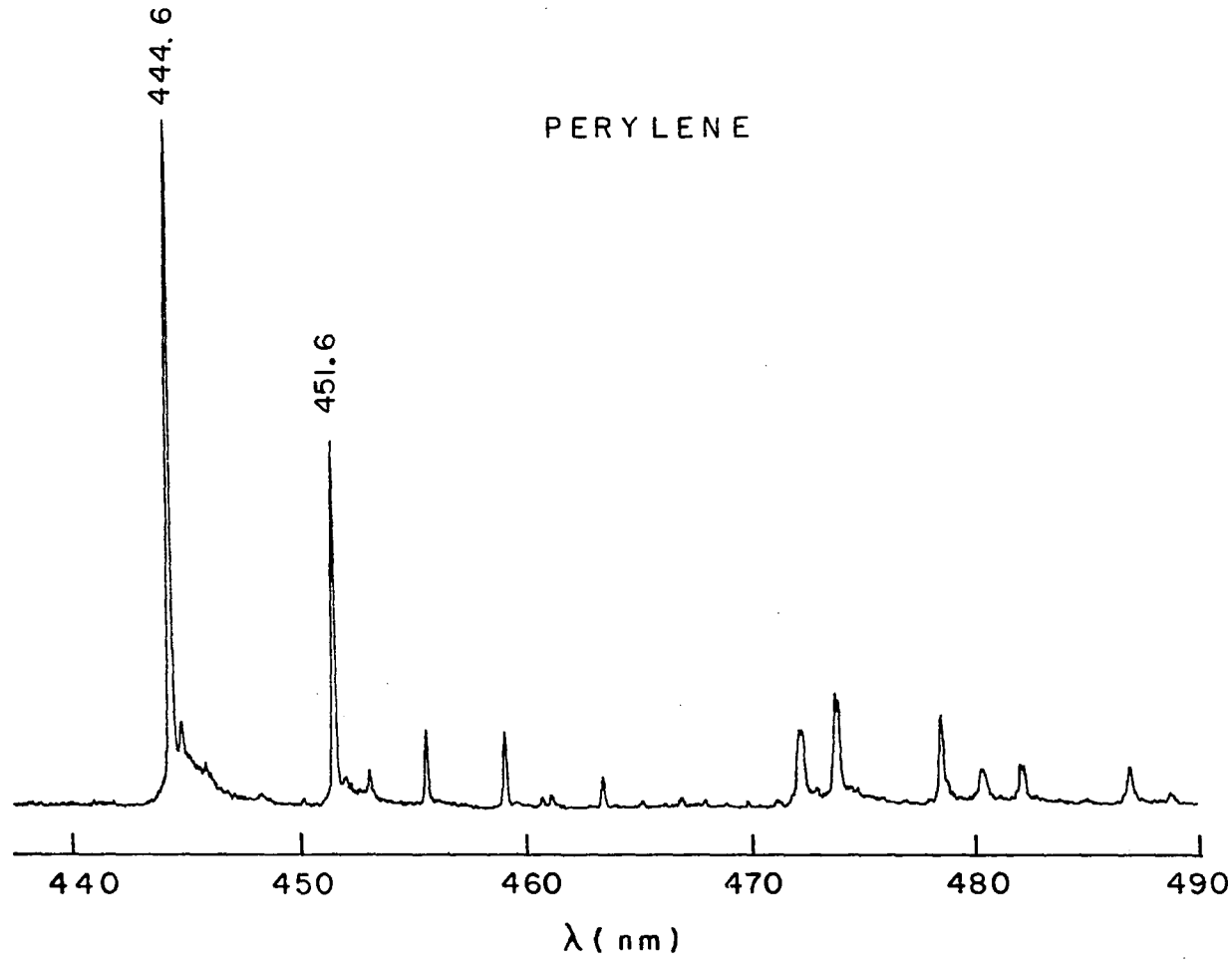

Figure 12H. LES spectrum of perylene in n-octane. λ_{ex}=420.3 nm.

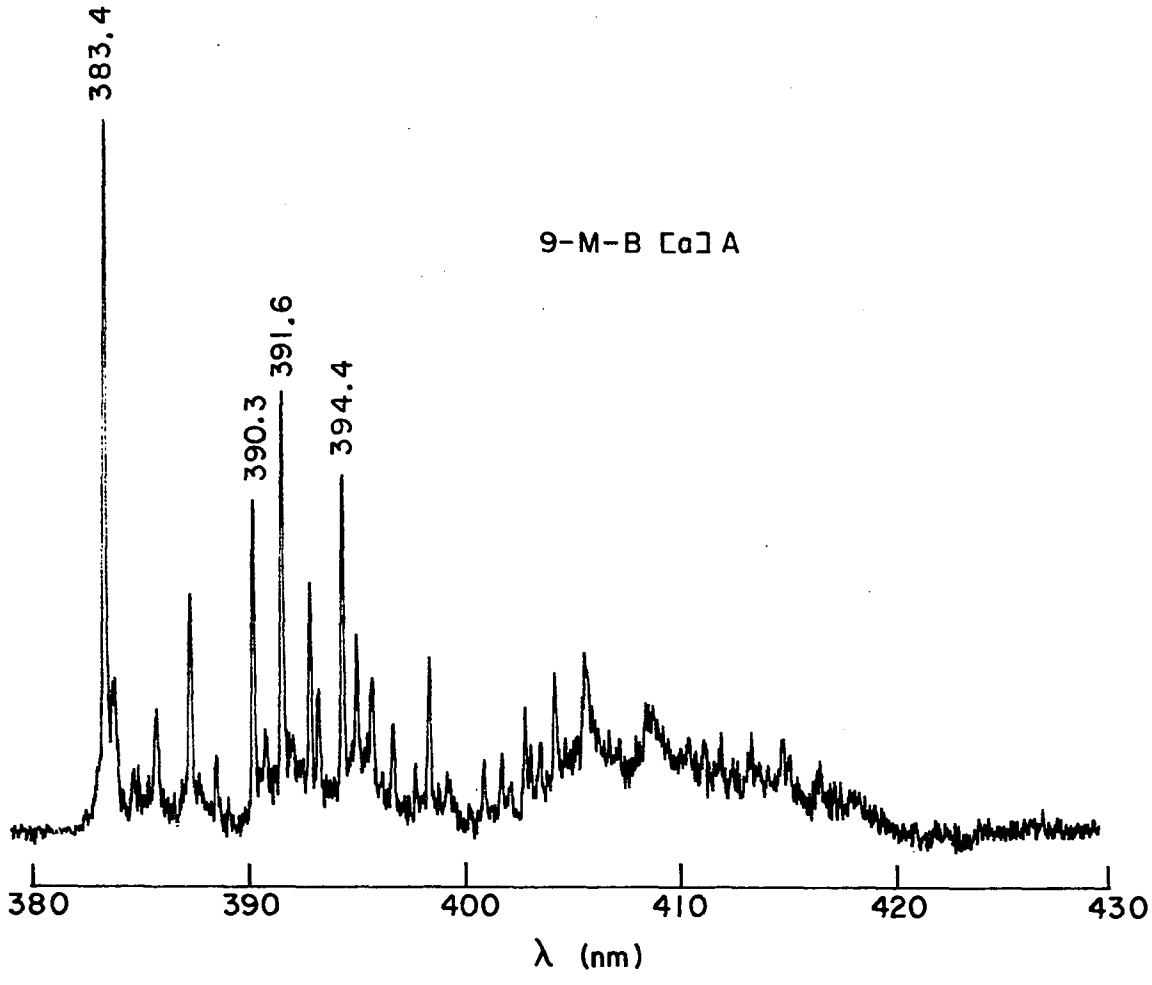

Figure 12I. LES spectrum of 9-M-B[a]A in n-octane. λ_{ex}=373.6 nm.

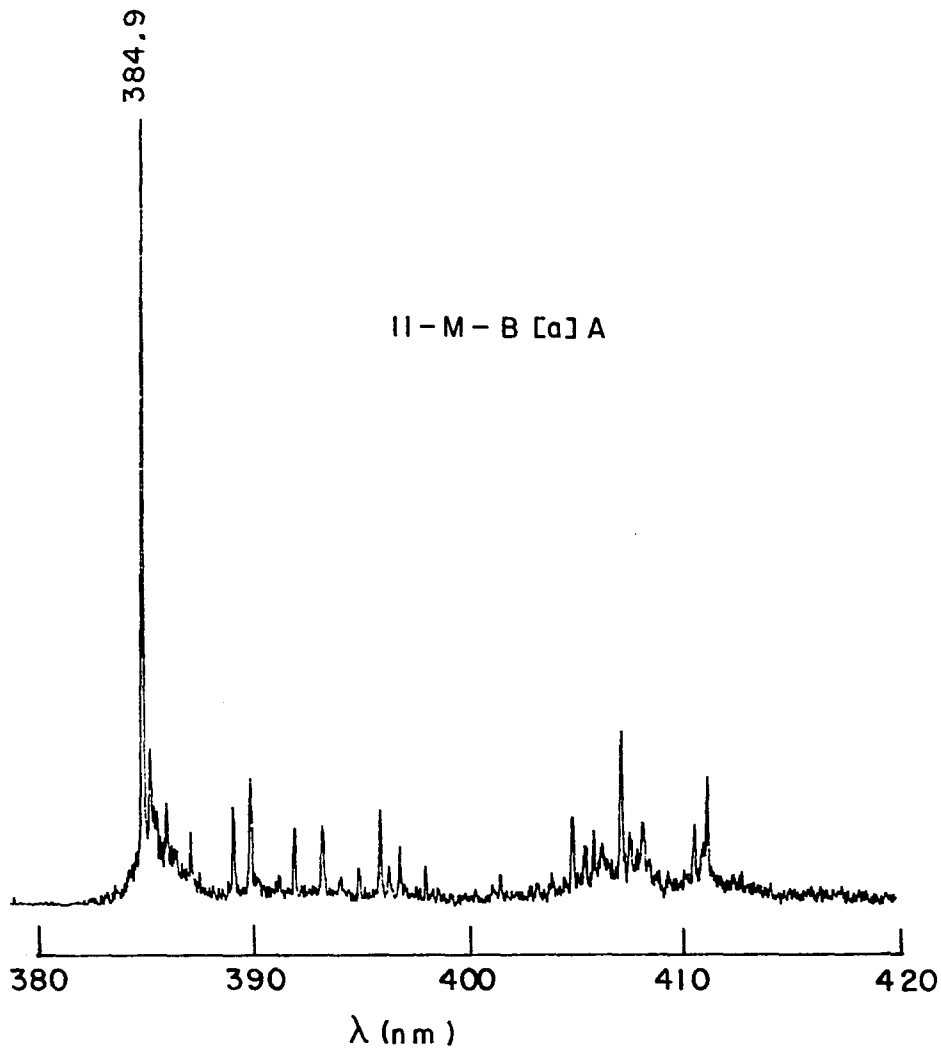

Figure 12J. LES spectrum of 11-M-B[a]A in n-octane. λ_{ex}=374.7 nm.

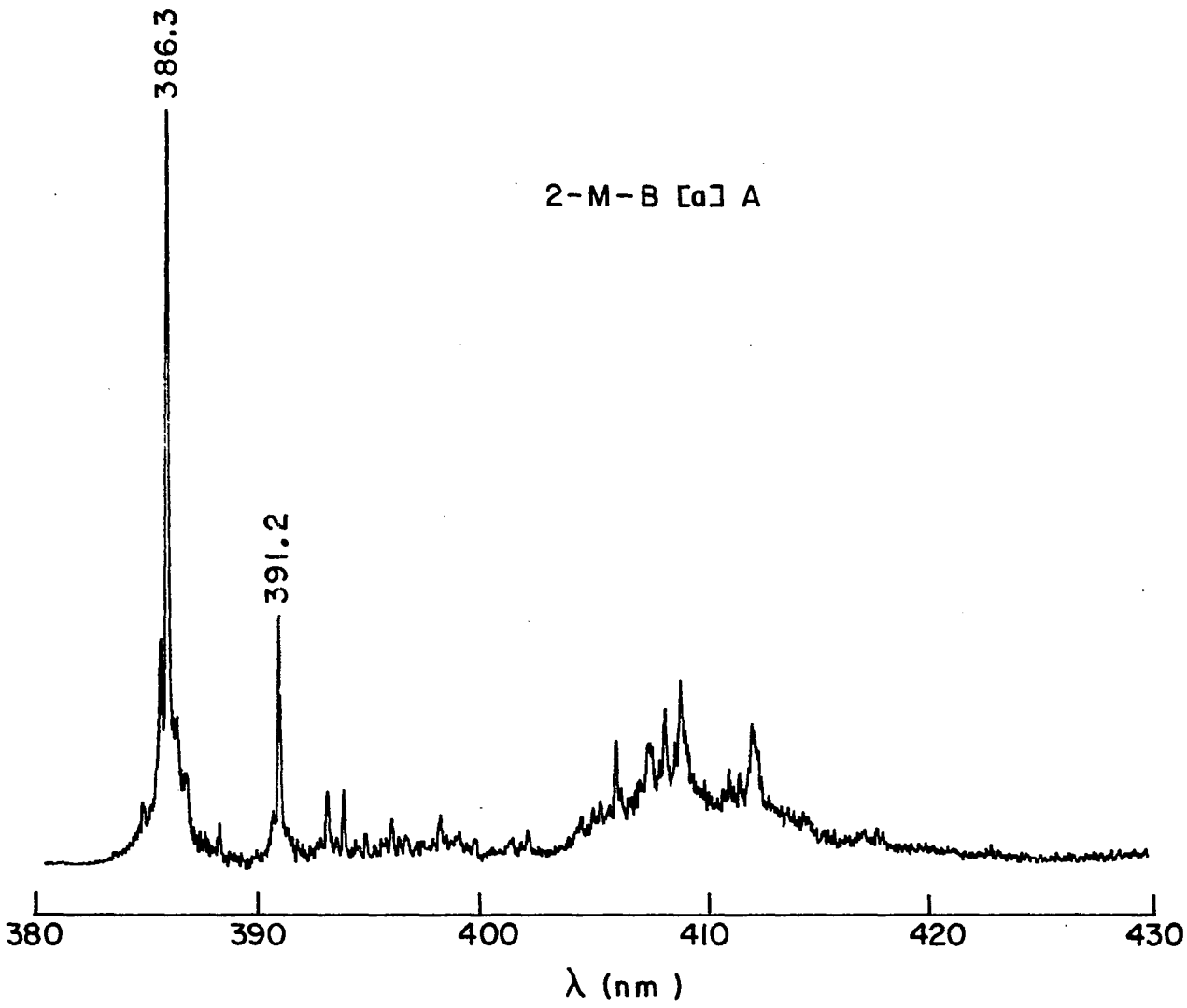

Figure 12K. LES spectrum of 2-M-B[a]A in n-octane. λ_{ex}=376.6 nm.

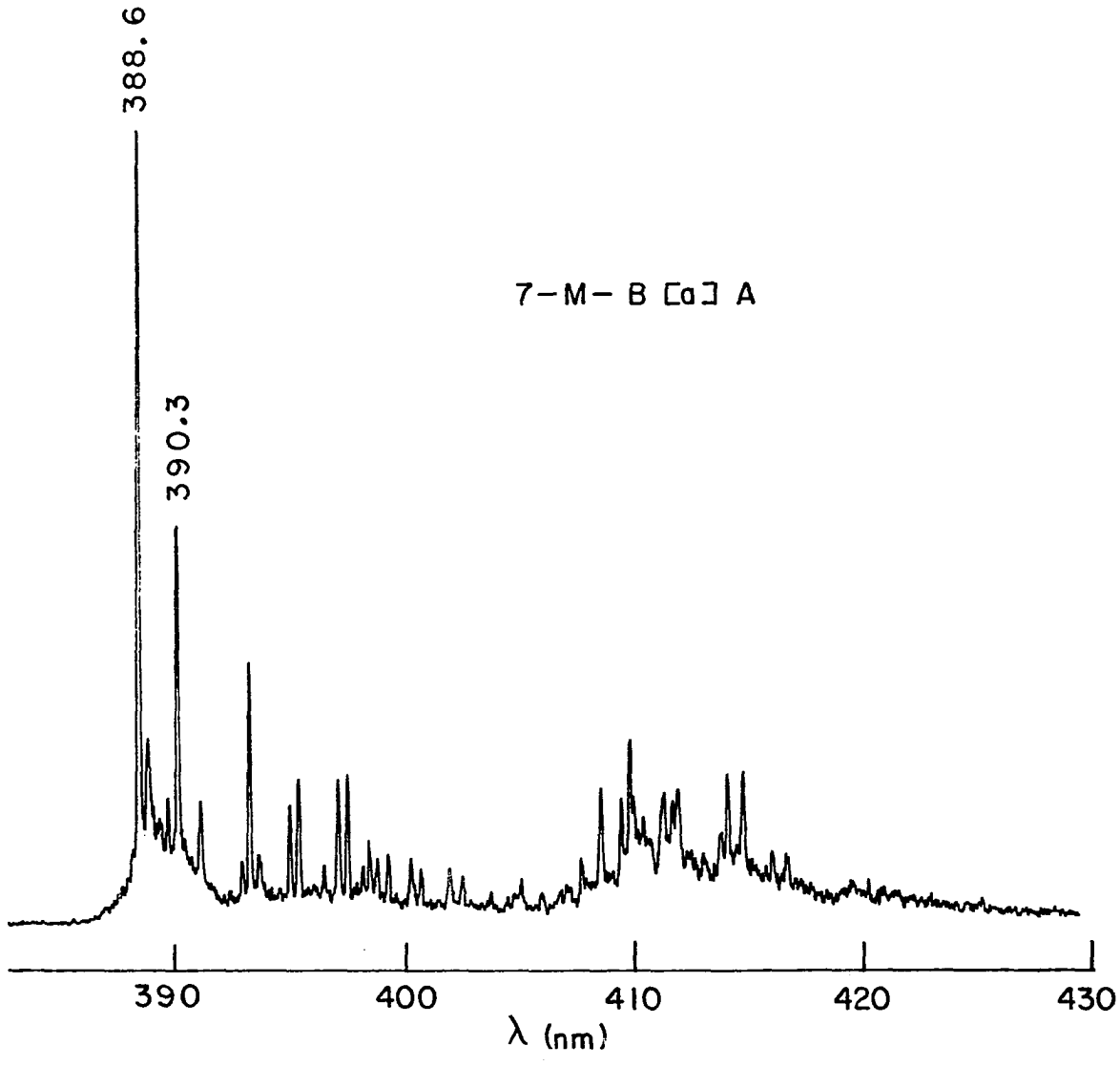

Figure 12L. LES spectrum of 7-M-B[a]A in n-octane. λ_{ex}=372.4 nm.

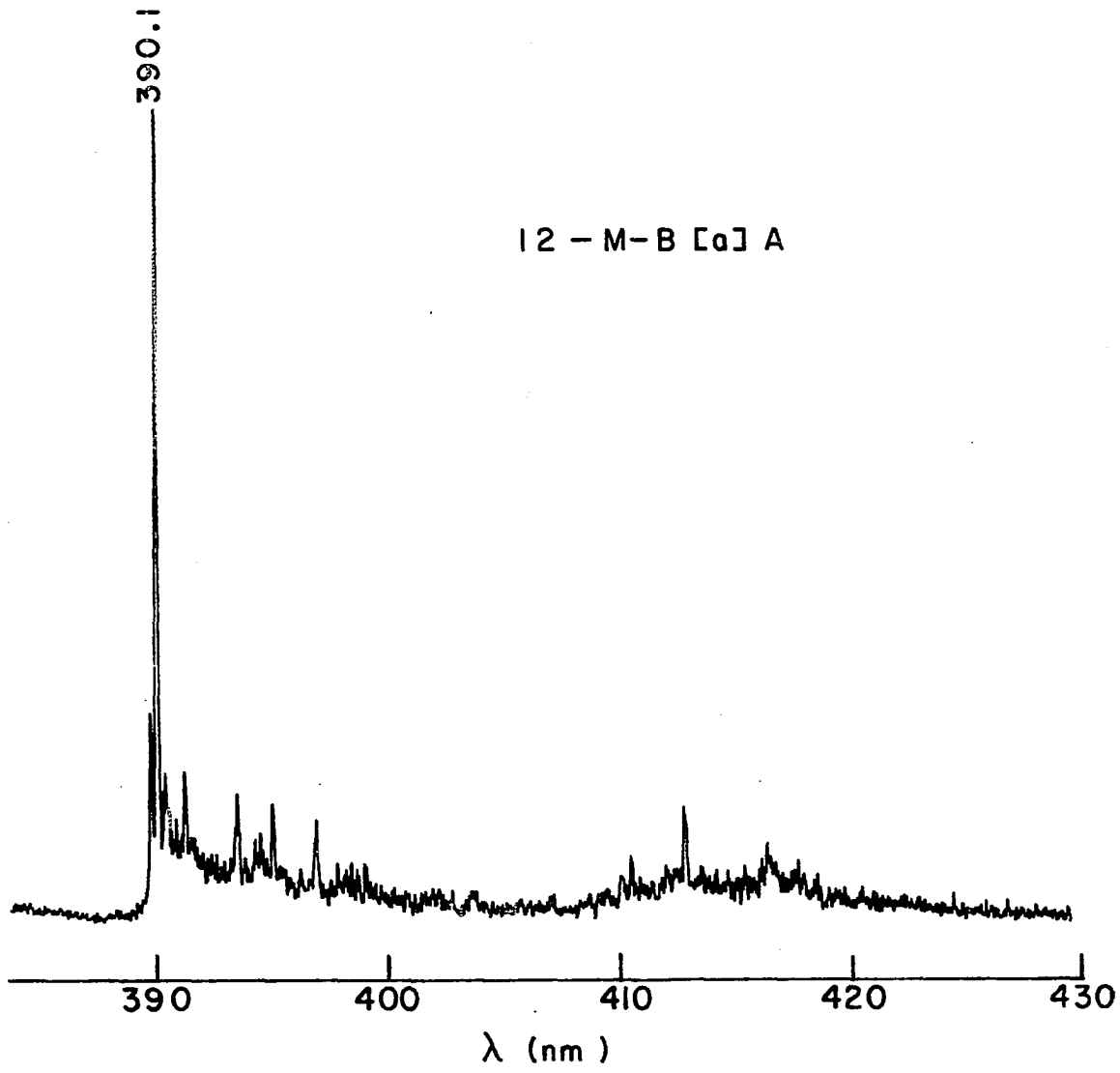

Figure 12M. LES spectrum of 12-M-B[a]A in n-octane. λ_{ex}=381.8 nm.

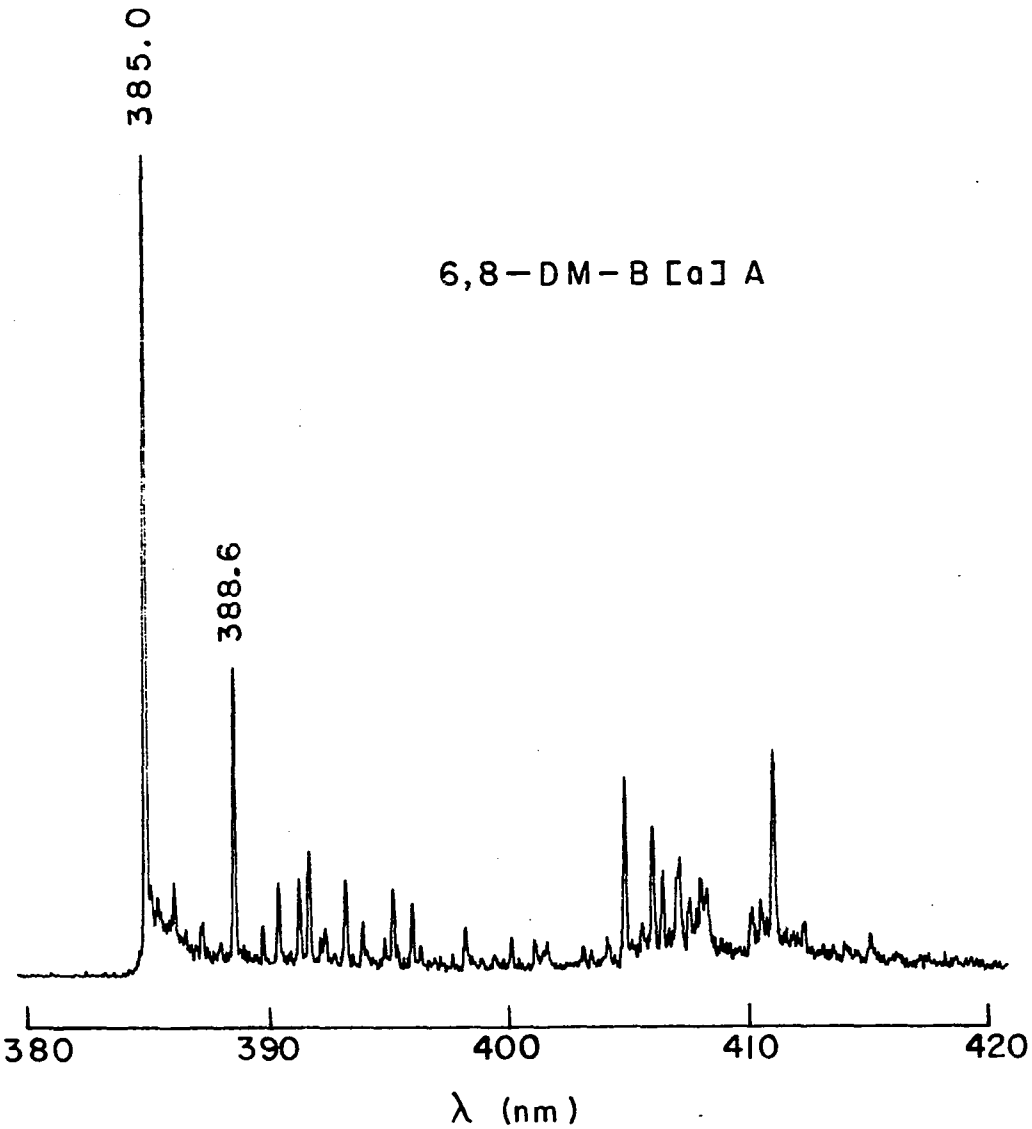

Figure 12N. LES spectrum of 6,8-DM-B[a]A in n-octane. λ_{ex}=375.0 nm.

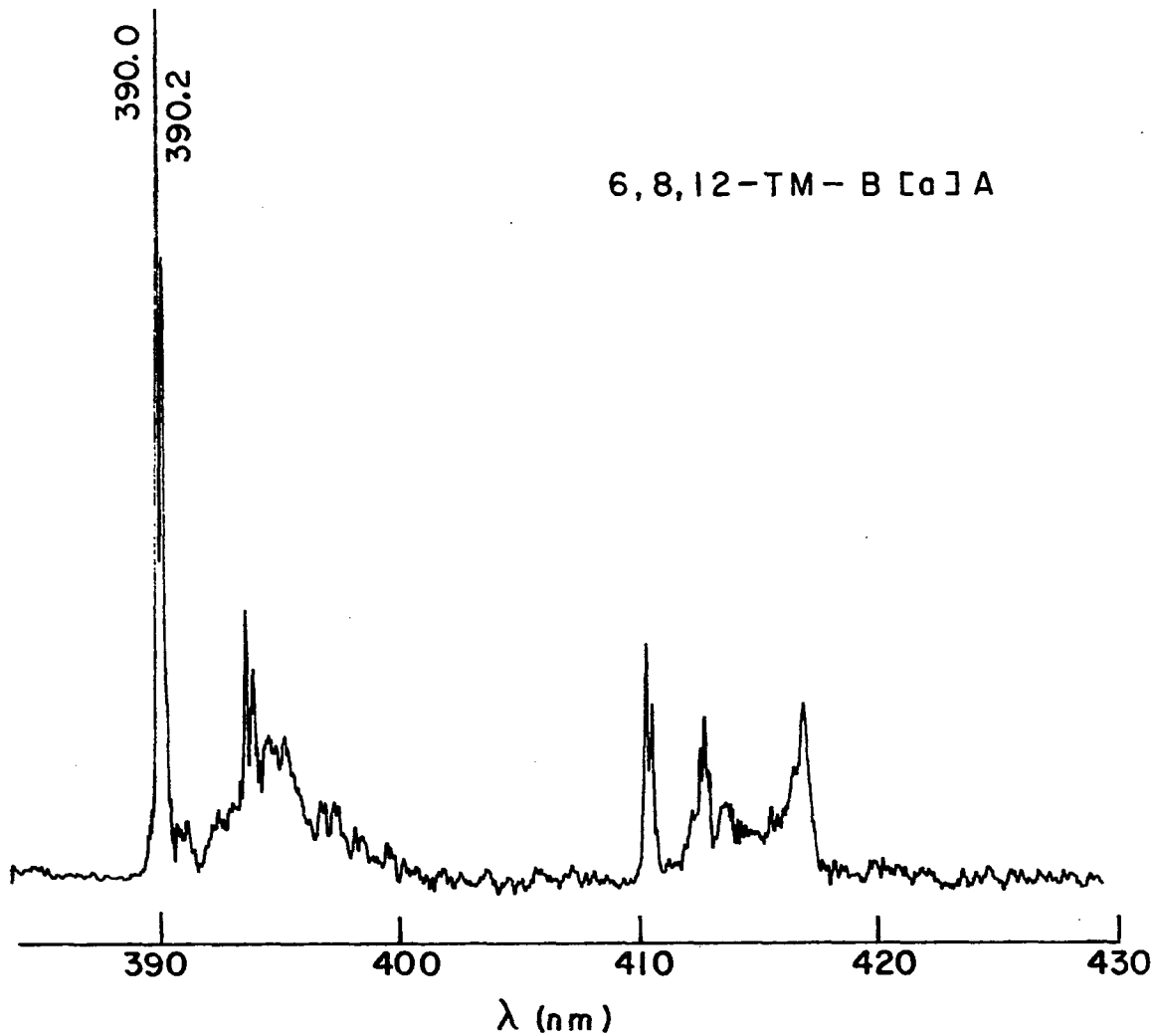

Figure 12P. LES spectrum of 6,8,12-TM-B[a]A in n-octane. λ_{ex}=380.0 nm.

benzo[a]pyrene, benzo[ghi]perylene and perylene were in good agreement with those recorded at 77 K by other workers (63,68). All of the spectra shown exhibited sharp line feature. The observed spectral half-bandwidth was of the order of ~0.1 nm. These laser excited Shpol'skii (LES) spectra comprised a number of vibronic lines which can be used as a fingerprint for identification of PAHs.

Selective Excitation of PAHs in Mixtures

The spectral positions of the 0-0 lines (principal origins) of some typical PAHs are shown schematically in Figure 13; the 0-0 lines of alkylated PAH derivatives can be expected to shift from those of their parent PAHs. The 0-0 lines correspond to the minimum energy required to excited a molecule. Compounds known to be carcinogenic are identified by an asterisk. It is seen in this figure that emissions of PAHs ranging from three to seven rings cover a spectral region of only about 110 nm. Thus, the emissions from literally hundreds of parent PAH compounds and their alkylated and multialkylated derivatives can be expected to be located within such a narrow "spectral window." In addition, each PAH compound also emits a number of vibronic lines (note that the luminescence spectrum is further complicated by multiplet structures as discussed earlier). Therefore, the unequivocal identification of an individual compound in a complex mixture may be greatly simplified through selective laser excitation.

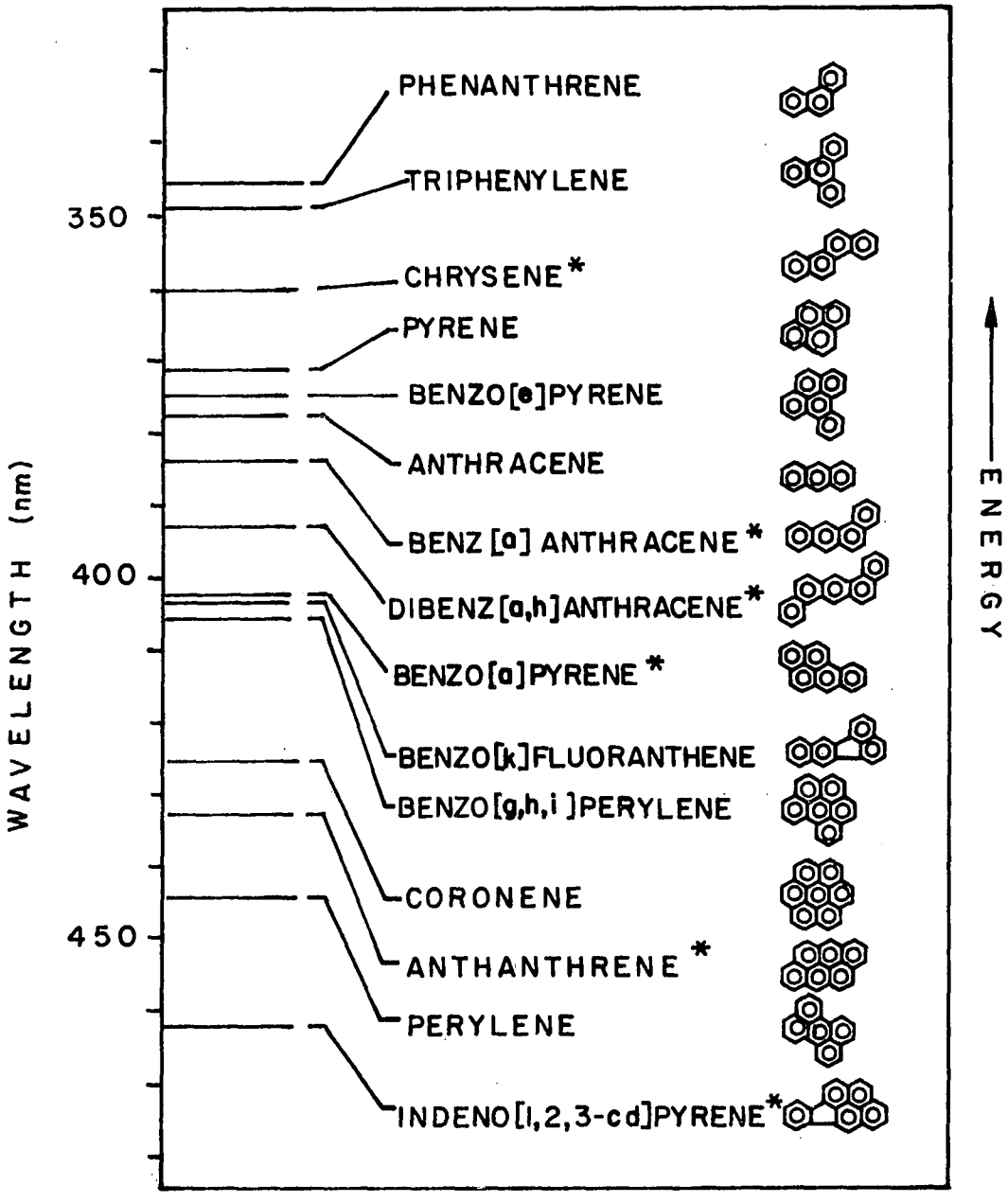

Figure 13. Spectral positions of the 0-0 lines of some PAHs.

Selective excitation usually relies upon the separation of principal origins, that is, if the PAH origins are sufficiently separated, λex can be set at a wavelength among them so that those PAHs with higher lying origins than λex (in energy) cannot be electronically excited and will not fluoresce. From Figure 13, three of the structural isomeric groups can be noted, i.e. the three-ring phenanthrene and anthracene; the four-ring triphenylene, chrysene, pyrene and benz[a]anthracene; and the five-ring benzo[e]pyrene, benzo[a]pyrene, benzo[k]fluoranthene and perylene. Compounds in these groups are often found difficult to be separate or distinguished by chromatographic and mass spectrometric techniques (89-91). Fortunately, these compounds exhibit significant separations in their principal origins (except B[a]P and B[k]F pair) that render the selective excitation an easy task. A more difficult situation is presented by B[a]P and B[k]F, where the origins lie so closely that selectivity in excitation will then rely primarily on the resolution achievable in the absorption spectrum of the mixture.

To study the selectivity provided by LESS, a synthetic mixture of B[a]P (0.3 ppm), B[k]F (1 ppm) and B[ghi]P (2 ppm) in n-octane was examined. The spectrum shown in Figure 14A was excited at a nonselective wavelength of 385.7 nm; under these conditions the marginally resolved spectral lines of B[a]P and B[k]F at 403 nm are evident. Laser excited, site selective excitation with the wavelengths shown in Figure 14B, C and D yielded the sequence of characteristic spectra of B[a]P, B[k]F and B[ghi]P. However, when compound and site selective excitation is

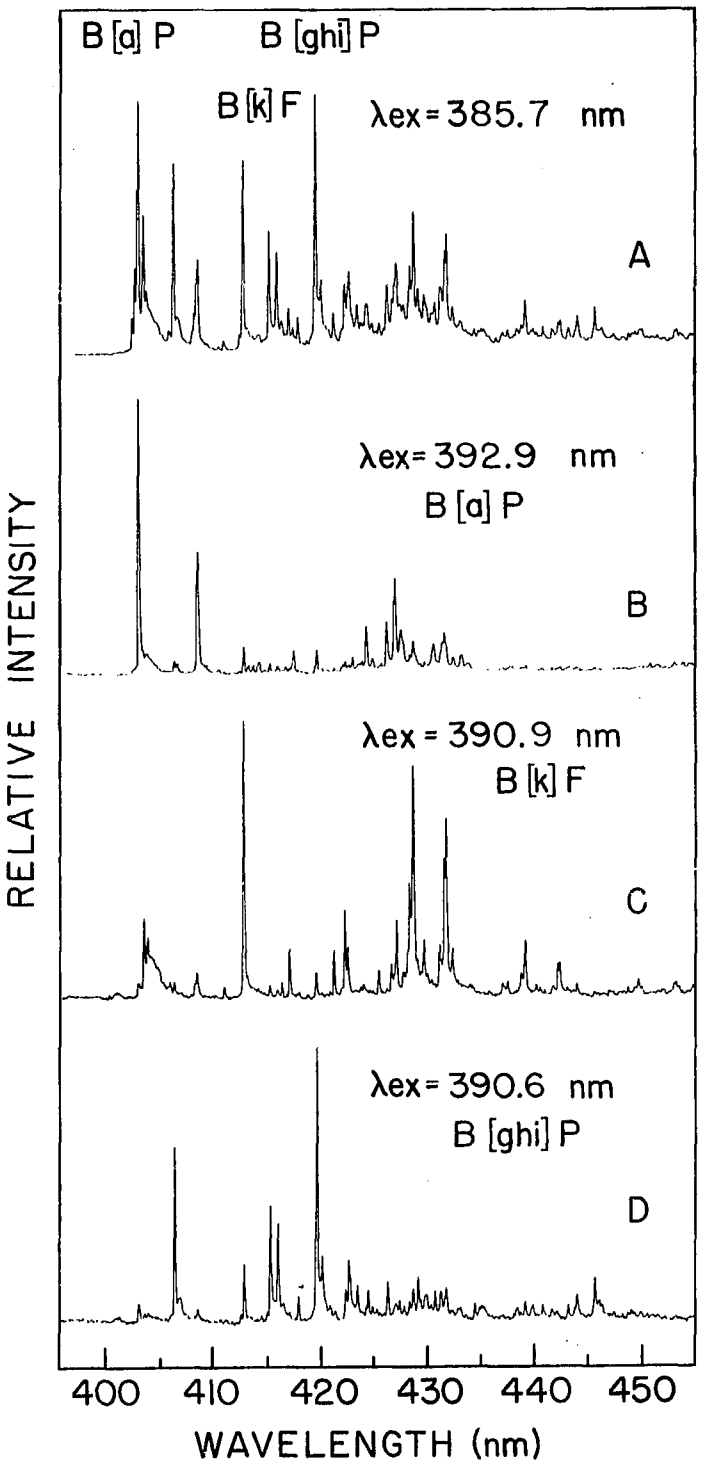

Figure 14. Selectively excited fluorescence spectra of the components of a mixture containing B[a]P, B[k]F and B[ghi]P in n-octane.

used for B[a]P no emission from B[k]F at 403 nm is observed, as shown in Figure 14B.

The site selective compound specific excitation of different alkylated derivatives of the same parent compound is illustrated in Figure 15. Nonselective excitation of this mixture via 366.5 nm laser radiation into the congested vibration manifold of 6,8-DM-B[a]A and 11-M-B[a]A led to the emission of the overlapping site spectra at 385 nm of both molecules. Four emission lines at 385 nm from the 0-0 transition in molecules occupying different sites were evident. In the relatively noncongested wavelength region (~370 to 380 nm), well-resolved absorption lines and associated excitation wavelengths could be selected with little or no spectral overlap from the other compounds in a manner analogous to that utilized in obtaining the site selected luminescence spectra in Figure 11. This selection process revealed that 375.0 nm and 374.7 nm, respectively were the best wavelengths for exciting site selective fluorescence of 6,8-DM-B[a]A and 11-M-B[a]A as shown in Figures 14B and 14C. It should be noted that the site selective fluorescence spectra at ~385 nm of the individual compounds consist of only a single prominent line characteristic of the individual compounds, with no overlap from the emission spectrum of the other compound.

Identification of Alkylated PAH Isomers

A variety of mutagenic alkylated and multialkylated PAHs have been

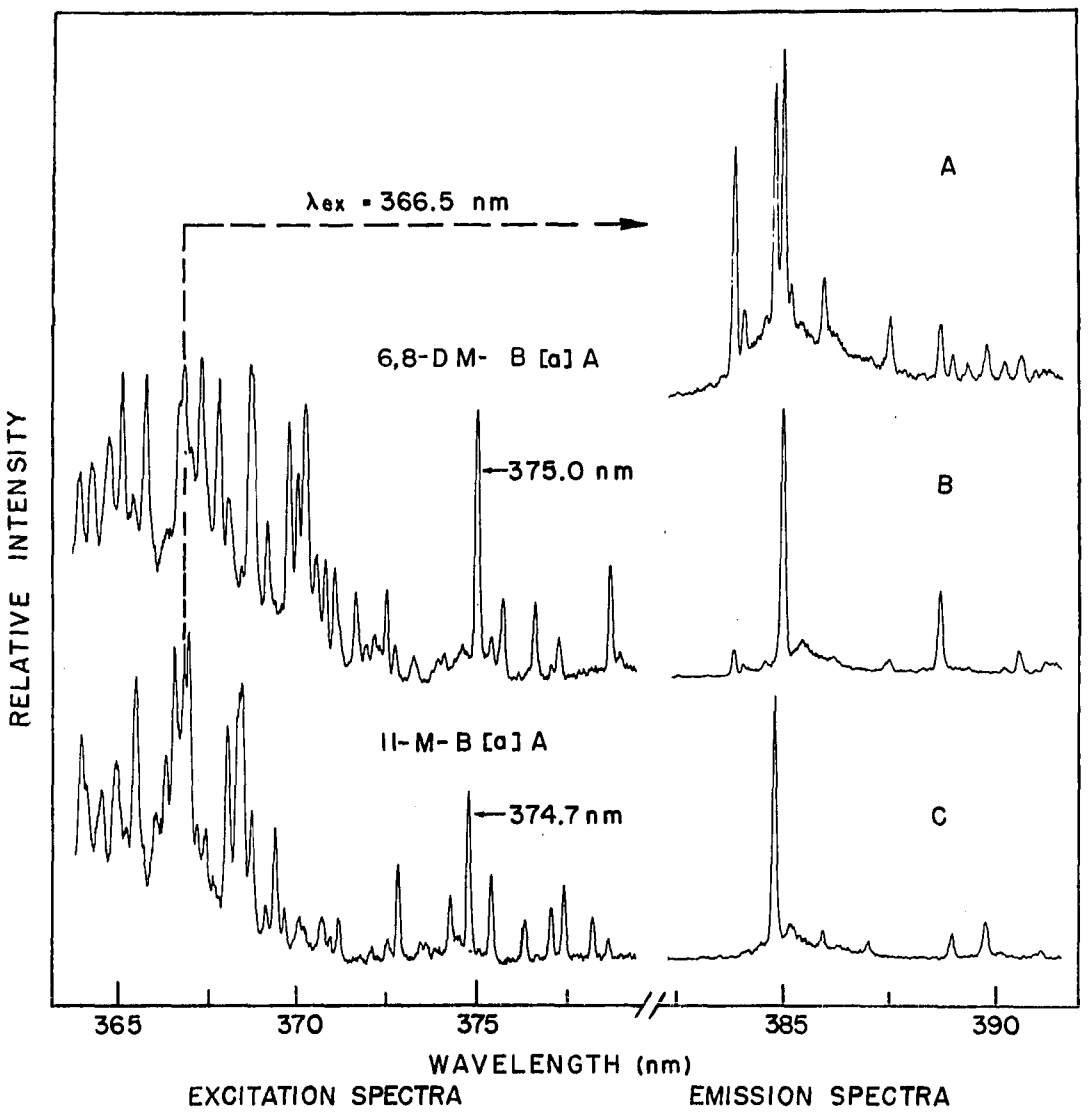

Figure 15. Selectively excited fluorescence spectra of the individual components in a mixture of 6,8-DM-B[a]A and 11-M-B[a]A.

found in cigarette smoke condensate (92) and multialkylated isomers of phenanthrene and benzo[a]anthracene have been reported to be major contributors to the mutagenicity of the PAH fraction isolated from a coal liquid (4). Typically, the mutagenicity of the alkylated isomers of B[a]A vary substantially (93,94). Thus, 7,12-DM-B[a]A is one of the most potent skin carcinogens known. In contrast, 1,2-DM-B[a]A is innocuous. Similar variations are known to occur with alkylated isomers of chrysene and phenanthrene. Because of the extremely similar chemical and physical properties of alkylated PAHs, the characterization of such complex mixtures is regarded as a difficult analytical task, which has to date been attempted only by capillary-column, gas chromatography-mass spectrometry (CC-GC-MS) (95), matrix isolation fluorescence (MIF) and Fourier transform infrared spectrometry (FTIR) (75). Resolutions adequate for the identification of alkylated phenanthrenes but not for the identification of alkylated B[a]A in synthetic mixtures has been achieved by CC-GC-MS (95). With MIF or FTIR only marginal resolution of the individual components present in a six-component mixture of methyl chrysenes was found possible (75). In an attempt to evaluate the potential application of LESS to such a challenging analytical task, a synthetic mixture of the parent compound and 11 alkylated derivatives of B[a]A dissolved in n-octane was examined.

The multiplet structure of the 0-0 transitions of some of the alkylated B[a]A compounds is shown schematically in Figure 16. The figure was assembled from data obtained on the pure compounds. The compounds

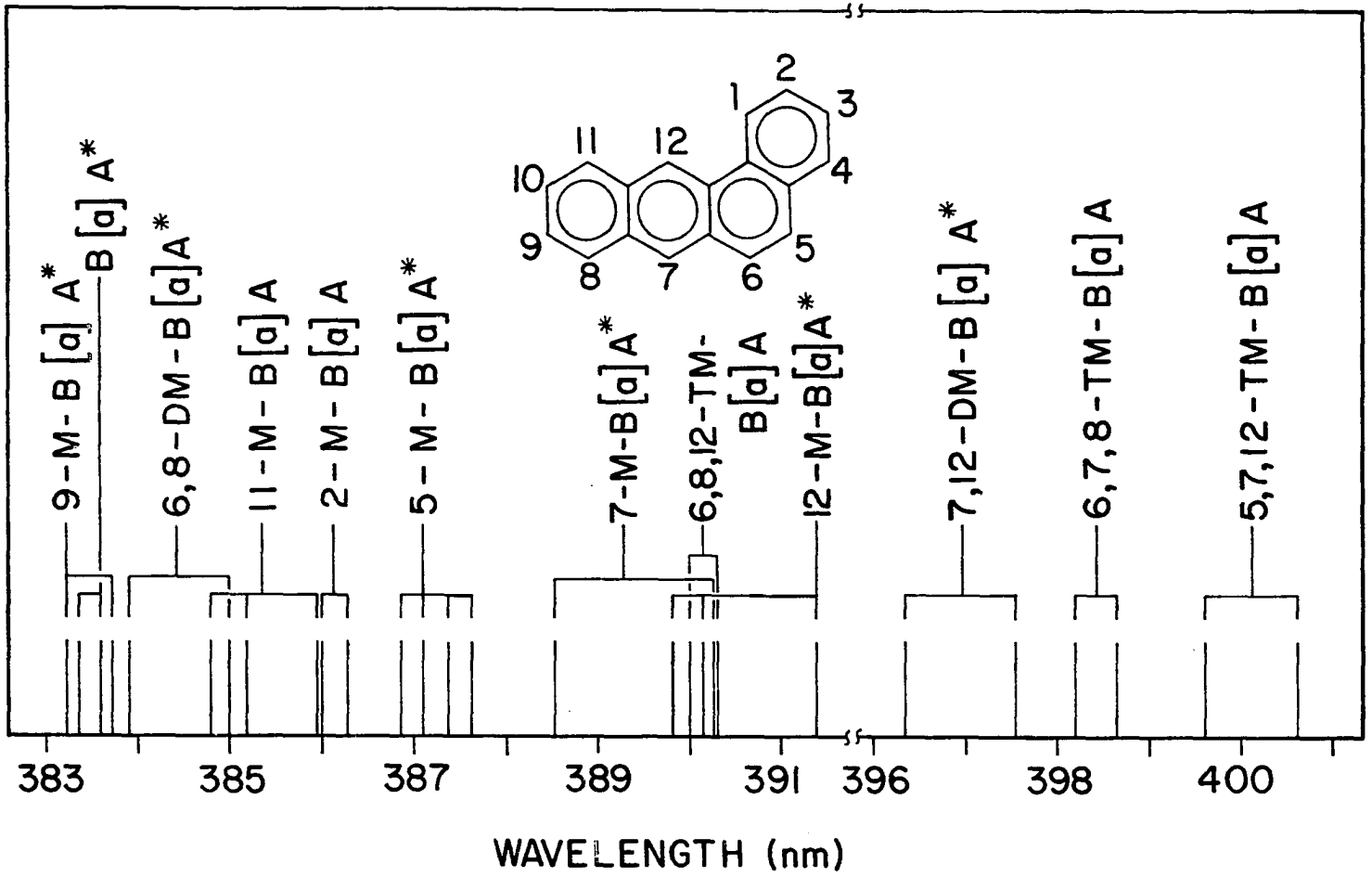

Figure 16. Spectral positions of 0-0 multiplets of B[a]A and several alkylated B[a]A.

known to be carcinogenic (93) are identified by an asterisk. As discussed earlier, the multiplet structures result from occupancy of the solute molecules in multiple nonequivalent sites. The site multiplets for the 12 compounds studied cover a spectral region of ~20 nm, with each compound exhibiting doublet, triplet or quartet structures. The wavelength interval covered by the 0-0 transition from molecules in nonequivalent sites can be as narrow as 0.3 nm (2-M-B[a]A) or as wide as 1.8 nm (7-M-B[a]A). From Figure 16 it is clear that the close proximity of the multiplet structures of several of the compounds may result in the spectral interferences when the mixture is excited by broadband UV or X-ray excitation. In the "worst case" example, it is seen that the multiplets of 6,8,12-TM-B[a]A are subject to spectral interferences from the multiplets of 7-M-B[a]A and 12-M-B[a]A. Thus, an ultra high resolution spectrometer would be required to resolve the fluorescence of 6,8,12-TM-B[a]A in the presence of the other two compounds, when nonselective excitation of Shpol'skii effect spectra is utilized.

When site and compound specific excitation is used, the spectral signatures of the compounds in the mixture are substantially simplified as is shown in Figure 17 A, C, D, E, F, G and H. The site specific excitation wavelengths are tabulated in the figure caption. An elegant example that illustrates the potential of LESS is the site and compound specific fluorescence of 6,8,12-TM-B[a]A shown in Figure 17G, which consists of only a single prominent line, with no spectral interference from 7-M-B[a]A and 12-M-B[a]A.

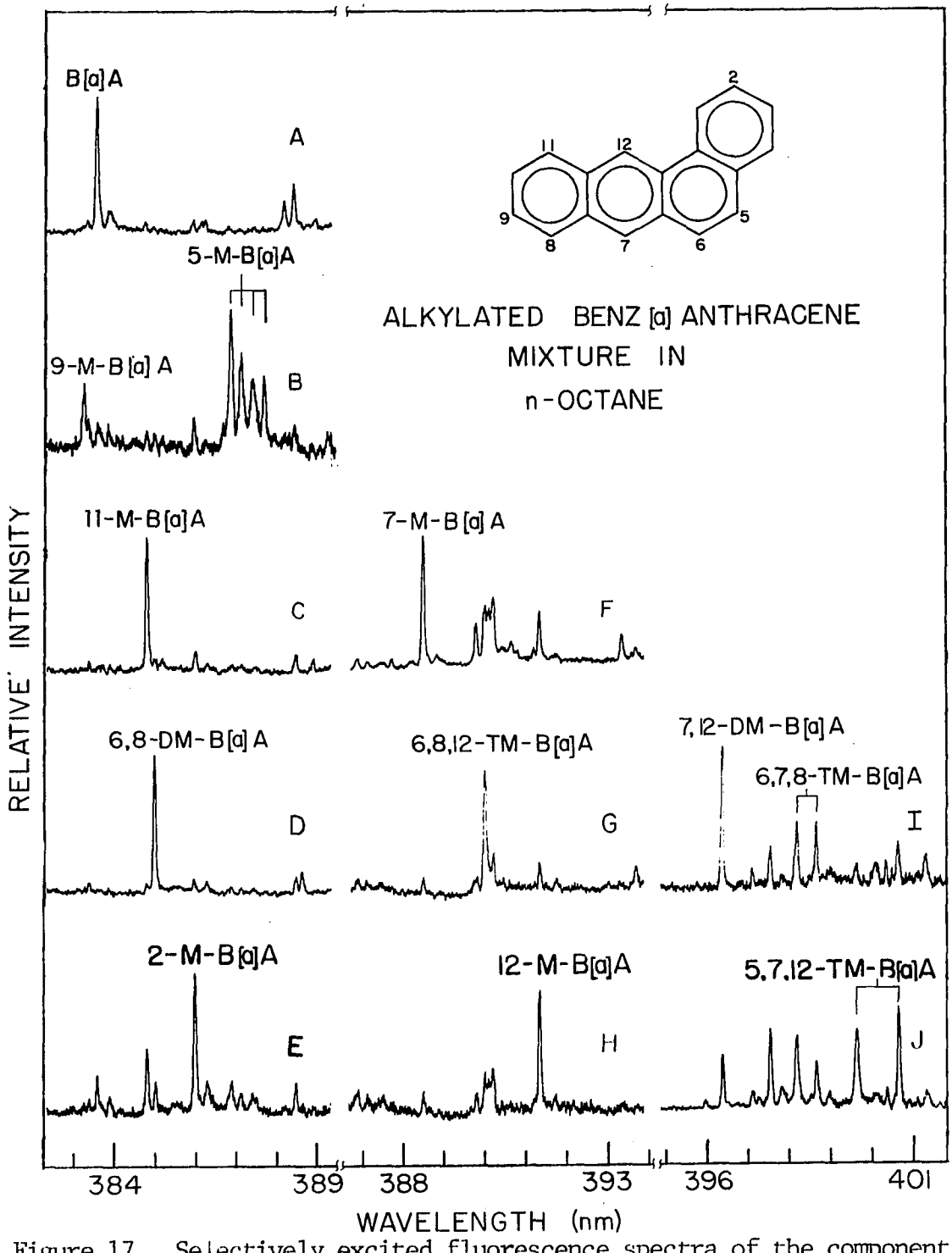

Figure 17. Selectively excited fluorescence spectra of the components of a mixture containing B[a]A and 11 alkylated B[a]A. Concentrations: 0.3-2.0 µg/ml in n-octane. λ_{ex}: A-376.9 nm, B-373.6 nm, C-374.7 nm, D-375.0 nm, E-375.4 nm, F-372.4 nm, G-380.0 nm, H-381.4 nm, I-389.7 nm, J-384.6 nm.

Examples of nonsite and compound specific excitation are shown in Figure 17 B, I and J. In Figure 17B it is seen that the site specific excitation of 9-M-B[a]A also leads to the simultaneous excitation of the fluorescence from all four sites of 5-M-B[a]A. No attempt was made to obtain site specific fluorescence of 5-M-B[a]A as the multiplets of the compound are not subject to spectral interferences from the multiplets of any other compounds in the mixture as is seen in Figure 16. The complexity of the spectra shown in Figure 17 I and J are a manifestation of a less than optimum choice in excitation wavelengths, which are located outside the laser output of the dyes used in this study. The complexity of the spectra did not pose any problems in the identification of 7,12-DM-B[a]A, 6,7,8-TM-B[a]A and 5,7,12-TM-B[a]A because the multiplets of the individual compounds are not subject to spectral interferences, as is evident in Figure 16. The fluorescence spectra shown in Figure 17 provide an elegant proof that site selective excitation utilizing LESS can provide unequivocal identification and potential quantification of the components of complex mixtures of alkylated benz[a]anthracene.

Analytical Studies

Site distribution dependence on concentrations

The quantitative aspects of conventional Shpol'skii method, i.e. linear concentration ranges, precision and detection limits,

have been demonstrated by previous workers in this field (62-65). Despite the numerous linear analytical curves that have been demonstrated, the potential analytical utility of the Shpol'skii effect for quantitation of trace levels of PAH compounds have been questioned (71,74,96). These questioning assertions were based on classical Shpol'skii effect studies on the luminescence spectrum dependency on concentrations (49,57,60). One of the major concerns has been the nonreproducibility in the relative intensities of the multiple site spectra. However, many of the earlier observations on site spectra were made at concentrations greater than 10^{-6}M. At these concentrations nonreproducible solute aggregate formation, resulting from variations in the cool-down procedures, may result in changes in the relative intensities in the multiple site spectra.

For quantitative analysis the population distribution of molecule among the different lattice sites that determines the intensity relationship within a multiplet structure should remain invariant, no matter what the concentration of the analyte molecule in typical samples. To demonstrate this invariance, the site spectra of various concentrations of B[a]P in n-heptane, excited at 385.6 nm were examined in frozen samples prepared under the controlled freezing regimes discussed earlier. As shown in Figure 18, the B[a]P molecules were basically distributed among four different sites. The spectra shown in Figure 18A and B were obtained at a B[a]P concentration of 1 ppm. The attenuations of the 0-0 lines at 402.3, 402.7 and 403.1 nm in Figure 18A were caused by self-absorption, which was alleviated on excitation with reduced laser

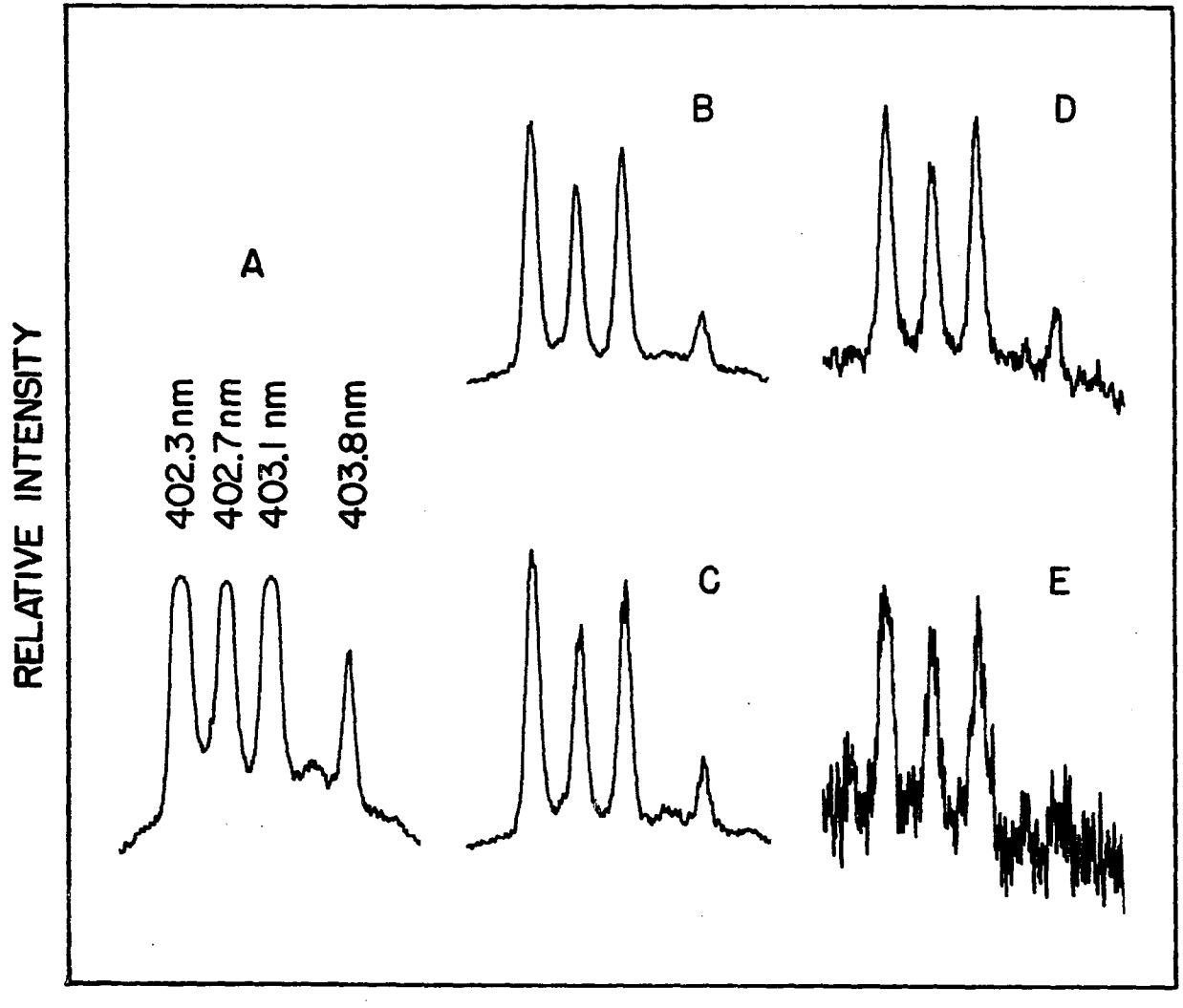

Figure 18. Multiple site spectra of B[a]P in n-heptane. Concentration: A,B-1 ppm, C-100 ppb, D-10 ppb, E-1 ppb. Excitation laser power: A-200 kW; B,C,D,E-40 kW.

power as shown in Figure 18B. Presently, the origin of this self-absorption dependency on excitation powers is not known. However, this self-absorption phenomenon has been observed in the fluorescence spectra of many other PAHs as well. Normally, the 0-0 line was the only line that would suffer from self-absorption, which could easily be detected from the changes in intensity ratios of the 0-0 line to other vibronic lines when the sample solution was diluted.

Multiple site spectra identical to those shown in Figure 18B to E were also observed for B[a]P in a n-heptane-diluted shale oil sample, indicating that these multiple patterns were independent of other constituents present in the sample. These results provide encouraging documentation that if the solute concentrations are maintained below ~1 ppm, the guest or impurity molecules are essentially isolated by the Shpol'skii host molecules, and consistent wavelengths and intensity ratio among the multiplet components can be achieved under controlled sample freezing regimes.

Analytical curve

Although the fluorescence intensity dependencies on concentrations of many PAHs have been studied previously, most of the studies were performed on single-component systems at liquid nitrogen temperature (77 K). The quantitation of one of the isomeric pair, B[a]P and B[k]F ($C_{20}H_{12}$) in the presence of the other is usually considered a difficult analytical task because of the similar chemical, physical and

spectroscopic properties of these compounds. The coexistence of these compounds in many environmental samples makes their determination particularly important. Thus, the potential of LESS for the quantitation of B[a]P in the presence of a relatively large excess of B[k]F and B[ghi]P was evaluated. In Figure 19 the selectively excited fluorescence spectrum of B[a]P present at a concentration of 1 ppb in a mixture containing B[k]F (1 ppm) and B[ghi]P (2 ppm) is shown. At relatively high concentration of B[k]F present in the mixture, relatively weak luminescence of B[k]F is obtained but the near baseline spectral resolution observed is more than adequate to quantitate trace levels of B[a]P. The spectral resolution observed in Figure 19 sharply contrasts with that obtained by utilizing time-resolved detection in conventional matrix isolation spectroscopy (77). A typical analytical curve for B[a]P present in this three-component mixture containing B[k]F (1 ppm) and B[ghi]P (2 ppm) is shown in Figure 20. It is seen that the linear concentration range extends over three decades. The correlation coefficient for the linear portion of the analytical curve was calculated to be 1.01, indicating a true linear relation between the fluorescence intensities and concentrations. The deviations from linearity in the analytical curve between 100 and 1000 ppb evidently arose from self-absorption effects on the 403.1 nm B[a]P line. This conclusion was supported by two independent observations. First, emission lines of B[a]P lines other than the 0-0 transition, e. g. the 408.5 nm line exhibited linearity up to 1000 ppb. Second, the linear concentration range shown in Figure 20 could be extended to higher

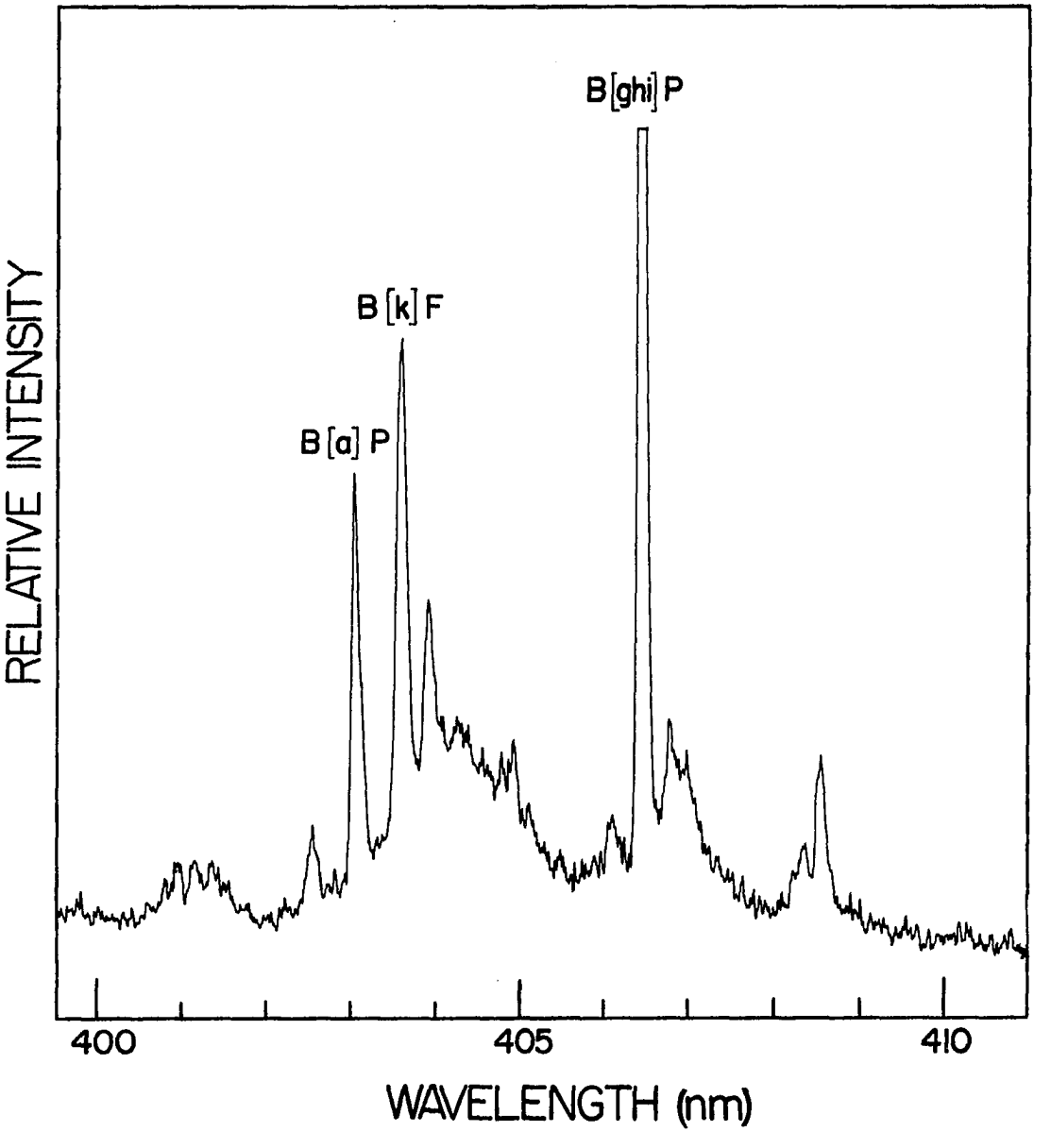

Figure 19. The spectral resolution obtained on the selective excitation of B[a]P (1 ppb) present in a mixture containing an excess of B[k]F (1 ppm) and B[ghi]P (2 ppm) in n-octane. λ_{ex}=392.9 nm.

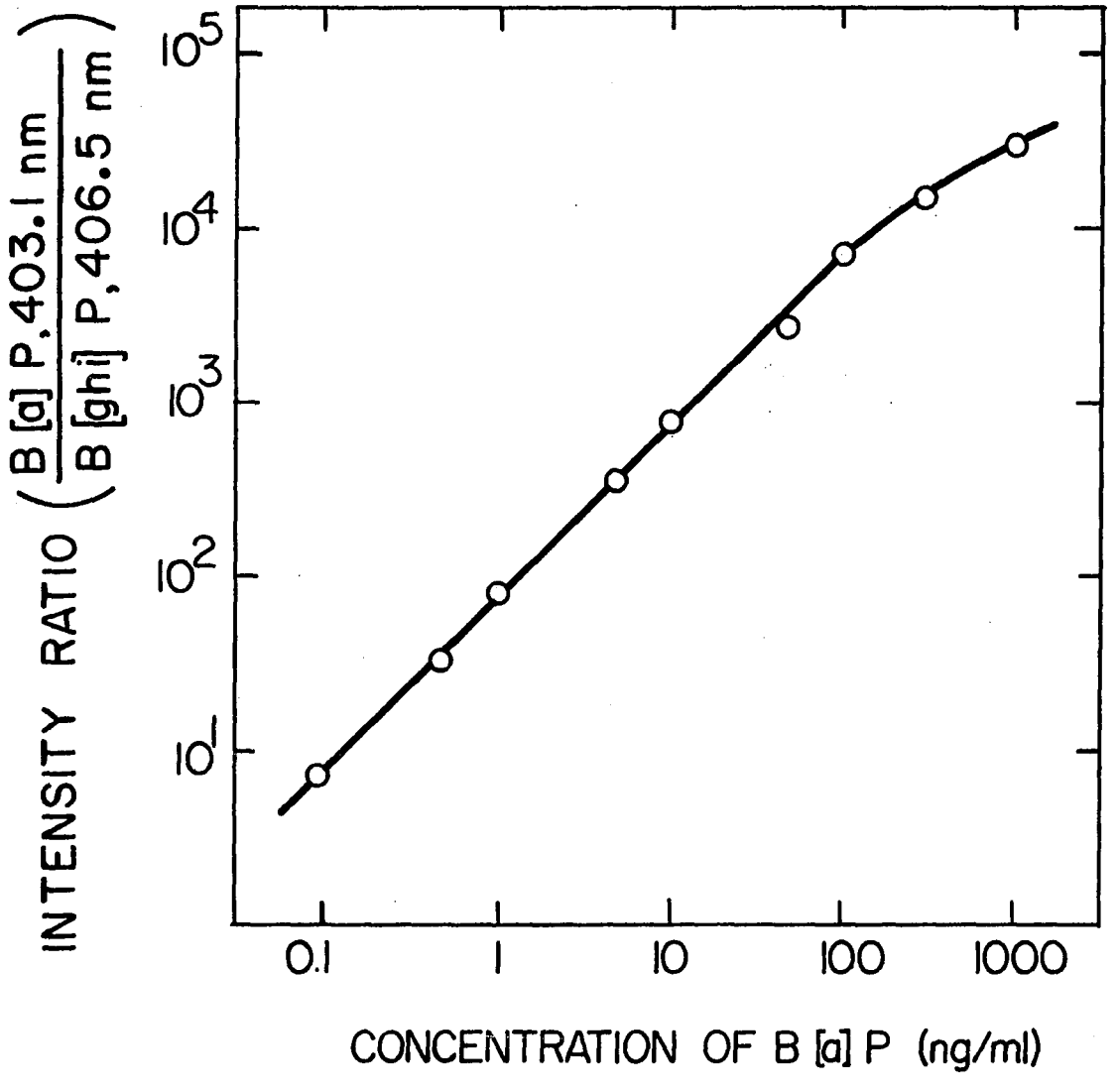

Figure 20. Analytical curve for B[a]P in the presence of B[k]F and B[ghi]P.

concentrations by simply reducing the laser power. Nonlinearity observed in the part-per-million concentration range evidently arose from self-absorption as well as aggregate formation, based on the attenuated 403.1 nm line of B[a]P and the appearances of broad emission bands (FWHM on the order of nanometers) characteristic of aggregates observed in the spectra. The aggregate formation phenomenon at relatively high concentration levels may explain, in part, the nonlinear characteristics of the analytical curves observed in the earlier analytical studies of PAHs by a X-ray excited optical luminescence-time resolution spectroscopy (XEOL-TRS) technique (97).

Detection limits

The detection limit of B[a]P in the presence of 1 ppm B[k]F was 0.07 ppb, calculated as the concentration of B[a]P which gave S/N=3, where S is the difference in intensities between B[a]P and background, and N is the background noise. This detection limit, as obtained using the N_2-laser pumped dye laser, corresponds to a 0.05 ng absolute detection, based on a 0.7 ml sample volume. This detection limit is significantly better than the value obtained by time-resolved matrix isolation method using conventional N_2 matrix (2 ng) (77). The detection limit of B[a]P in the absence of the B[k]F interferant, obtained using the higher power excimer laser pumped dye laser, was 8 ppt (parts-per-trillion), which corresponds to a 6 pg absolute detection. Because only ~1/200 of the total sample surface was exposed to the laser beam, only ~30 fg of B[a]P was

actually being detected. In any event, this limit of detection of B[a]P is significantly better than that obtained by conventional Shpol'skii spectroscopy (5 ppb), based on using Hg lamp as the excitation source (63).

The above results do not imply that an increased excitation power would necessarily result in an improvement in limit of detection, because the associated scatter of the excitation radiation is also enhanced. Scatter radiation is generally regarded as the ultimate limiting factor in fluorimetric determinations of ultra-trace species. Detection limit is usually affected by such parameters as collection optic efficience, detection electronics, excitation source intensity, absorption cross-section, luminescence quantum efficiency of species of interest, and noise source. Typically, the absorption extinction coefficient of PAHs ranges from 10^2 to 10^5 $M^{-1}cm^{-1}$, and the luminescence quantum yield from 10% to 90% (98). Thus, the detection limits of those PAHs other than B[a]P would also be expected to be in the parts-per-trillion concentration levels. Presently, the principal source of noise is laser scatter radiation. Although the scattered radiation background can be suppressed through time-resolution (the scatter radiation decays at the same rate as the laser pulse, ~10 ns), there is a trade-off between gate-delay, i.e. time resolution, and the magnitude of fluorescence signal. Another noteworthy source of noise is the shot-to-shot laser intensity jitter, which could undoubtedly be reduced by employing a reference channel in the detection system that monitors the variation of the laser radiation directly.

Analytical Applications

Coal liquids, petroleum crude oil and crude shale oil are known to contain substantial concentrations of potentially carcinogenic and mutagenic PAHs. The extremely complex nature of these liquid fuels, which are known to contain hundreds of low and high molecular weight organic compounds, has made it difficult to directly analyze the liquid fuels for PAH compounds. Presently, the PAHs are usually first isolated as a compound class through solvent extraction, column or liquid chromatography, followed by isolation and characterization of the individual PAHs via thin layer chromatography, capillary column gas chromatography with flame ionization detection or mass spectroscopic characterization, or high performance liquid chromatography with fluorescence detection. These techniques are often inadequate for resolving the complex mixtures of PAHs present in the energy related materials, and they are not readily adaptable to the direct determination of selected high potency species without resorting to time consuming prior separations.

The applications of LESS for the determination of PAHs in some nine liquid fuel samples (as given in Table 5) were studied. The demonstrated selectivity and sensitivity of LESS should facilitate the direct identification and determination of PAHs in complex matrices. Moreover, LESS is particularly selective for PAHs in the sense that only PAHs and their heterocyclic analogue in the sample would be subject to the Shpol'skii effect and give rise to sharpline emissions.

Selection of solvent for sample dilution

The Shpol'skii solvents, i.e. n-paraffins, are probably more compatible with these oil-type liquid fuel samples than any other organic solvent that facilitate direct sample dilutions. Among the n-paraffins, n-octane was selected as the solvent for two reasons. First, a single solvent, such as n-octane, suffices for the development of the sharpline spectra of PAHs ranging from four to seven ring compounds. Second, a lesser number of site is usually occupied by the analyte in the n-octane host. Generally, the samples were diluted by a minimum factor of 10^3 to minimize the precipitation of n-octane-insoluble asphaltenes.

Asphaltenes consist of a complex mixture of the most polar and highest molecular weight molecules in the liquid fuel samples. To alleviate asphaltene precipitation during our studies, n-octane containing 10-20% of methylene chloride, acetone, dimethyl sulfoxide, or ethanol (immiscible with n-octane) was initially used for sample dilution for fear of potential loss of PAH through occlusion during the precipitation process. However, the increases in the solvent polarity did not cause noticeable changes in the amount of precipitates. Many complex liquid fuels consist of a delicately balanced mixture of compounds that depend on each other for solubility (99). Primarily two factors, (a) the ratio of polar to nonpolar molecules; and (b) the ratio of low molecular weight compounds to high molecular weight compounds, are responsible for maintaining the mutual solubility of the compounds in the complex mixture. In liquid fuels, polar and nonpolar, and low molecular weight and high molecular weight compounds are miscible, and homogeneous solutions are

maintained as long as suitable ratios of polar to nonpolar and low molecular weight to high molecular weight molecules are maintained. When these two ratios are changed, for example, by adding large amounts of low molecular weight, nonpolar solvent such as n-octane, the balance is upset, and polar molecules as well as high molecular weight compounds are less soluble and precipitate as asphaltenes. Evidently, the amount of asphaltene precipitated depends on the hydrocarbon solvent, the volume ratio of solvent to sample, and the composition of the sample. Thus, it was not surprising that no single solvent or combination of solvents was capable of dissolving all the compounds in some complex mixtures at dilution ratios of 10^3 to 10^4. In the present study, no attempt was made to isolate the trace precipitates from the dilute sample solutions except allowing them to settle to the bottom of the solution flasks.

Identification of PAHs in liquid fuels

This investigation was not meant to identify as many PAHs as possible in one sample, but to examine the feasibility of utilizing LESS to identify selected PAH compounds in a number of samples of various complexity. The compounds selected and the liquid fuels analyzed are shown in Table 6. The PAHs that were searched for in each sample are indicated either by a check mark (identified), or by ND (not detected). The PAHs not detected were either absent in the sample, or occurred below their detection limits.

Table VI. Liquid fuels analyzed and the compounds detected by the LESS technique

PAH	SRC-I Solvent	SRC-II	Syncrude Oil	Petroleum Mix	Synthoil	Shale Oil
Pyrene	✓	✓	✓	✓	✓	✓
4-Methyl-pyrene	✓	✓	✓	ND[a]	✓	—
B[a]P	✓	✓	✓	✓	✓	✓
B[e]P	✓	✓	—	—	—	—
B[k]F	✓	✓	✓	ND	✓	—
B[ghi]P	—	—	✓	ND	✓	—

[a]ND=not detected.

The typical, selectively excited luminescence spectra of pyrene, 4-methyl-pyrene, B[a]P, B[k]F and B[e]P in the liquid fuel samples are shown in Figure 21 and 22. These spectra were obtained after dilution of the SRC-II sample by 1 X 10^3 with n-octane. The observed spectra comprise a number of well-resolved vibronic lines that provide for the unequivocal identification of the individual PAHs via comparison with their reference LES spectra in Figure 12, or as for 4-methyl-pyrene by comparison with the literature reference spectrum (100). The selectivity in absorption can be noted from the drastic change in the fluorescence spectra of pyrene and 4-M-P when the λex was altered from 363.3 to 363.2 nm. The λex selected for B[a]P and B[k]F caused weak emission from B[k]F and B[a]P respectively, because of the partial overlap of primary absorption lines of these two compounds at the excitation wavelength. However, the emission lines are sufficiently resolved to permit

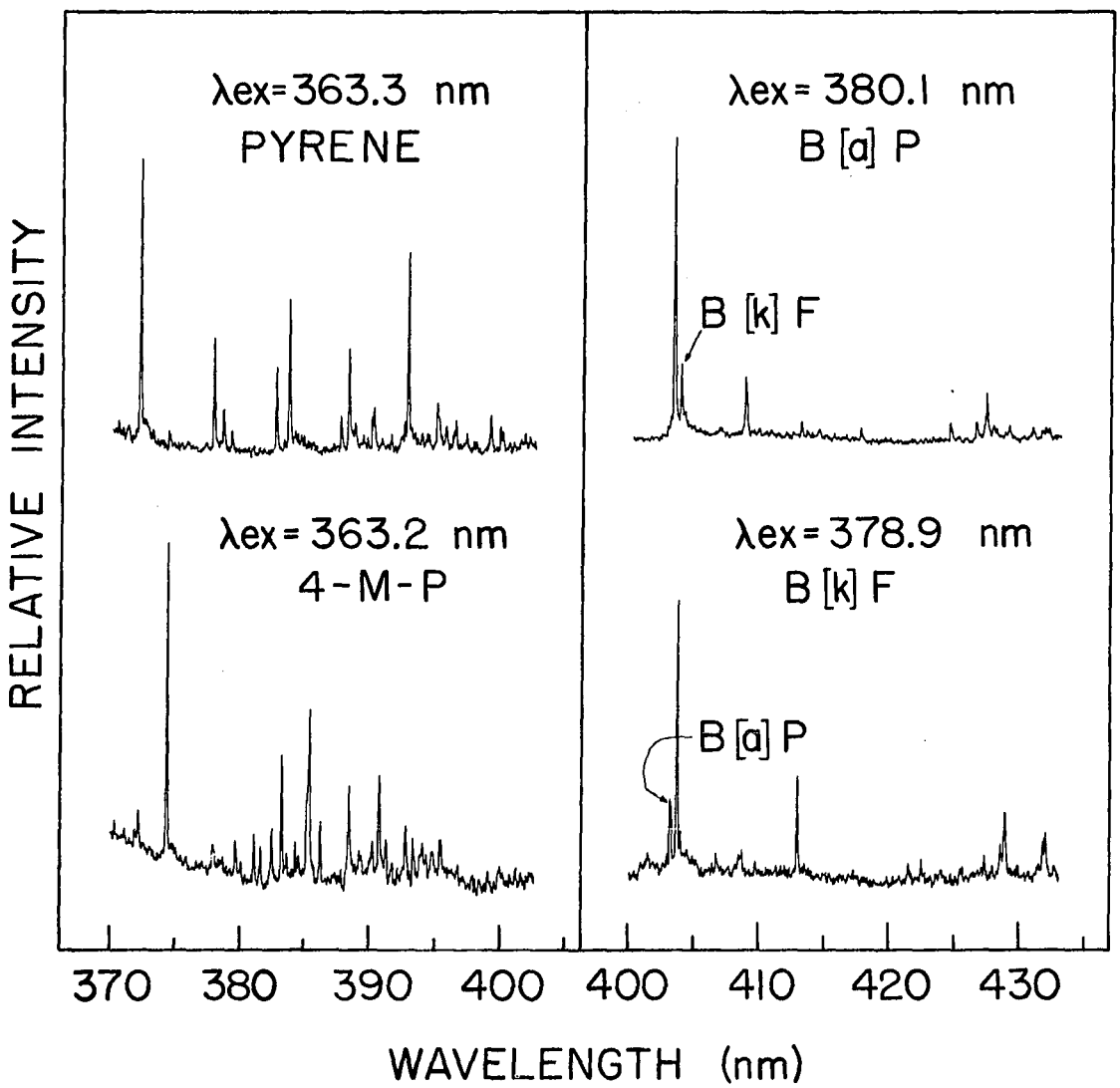

Figure 21. Selectively excited fluorescence spectra of pyrene, 4-M-P, B[a]P and B[k]F in a solvent refined coal liquid (SRC-II) sample.

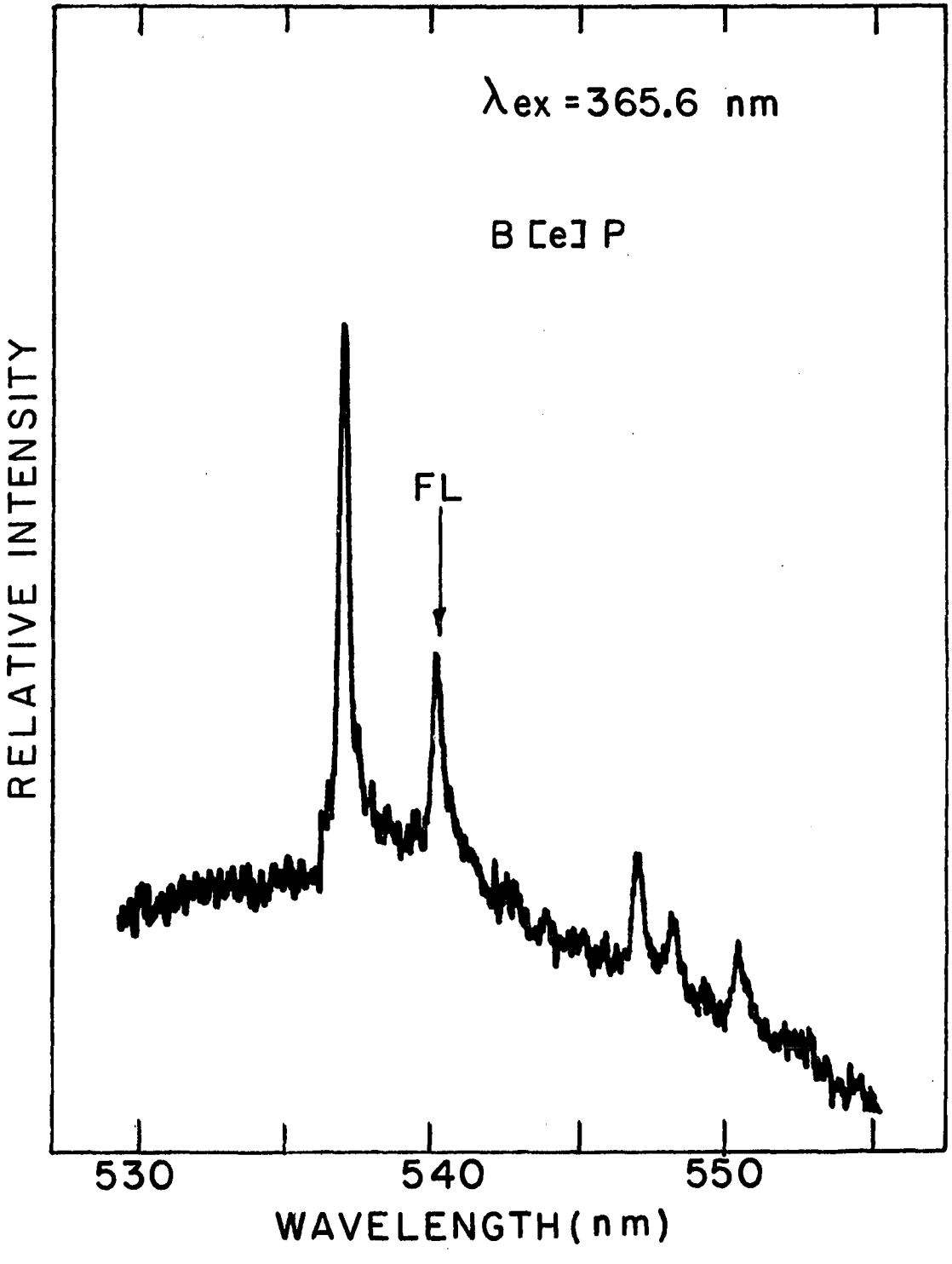

Figure 22. Selectively excited phosphorescence spectrum of B[e]P in a SRC-II sample. FL:fluoranthene.

quantitative determination of these compounds in mixtures. In Figure 22, benzo[e]pyrene was identified by its phosphorescence spectrum (Figure 12B) because of the more optimum phosphorescence intensity observed for B[e]P. Similarly, the λex selected for B[e]P caused weak emission from fluoranthene that does not pose any spectral interference. The sloping baseline seen in Figure 22 is typical of emissions from the compounds in the sample that were not subject to the line-narrowing Shpol'skii effect.

Quantitative analysis - The standard additions approach

Because of the complex composition of unrefined coal liquefaction products and shale oil, the "inner filter effect" may result in quenching of luminescence (101). The analytical bias that may be occasioned by this effect can usually be eliminated through the standard additions approach (63). In the standard additions approach, equal quantities of the sample are added to a series of standard solutions containing varying quantities of the analyte of interest. The analyte emission readings for these solutions are then corrected for background and plotted against the concentration of the standard present in the solution. The resulting extrapolated line intersecting the concentration axis indicates the concentration of the analyte in the sample.

Analytical calibration curves obtained via this approach on a shale oil sample diluted by 10^3 are shown in Figure 23. To compensate for any variation in the experimental conditions during the course of an analytical calibration-quantitation run, the luminescence intensity of

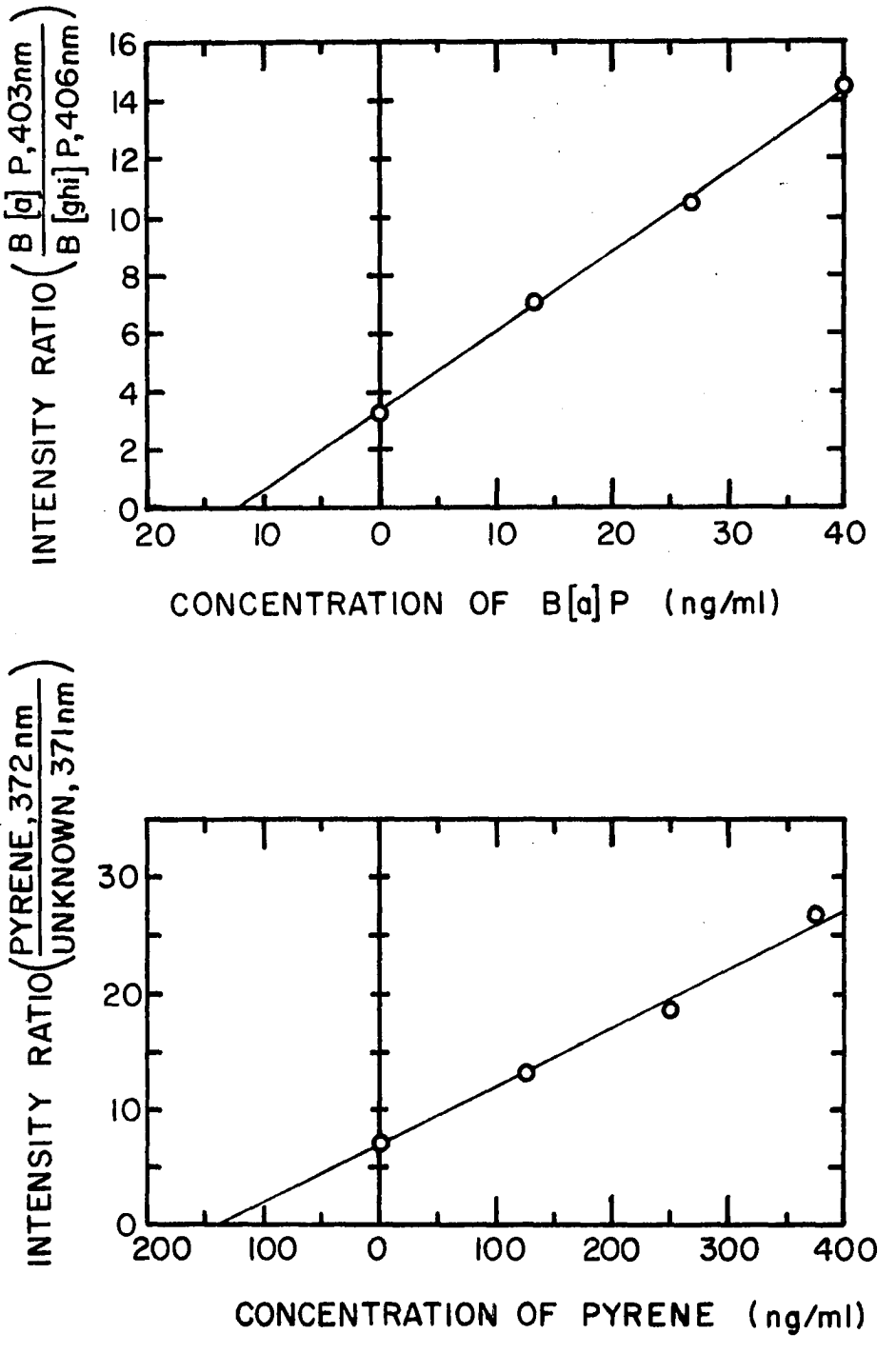

Figure 23. Calibration curves for B[a]P and pyrene in shale oil, obtained by the method of standard additions.

another PAH in the sample was concurrently measured along with the analyte emission. For the analytical curve shown in Figure 23, the intensity ratio of analyte/internal reference was related to concentration. The analytical results obtained in the manner discussed above for the shale oil sample are summarized in Table 7 under the caption LESS.

Table VII. Analytical data (μg/g) on shale oil

	Ames Lab			NBS	Mean
Compound	LESS	GC-MS	HPLC		
Pyrene	147	161	138	107	138
B[a]P	13	14	19	20	16

The analytical methodology employed by NBS, which also performed the analysis, involved several fractionation procedures including acid-base extraction or high performance liquid chromatography. The individual PAHs were then isolated via gas chromatography-mass spectrometry (GC-MS) or high performance liquid chromatography (HPLC) and quantitated by utilizing the external, internal and/or standard additions procedures (102). The Ames Lab GC-MS and HPLC methods generally followed those suggested by NBS. A comparison of the LESS results with those obtained by chromatographic techniques reveals a level of disagreement that is symptomatic of the lack of absolute accuracy of existing methodologies for the determination of trace concentrations of PAHs in complex mixtures, such as shale oil. However, it is seen that the LESS values agree within the estimated experimental uncertainty of ~20% with the average values.

A more critical evaluation of the LESS technique was demonstrated for the direct determination of some target PAHs in a solvent refined coal (SRC-II) product. The SRC-II sample was provided by NBS as part of the round-robin analysis for the NBS surrogate reference material program. The objective of this program is to evaluate, with provided material, the efficacy of the various technique utilized by different laboratories for the determination of trace organic constituents in alternate fuels. The target compounds include phenol, o-cresol, acridine, carbazole, dibenzothiophene, pyrene, B[a]P and B[e]P. Unfortunately, the former five compounds could not be excited and examined by the current LESS facilities without frequency-doubling the laser output.

Figure 24 and 25 show the analytical calibration curves obtained via the standard additions approach, for the SRC-II sample diluted by 2.5×10^3, 5×10^3, 1×10^3 and 2.5×10^3 for pyrene, B[a]P, B[e]P and B[k]F, respectively. Again, linearity was observed in all the curves shown. The analytical results obtained along with those obtained by other laboratories are summarized in Table 8. Among the various methods employed by different laboratories, LESS, FLNS (fluorescence line-narrowing spectrometry), SF (synchronous fluorimetry) and RTP (room temperature phosphorimetry) were luminescence techniques, and the remainder all involved chromatographic procedures. Only the LESS, FLNS, SF, RTP and Ames Lab GC-MS techniques involved direct analysis of the SRC-II sample without resorting to any prior fractionation procedure. A comparison of the data obtained by these independent techniques shows serious disagreements. In general, the LESS results were in excellent

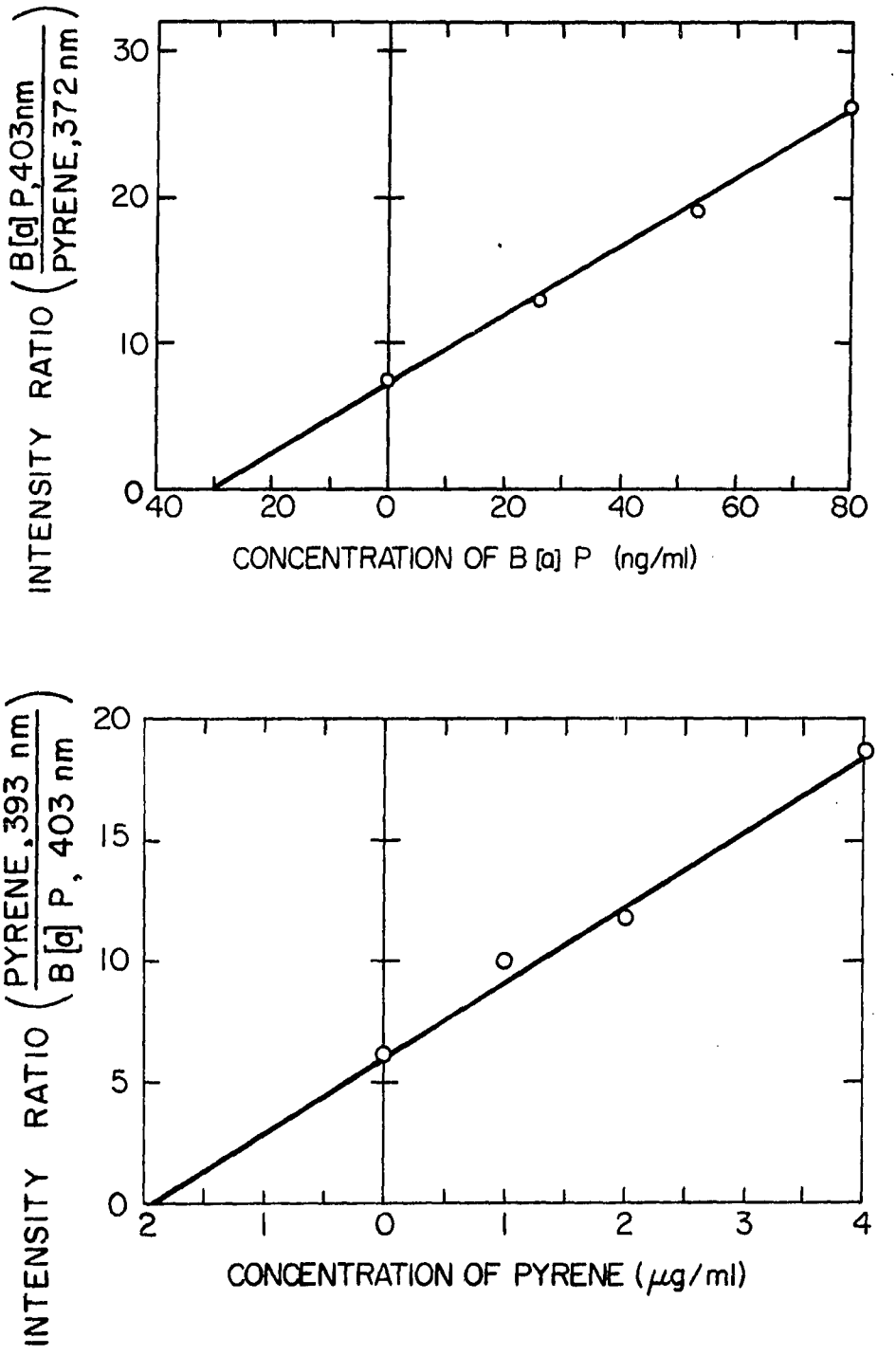

Figure 24. Calibration curves for pyrene and B[a]P in SRC-II, obtained by the method of standard additions.

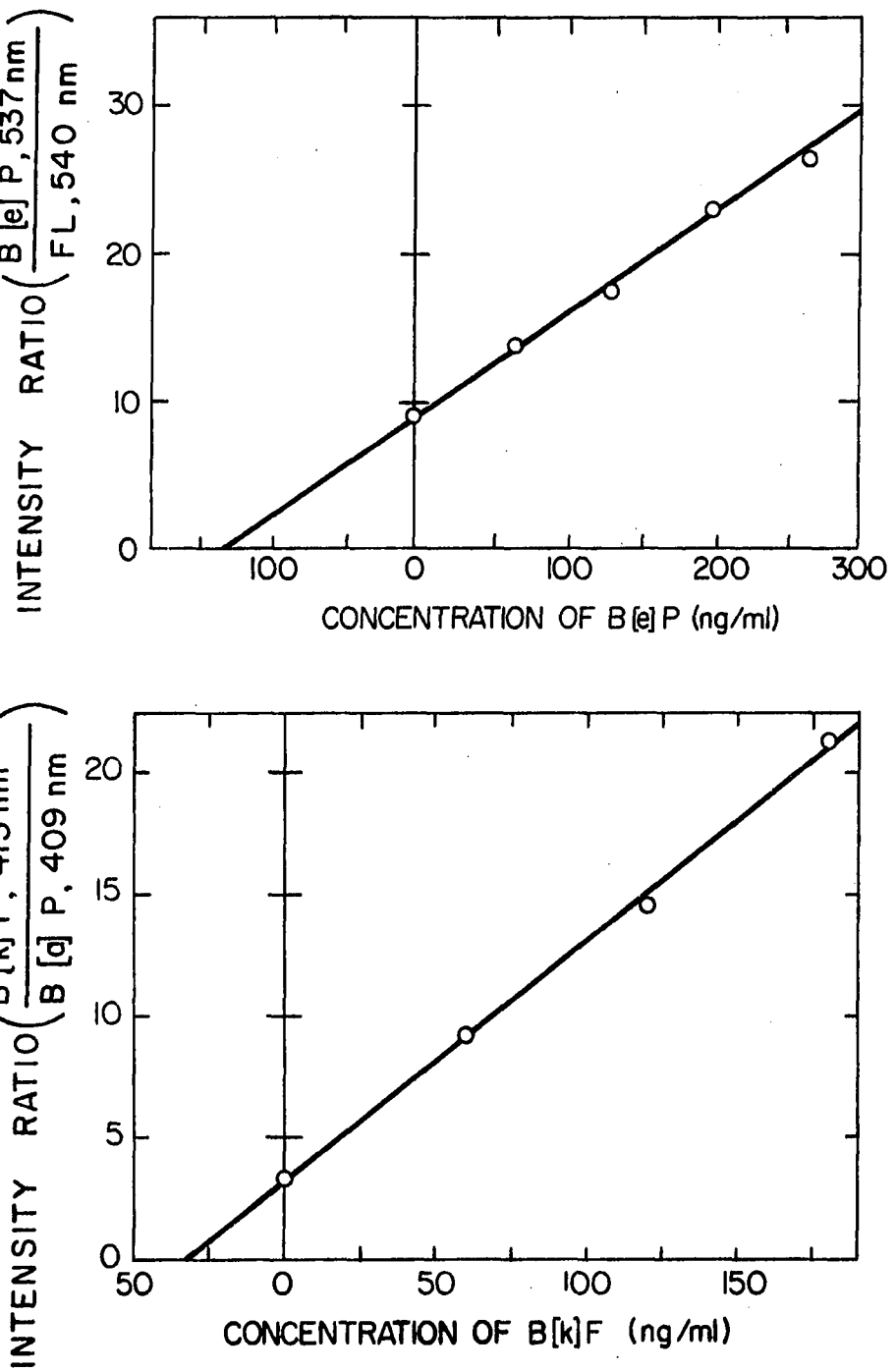

Figure 25. Calibration curves for B[k]F and B[e]P in SRC-II, obtained by the method of standard additions.

Table VIII. Analytical data (μg/g) on solvent refined coal (SRC-II) surrogate reference material

	Ames Lab				ORNL[a]		LLL[b]	ANL[c]	LASL[d]	NBS	Mean
Compound	LESS	GC-MS	HPLC	FLNS	SF	RTP					
Pyrene	4605	7607	4080	830	6000	3600	4900	10000	6490	6000	5411
B[a]P	145	208	130	95	129	—	180	126	235	134	154
B[e]P	126	208	225	56	—	117	230	107	205	143	157
B[k]F	78	—	—	—	—	—	—	—	—	—	—

[a]ORNL - Oak Ridge National Laboratory.

[b]LLL - Lawrence Livermore Laboratory.

[c]ANL - Argonne National Laboratory.

[d]LASL - Los Alamos Scientific Laboratory.

agreement with most of the data, specifically with the NBS results. The deviations of the LESS values from the average values for pyrene, B[a]P, and B[e]P were 15%, 6% and 20%, respectively. The FLNS data were the only ones obtained without employing the standard additions procedures among the various direct determination methods. It was surprising to learn that when HPLC was utilized to fractionate the SRC-II sample into much less complex fractions, the FLNS technique found ~4000 μg/g for pyrene, which was comparable with the NBS or the mean value. The disagreement of the FLNS data (which were low) with those of others shown in Table 8, lends some doubt to the claim (72) that quantitation can be achieved by this approach without preseparation or recourse to the standard addition or internal reference methods.

Quantitative analysis - The internal reference approach

Although the standard addition procedure has consistently provided accurate analytical data, the necessity of establishing an analytical curve for each analyte and for each samples renders this approach impractical for routine analyses. Thus, an alternate but relatively simple procedure to obtain unambiguous quantitative data was evaluated, by employing completely deuterated PAHs as the internal reference compounds. In principle, luminescent quenching or enhancement effects may be internally compensated by comparing the analyte luminescence to an internal reference compound that

responds to these effects to the same degree as the analyte. From a consideration of first principles (see Selection Criteria discussion below), deuterated analogues of the analytes added at constant concentration levels to each sample should, therefore, serve as virtually ideal internal reference compounds. In this investigation, the efficacy of this approach was demonstrated for the quantitative determination of benzo[a]pyrene and perylene. Benzo[a]pyrene was particularly selected as the target compound because it is a well-known potent carcinogen and is probably the most widely accepted indicator of PAH content of environment samples.

Selection criteria of an internal reference compound in LESS

The normal requirements of an effective internal reference element in analytical atomic spectroscopy are well known. In the analysis of complex organic matrices such as coal liquids and shale oil utilizing LESS, the following criteria are considered important.

1. Its spectroscopic properties should be as similar as possible to those of the analyte being determined so that the internal reference compound will provide adequate compensation for the emission variation associated with intermolecular interactions and inner filter and enhancement effects.
2. It should be absent in the sample.

3. It should be in a high state of purity with respect to the analyte being determined.
4. The luminescent lines of the internal reference and analyte compound of interest should be free of spectral interferences arising from emissions of other sample constituents.
5. Both of the lines selected should be free of self-absorption.
6. It is preferable to employ the same excitation wavelength for the reference and analyte, whenever possible.

Deuterated organic compounds are known to have similar chemical and physical properties as their undeuterated analogues. Because they are available commercially with high purity, and are unlikely to be present in "real" samples, these compounds satisfy the stated criteria to an unusually high degree.

Isotopic effects on the Shpol'skii-effect spectra Spectral line shifts resulting from isotopically enriched solute and solvent have often been reported for Shpol'skii systems (103-106). Observations on the deuteration effect on the luminescence spectrum of pyrene dissolved in n-pentane and frozen to a solid at 10 K, revealed that similar excitation and emission spectra are observed for pyrene and pyrene-d_{10}, and that the spectral line shift between the 0-0 lines were ~100 cm^{-1} (103). In the present work, similar spectral shifts were observed for deuterated PAHs. Figure 26

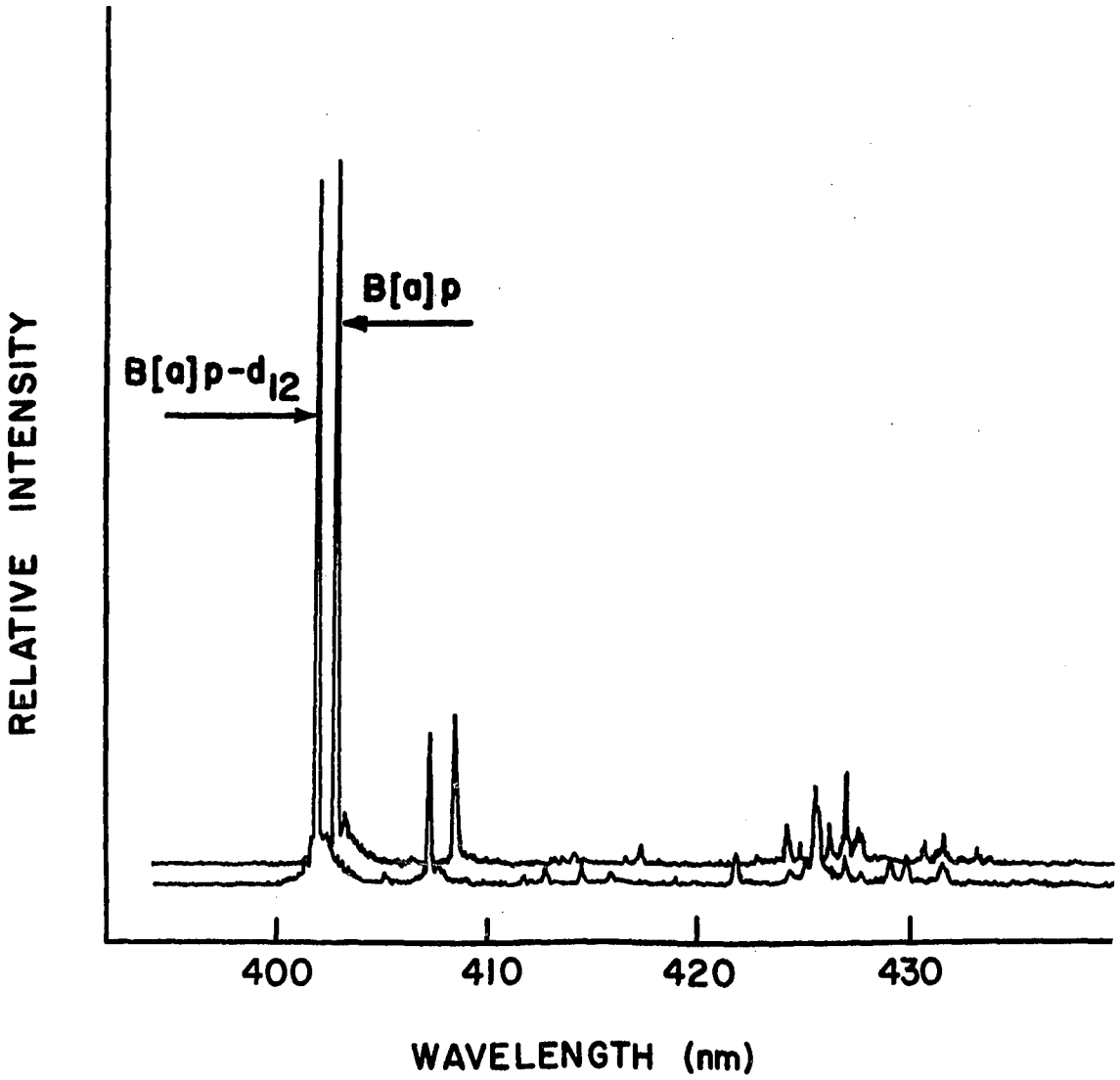

Figure 26. Fluorescence spectrum of B[a]P-d_{12} in n-octane, λ_{ex}=379.5 nm superimposed on the reference LES spectrum of B[a]P, λ_{ex}=380.2 nm.

shows the observed fluorescence spectrum of B[a]P-d_{12} in n-octane, superimposed on the reference LES spectrum of B[a]P. It is seen in this figure that B[a]P-d_{12}, as well as B[a]P, exhibits quasilinear features (FWHM ~0.1 nm), and both spectra resemble each other (identical to the multiple site spectrum case discussed earlier in this thesis). The effect of deuterium on the fluorescence of B[a]P resulted in a 1 nm (~55 cm^{-1}) blue-shift in the 0-0 line. Similar spectral line shifts were also observed for perylene-d_{12} as shown in Figure 27. Such spectroscopic properties of deuterated PAH are desirable for an internal reference compound in determination of PAHs in complex matrices. The proximity of the analytical line pair would assure that both the analyte and internal reference line intensities will vary to a similar extent by the "inner filter and enhancement effects," because the absorption spectrum of liquid fuel would be expected to be broad and structureless, i.e. the extinction coefficient of a complex mixture remains approximately constant over a small wavelength internal.

Analytical studies To evaluate the feasibility of the internal reference approach utilizing deuterated PAH analogues, oil samples of widely differing B[a]P contents and complexities were examined. These samples included a petroleum crude, two coal-derived fuels, and two shale-derived crude oils. The analytical calibration curve for the determination of B[a]P

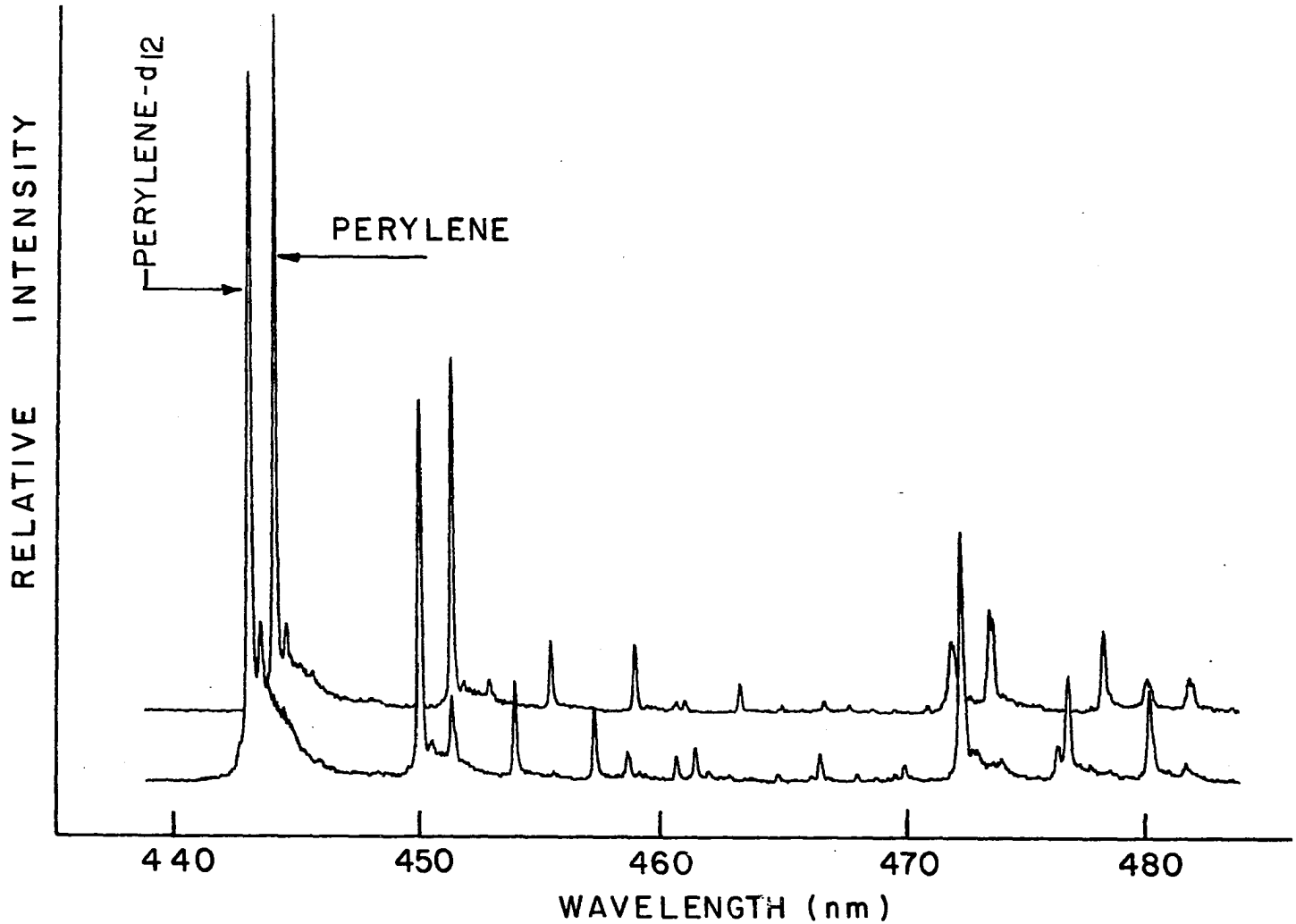

Figure 27. Fluorescence spectrum of perylene-d_{12} in n-octane, λ_{ex}=417.7 nm superimposed on the reference LES spectrum of perylene, λ_{ex}=420.3 nm.

in the concentration range of 0.1 to 100 ppb is shown in Figure 28. For this analytical curve, the 0-0 lines at 402 nm and 403 nm, the most intense lines shown in Figure 26, were selected as the analytical line pair in obtaining the data. Typical fluorescence spectra of B[a]P and perylene, and their deuterated analogues in the liquid fuel sample spiked with 10 ppb B[a]P-d_{12} and 160 ppb perylene-d_{12} are shown in Figure 29 and 30. The same excitation wavelengths, 380.2 nm (Figure 29) and 420.3 nm (figure (Figure 30), were utilized for excitation of both analyte and reference compounds as were done for establishing the analytical calibration curves. It is seen in Figure 29 and 30 that both analytical lines are free of spectral interferences.

Typical analytical results obtained by the internal reference method are shown in Table 9, where B[a]P contents measured on five samples and perylene contents on two samples are compared with those values obtained by the standard addition method and by other investigators who employed independent analytical methodologies. Various dilution factors were chosen for these samples (SRC-II, 5 X 10^3; shale oil, 10^3; Wilmington crude, 10^3; coal-derived fuel oil, 5 X 10^3; and shale-derived diesel fuel, 50) so that the analyte B[a]P concentration in the diluted sample would fall within the linear range of the analytical calibration curve. The dilution factor of 50 used for shale-derived diesel fuel was the minimum factor required to avoid spectral

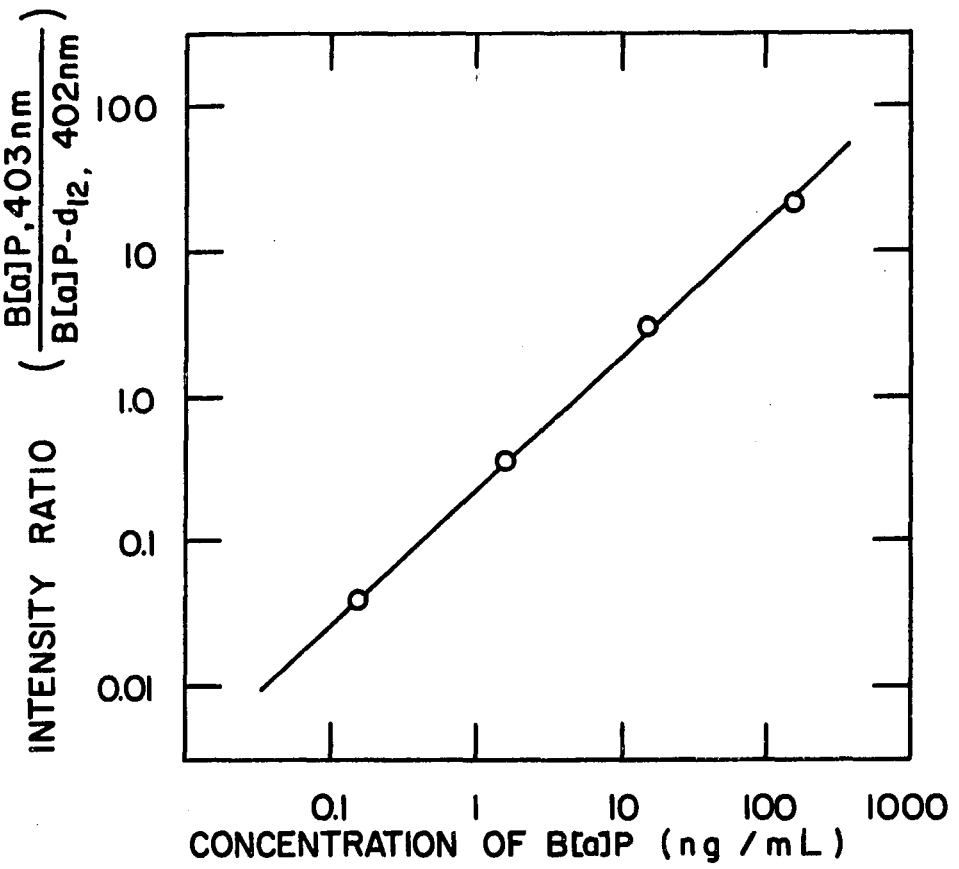

Figure 28. Analytical calibration curve for B[a]P utilizing B[a]P-d_{12} (10 ppb) as internal reference. The λ_{ex} was 380.2 nm for both the analyte and internal reference compounds.

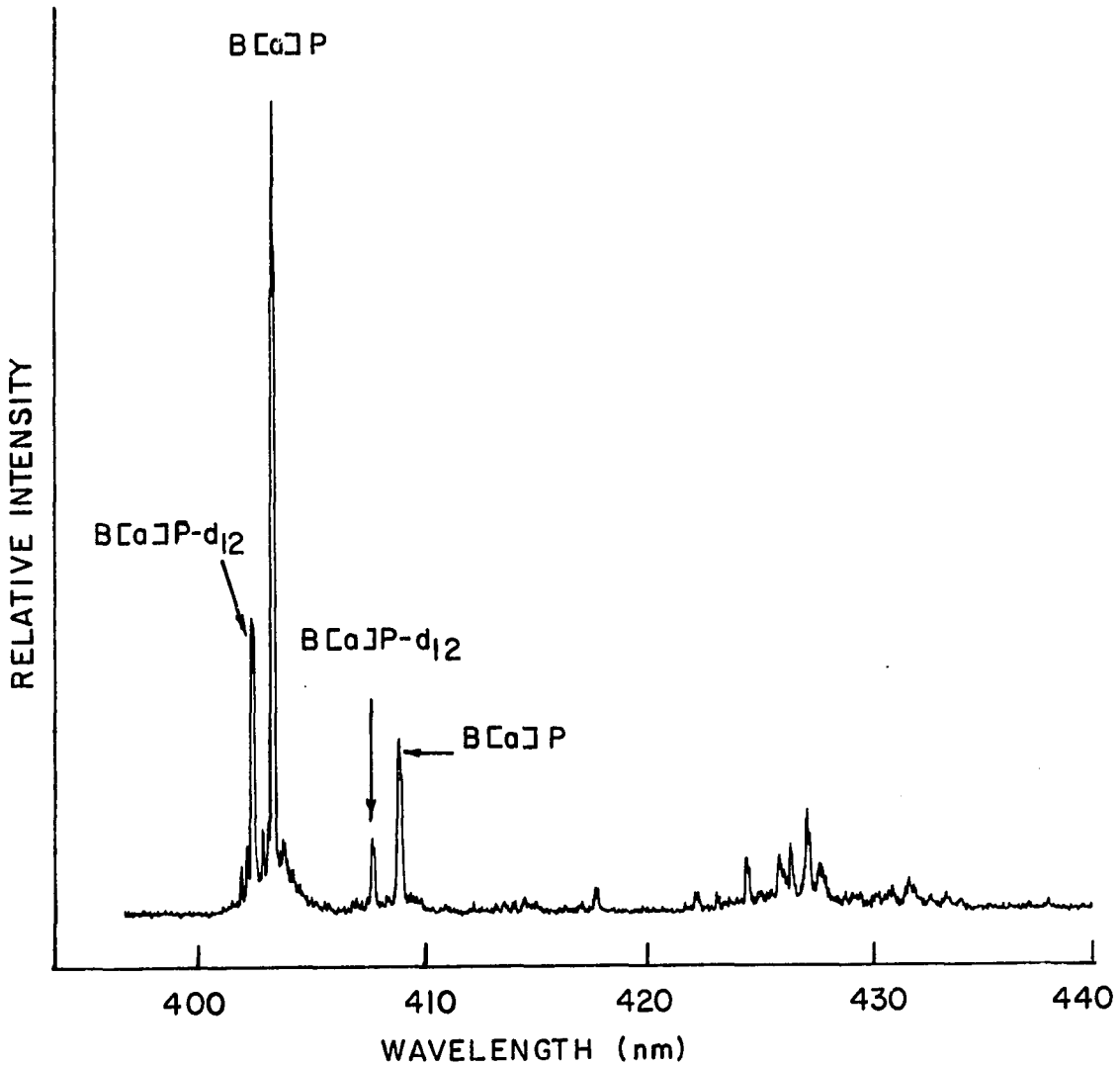

Figure 29. Selectively excited fluorescence spectrum of B[a]P in a shale oil sample with 10 ppb B[a]P-d_{12} added as the internal reference.

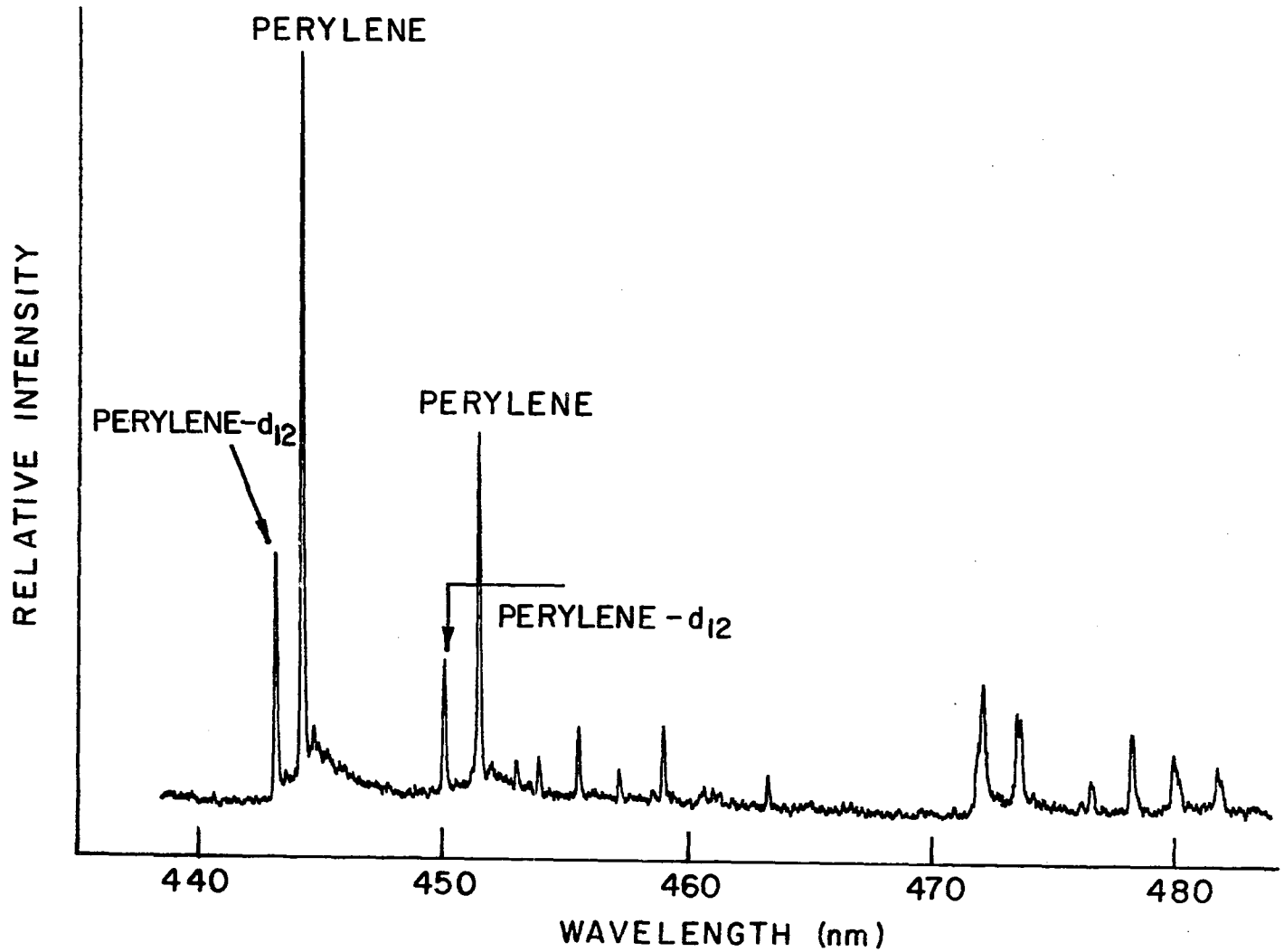

Figure 30. Selectively excited fluorescence spectrum of perylene in a Wilmington crude oil sample with 160 ppb perylene-d_{12} added as the internal reference.

Table IX. Concentrations of B[a]P and perylene in liquid fuels (μg/g)

Sample	Standard Addition Method	Internal Reference Method	Reference Data
		B[a]P Concentrations	
SRC-II	145	163	134/129[a]
Shale oil	13	15	21[a]
Wilmington crude	—	3	2[a]; 2.5/2.7[b]
Coal-derived fuel oil	—	88	82.3/91.8[b]
Shale-derived diesel fuel	—	0.056	0.030/0.045[b]
		Perylene Concentrations	
SRC-II	—	29	26[c]
Wilmington crude	—	40	38[c]

[a](102).

[b](107).

[c]NBS data.

line-broadening observed for samples diluted to a lesser extent. However, no asphaltene precipitation was visually detected in dilution of the diesel fuel sample by any factor. The analytical methodologies employed for obtaining the reference values shown in Table 9 have generally involved considerable fractionation and separation procedures. For example, in Tomkins's method (107), which required a minimum of three man-days to determine the B[a]P content of one sample, a B[a]P tracer, 7,10-C^{14}-B[a]P, was added to the samples to evaluate the B[a]P losses throughout the isolation procedures, and the quantitative data were corrected for the B[a]P recovery factor. Thus, Tomkins's data were probably the most reliable ones available to date.

A comparison of the data obtained by the internal reference approach with values obtained by other methodologies reveals a level of agreement that is considered excellent in terms of present capabilities. Because the deuterated analogues of the analytes satisfy the operating criteria of an internal reference compound to such a high degree, the direct determination of selected PAHs in complex mixtures in a rapid and simple fashion is portended by the results shown in Table 9. In contrast to other methodologies, only a sample dilution step, the addition of the internal reference compound, and cooling to 15 K are

required prior to the spectroscopic observations. The total elapsed time for an analysis is approximately one hour.

CHAPTER 5. CONCLUSIONS AND RECOMMENDATIONS FOR FURTHER WORK

The results presented in this dissertation demonstrate the feasibility of utilizing the LESS approach for the analysis of complex mixtures of PAHs, including alkylated derivatives. The use of deuterated internal reference compound coupled with LESS, in particular, provided a simple and novel approach for the direct qualitative and quantitative determination of specific, highly carcinogenic PAHs in real samples, without any prior separation of the PAHs. The LESS technique could obviously be applied to other organic luminescent systems, such as heterocyclic compounds that also exhibit Shpol'skii effect. As the scope expends to other organic systems, other types of "Shpol'skii" solvents, which are amenable to more polar PAH derivatives, should be searched. Tetrahydrofuran (THF) is known to be one of such choices (64). In addition, some compounds that exhibit strong guest-host interactions even at low temperature may necessitate the freezing of the sample to liquid helium (~4 K) or even lower temperature. To excite those compounds that absorb and emit in the UV, frequency-doubling of the dye laser output will also be required.

Although LESS in the present state of development appears to be a promising analytical technique, the PAH problem is

quite complex, and other analytical techniques will undoubtedly be required to characterize PAHs in samples from various sources.

BIBLIOGRAPHY

1. Bridbord, K.; French, J. G. "Carcinogenesis, Vol. 3: Polynuclear Aromatic Hydrocarbons" P. W. Jones and R. I. Freundenthal, Eds., Raven Press, New York, NY, 1978, p. 451.

2. Dipple, A. In "Chemical Carcinogens," C. E. Searle, Ed., American Chemical Society, Washington, D. C., 1976, p. 245.

3. Jones, D. W. Prog. Med. Chem., 1974, 10, 159.

4. Griest, W. H.; Tomkins, B. A.; Epler, J. L.; Rao, T. K., in "Polynuclear Aromatic Hydrocarbons" P. W. Jones and P. Leber, Eds.; Ann Arbor Science Publishers, Ann Arbor, MI, 1979, p. 395.

5. Hoffman, D.; Wynder, E. L. Cancer, 1971, 27, 848.

6. Winefordner, J. D.; Schuiman, S. G.; and O'Haver, T. C. "Luminescence Spectroscopy in Analytical Chemistry," Wiley-Interscience, New York, NY, 1972.

7. Bradley, A. B.; Zare, R. N. J. Am. Chem. Soc. 1976, 98, 620.

8. Richardson, J. H.; Ando, M. E. Anal. Chem. 1977, 49, 955.

9. Richardson, J. H.; Wallin, B. W.; Johnson, D. C.; Hrubesh, L. W. Anal. Chim. Acta 1976, 86, 26.

10. Richardson, J. H.; Larson, K. M.; Haugen, G. R.; Johnson, D. C.; Clarkson, J. E. Anal. Chim. Acta 1980, 116, 407.

11. Rayner, D. M.; Szabo, A. G. Appl. Opt. 1978, 17, 1624.

12. Lytle, F. E.; Kelsey, M. S. Anal. Chem. 1974, 46, 855.

13. Winefordner, J. D.; Boutilier, G. D. Anal. Chem. 1979, 51, 1384.

14. Keirs, R. J.; Britt, R. D.; Wentworth, W. E. Anal. Chem. 1957, 28, 202.

15. Singer, L.; Baram, Z.; Ron, A.; Kimel, S. Chem. Phys. Lett. 1977, 47, 372.

16. Sepaniak, M. J.; Yeung, E. S. Anal. Chem. 1977, 49, 1554.

17. Wirth, M. J.; Lytle, F. E. Anal. Chem. 1977, 49, 2054.

18. Vo-Dinh, T. Anal. Chem. 1978, 50, 396.

19. Vo-Dinh, T.; Gammage, R. B. Anal. Chem. 1978, 50, 2054.

20. Philip, J.; Souter, I. Anal. Chem. 1976, 48, 420.

21. Vo-Dinh, T.; Hooyman, J. R. Anal. Chem. 1979, 51, 1915.

22. Vo-Dinh, T.; Winefordner, J. D. Appl. Spectrosc. Rev. 1977, 13, 261.

23. Vo-Dinh, T.; Martinex, P. R. Anal. Chim. Acta, in press.

24. Kasha, M. J. Chem. Phys. 1952, 20, 71.

25. Aaron, J. J.; Mousa, J. J.; Winefordner, J. D. Talanta 1973, 20, 279.

26. Personov, R. I.; Al'shits, E. I.; Bykovskaya, L. A. Opt. Commun. 1973, 7, 417.

27. Meyer, B. "Low Temperature Spectroscopy," American Elsevier, New York, NY, 1971.

28. McClure, D. S. J. Chem. Phys. 1954, 22, 1968.

29. Ostertag, R.; Wolf, H. C. Phys. Status Solidi 1969, 31, 139.

30. Shpol'skii, E. V. Sov. Phys. Usp. 1960, 3, 372.

31. Rebane, K. K.; Khizhnyakov, V. V. Opt. Spectrosc. 1963, 14, 193.

32. Richards, J. L.; Rice, S. A. J. Chem. Phys. 1971, 54, 2014.

33. Osad'ko, I. S.; Personov, R. I.; Shpol'skii, E. V. Izv. Akad. Nauk SSSR, Ser. Fiz. 1973, 37, 540.

34. Rebane, K. K. "Impurity Spectra of Solids," Plenum Press, New York, NY, 1970, p. 35.

35. Dibartolo, B.; Powell, R. C. "Phonons and Resonance in Solids," Wiley, New York, NY, 1976, p. 348.

36. Szabo, A. Phys. Rev. Lett. 1970, 25, 924.

37. Szabo, A. Phys. Rev. Lett. 1971, 27, 343.

38. Kohler, B. E. In "Chemical and Biochemical Applications of Lasers," Moore, C. B., Ed.; Academic Press, New York, NY, 1979, Vol. 4, p. 31.

39. Shpol'skii, E. V.; Il'ina, A. A.; Klimova, L. A. Dokl. Akad. Nauk SSSR, 1952, 87, 935.

40. Shpol'skii, E. V. Sov. Phys. Usp. 1963, 6, 411.

41. Dekkers, J. J.; Hoornweg, G. Ph.; Visser, G.; Maclean, C.; Velthorst, N. H. Chem. Phys. Lett. 1977, 47, 357.

42. Nurmukhametov, R. N. Russian Chem. Rev. 1969, 38, 180.

43. Shpol'skii, E. V.; Klimova, L. A. "Physical Problems of Spectroscopy," Akad. Nauk SSSR, Moscow, 1962.

44. Colmsjö, A. L.; Stenberg, U. Chem. Scripta 1976, 9, 227

45. Pfister, C. Chem. Phys. 1973, 2, 171

46. Dokunikhin, N. S.; Kizel, V. A.; Sapozhnikov, M. N.; Solodar, S. L. Opt. Spectrosc. 1968, 25, 42.

47. Colmsjö, A. L.; Stenberg, U. Chem. Scripta 1977, 11, 220.

48. Dinse, K. P.; Winscom, C. J. J. Lumin. 1979, 18/19, 500

49. Mishina, L. A.; Nakhimovskaya, L. A.; Sviridova, K. A. Izv. Akad. Nauk SSSR, Ser. Fiz 1975, 39, 2387.

50. Personov, R. I. Zh. Analit. Khimii 1962, 17, 506.

51. Lamotte, M.; Merle, A. M.; Risemberg, S. J. Lumin. 1979, 18/19, 505.

52. Lamotte, M; Joussot-Dubien, J. Chem. Phys. 1973, 2, 245.

53. Merle, A. M.; Pitts, W. M.; El-Sayed, M. A. Chem. Phys. Lett. 1978, 54, 211.

54. Merle, A. M.; Nicol, M. F.; El-Sayed, M. A. Chem. Phys. Lett. 1978, 59, 386.

55. Svischev, G. M. Opt. Spectrosc. 1965, 18, 350.

56. Vo-Dinh, T.; Wild, U. P. J. Lumin. 1973, 6, 296.

57. Bolotnikova, T. N.; Naumova, T. M. Opt. Spectrosc. 1968, 25, 253.

58. Dekkers, J. J.; Hoornweg, G. Ph.; MacLean, C.; Velthorst, N. H. J. Mol. Spectrosc. 1977, 68, 56.

59. Nakhimovskaya, L. A. Opt. Spectrosc. 1968, 24, 105.

60. Shpol'skii, E. V.; Klimova, L. A.; Nersesora, G. N.; Glyodkoskii, V. I. Opt. Spectrosc. 1968, 24, 25.

61. Shpol'skii, E. V.; Bolotnikova, T. N. Pure Appl. Chem. 1974, 37, 183.

62. Gaeyava, T. Y.; Khesina, A. Y. Russ. J. Anal. Chem. 1974, 29, 1913.

63. Kirkbright, G. F.; de Lima, C. G. Analyst 1974, 99, 338.

64. Kirkbright, G. F.; de Lima, C. G. Chem. Phys. Lett. 1976, 37, 165.

65. Khesina, A. Y.; Smirnov, G. A.; Ermakov, E. A.; Knyazeva, A. A.; Yashin, Y. I. Zh. Analit. Khimii 1978, 33, 2032.

66. D'Silva, A. P.; Oestreich, G. J.; Fassel, V. A. Anal. Chem. 1976, 48, 915.

67. Woo, C. S.; D'Silva, A. P.; Fassel, V. A.; Oestreich, G. J. Environ. Sci. Technol. 1978, 12, 173.

68. Woo, C. S.; D'Silva, A. P.; Fassel, V. A. Anal. Chem. 1980, 52, 159.

69. Colmsjö, A.; Stenberg, U. Anal. Chem. 1978, 51, 145.

70. Colmsjö, A.; Östman, C. E. Anal. Chem. 1980, 52, 2093.

71. Brown, J. C.; Edelson, M. C.; Small, G. J. Anal. Chem. 1978, 50, 1394.

72. Brown, J. C.; Hayes, J. C.; Small, G. J. In "Lasers and Chemical Analysis;" Hieftje, G. M.; Lytle, F. E.; Traxis, J. C., Eds.; Humana Press, Clifton, NJ, 1980.

73. Brown, J. C.; Duncanson, Jr., J. A.; Small, G. J. Anal. Chem. 1980, 52, 1711.

74. Stroupe, R. C.; Tokousbalides, P.; Dickinson, R. B.; Wehry, E. L.; Mamantov, G. Anal. Chem. 1977, 49, 701.

75. Tokousbalides, P.; Hinton, E. R.; Dickinson, R. B.; Bilotta, P. V., Wehry, E. L.; Mamantov, G. Anal. Chem. 1978, 50, 1189.

76. Wehry, E. L.; Mamantov, G. Anal. Chem. 1979, 51, 643A.

77. Dickinson, R. B.; Wehry, E. L. Anal. Chem. 1979, 51, 778.

78. Maple, J. R.; Wehry, E. L.; Mamantov, G. Anal. Chem. 1980, 52, 920.

79. Maple, J. R.; Wehry, E. L. Anal. Chem. 1981, 53, 266.

80. Reedy, G. T.; Bourne, S.; Cunningham, P. T. Anal. Chem. 1979, 51, 1535.

81. Tokousbalides, P.; Wehry, E. L.; Mamantov, G. J. Phys. Chem. 1977, 81, 1789.

82. Allkins, J. R. Anal. Chem. 1975, 47, 752A.

83. Wright, J. C.; Wirth, M. J. 1980, 52, 988A, 1087A.

84. Yang, Y.; D'Silva, A. P.; Fassel, V. A.; Iles, M. Anal. Chem. 1980, 52, 1350.

85. Hänsch, T. W. Appl. Opt. 1972, 11, 895.

86. Lytle, F. E. Anal. Chem. 1974, 46, 545A.

87. Klauminzer, G. K. Laser Focus Mag. 1975, Nov., 35.

88. Boxcar Integrator Operating and Service Manual, Princeton Applied Research, 1976.

89. Giger, W.; Schaffner, G. Anal. Chem. 1978, 50, 243.

90. Fox, M. A.; Staley, S. W. Anal. Chem. 1976, 48, 992.

91. Das, B. S.; Thomas, G. H. Anal. Chem. 1978, 50, 967.

92. Snook, M. E.; Severson, R. F.; Higman, H. C.; Arrendale, R. F.; Chortyk, O. T. "Polynuclear Aromatic Hydrocarbons," Jones, P. W.; and Leber, P., Eds.; Ann Arbor Science Publishers, Ann Arbor, MI, 1979, p. 231.

93. Morgan, D. D.; Warshawsky, D.; Atkinson, T. Photochem. Photobiol. 1977, 25, 31.

94. Snook, M. E.; Severson, R. F.; Higman, H. C.; Arrendale, R. F.; Chortyk, O. T. Beitr. Tabakforsch. 1978, 9, 222.

95. Lee, M. L.; Vassilaros, D. L.; White, C. M.; Novotny, M. Anal. Chem. 1979, 51, 768.

96. Lukasiewicz, R. J.; Winefordner, J. D. Talanta 1972, 19, 381.

97. Oestreich, G. J. Ph.D. Dissertation, Iowa State University, Ames, IA, 1979.

98. Berlman, I. B. "Handbook of Fluorescence Spectra of Aromatic Molecules," 2nd ed., Academic Press, New York, NY, 1971.

99. McKay, J. F.; Amend, P. J.; Cogswell, T. E.; Harnsberger, P. M.; Erickson, R. B.; Latham, D. R. In "Analytical Chemistry of Liquid Fuel Sources," Uden, Siggia and Jensen, Eds. Amer. Chem. Soc., 1978, p. 128.

100. Colmsjö, A.; Stenberg, U. In "Polynuclear Aromatic Hydrocarbons, Hydrocarbons," Jones, P. W.; Leber, P., Eds., Ann Arbor Science Publishers, Inc., Ann Arbor, MI, 1979, p. 121.

101. Parker, C. A., "Photoluminescence of Solutions," Elsevier, Amsterdam, 1968.

102. Hertz, H. S.; Brown, J. M.; Chesler, S. N.; Guenther, F. R.; Hilpert, L. R.; May, W. E.; Parris, R. M.; and Wise, S. A. Anal. Chem. 1980, 52, 1650.

103. Cunningham, K.; Siebrand, W.; Williams, D. F. Chem. Phys. Lett. 1973, 20, 496.

104. Meyer, B.; Metzger, J. L. Spectrochim. Acta 1972, 28A, 1563.

105. LeBel, G. L.; Laposa, J. D. J. Mol. Spectrosc. 1972, 41, 249.

106. Schettino, V. J. Mol. Spectrosc. 1970, 34, 78.

107. Tomkins, B. A.; Kubota, H.; Griest, W. H.; Caton, J. E.; Clark, B. R.; Guerin, M. R. Anal. Chem. 1980, 52, 1331.

ACKNOWLEDGMENTS

I wish to express my sincere gratitude to Dr. Velmer A. Fassel for his guidance and critical review of the work presented in this dissertation. I would also like to express my appreciation to Mr. Arthur P. D'Silva for his guidance and suggestions which made this research possible. Special thanks are given to Mr. Malvern K. Iles, who helped me solve many of the instrumental problems, and to Dr. Robert S. Houk, who gave me numerous valuable advice throughout my graduate career.

The financial assistance granted me by the U. S. Department of Energy, Office of Health and Environmental Research is greatly appreciated.

I am also deeply indebted to my wife, Su-Mei, for her love, patience and encouragement, and the sacrifices she made over the past several years. To my daughter, San-San, I must apologize for the many hours, rightfully hers, that were consumed by this work.

Above all, I thank my father, Chung-Cheih Yang, for the love and support given me over the years. I would like to dedicate this dissertation to him.